Locally heterogeneous three-dimensional fibrous media : Representative elementary volumes and calculation of acoustic properties

Quang Vu Tran

UNIVERSITÉ GUSTAVE EIFFEL
MSME UMR 8208 CNRS
Laboratoire Modélisation et Simulation Multi Echelle

UNIVERSITÉ DE SHERBROOKE
Faculté de génie
Département de génie mécanique

THÈSE

pour obtenir le grade de

DOCTEUR DE L'UNIVERSITÉ GUSTAVE EIFFEL

Spécialité : Mécanique

Présentée par

Quang Vu TRAN

Milieux fibreux tridimensionnels localement hétérogènes : Volumes élémentaires représentatifs et calcul des propriétés acoustiques

Soutenue le 21 décembre 2023 devant le jury composé de

N. ATALLA :	Université de Sherbrooke (CA)	Examinateur
S. DARTOIS :	Sorbonne Université (FR)	Examinatrice
N. DAUCHEZ :	Université de Technologie de Compiègne (FR)	Rapporteur
B. DUBUS :	IEMN (FR)	Rapporteur
M. A. GALLAND	Ecole Centrale de Lyon (FR)	Présidente
V. MARCEL :	Adler Pelzer Group, Acoustic TechCenter R&D (FR)	Invitée
V. MONCHIET :	Université Gustave Eiffel (FR)	Examinateur
R. PANNETON :	Université de Sherbrooke (CA)	Co-Directeur
C. PERROT :	Université Gustave Eiffel (FR)	Directeur

Champs-sur-Marne, France

Sherbrooke (Québec), Canada

Remerciement

Après avoir mené à bien ce travail de recherche, je suis convaincu que la thèse de doctorat n'est pas un travail solitaire. En effet, cette réalisation n'aurait pas été possible sans le soutien d'un grand nombre de personnes durant cette phase délicate de "l'apprenti chercheur".

Cette thèse a été réalisée dans le cadre d'un projet de recherche partenarial entre Ader Pelzer et le laboratoire Modélisation et Simulation Multi Echelle (MSME UMR 8208 CNRS) de l'Université Gustave Eiffel en France avec la collaboration du Centre de Recherche en Acoustique-Signal-Humain de l'Université de Sherbrooke (CRASH-UdeS) au Québec, Canada depuis octobre 2020, sous convention CIFRE No. 2020/0122. A ce titre, je tiens tout d'abord à remercier l'ANRT et Adler Pelzer qui ont permis, grâce à leurs financements, la mise en place de ce travail de recherches. Mes remerciements vont également à tous membres du laboratoire MSME ainsi que les personnes au CRASH-UdeS pour y avoir fait régner une ambiance amicale au travail.

Je remercie particulièrement mes directeurs, le Professeur **Camille Perrot** et le Professeur **Raymond Panneton**, pour leure grande contribution à ce travail, pour leur soutien, leurs conseils et leur culture scientifique à travers de ces trois années de thèse. Avec eux nous avons formé une belle équipe de travail.

J'exprime toute ma reconnaissance aux membres du jury : **Noureddine ATALLA**, **Sophie DARTOIS**, **Nicolas DAUCHEZ**, **Bertrand DUBUS**, **Marie-Annick GALLAND**, **Valérie MARCEL**, **Vincent MONCHIET** pour le temps qu'ils ont passé à évaluer mon travail. Leurs remarques constructives, leurs questions intéressantes ont suscité une réflexion ouvrant d'autres perspectives à mon travail.

Un grand merci à Messieurs **Minh Tan HOANG**, **Ludovic DEJAEGER**, **Mathieu JOUVE** (Acoustic TechCenter, Adler Perzer Group) avec qui j'ai eu de nombreuses discussions autour du travail de thèse et pour leurs expertises et conseils, en particulier sur les aspects applicatifs du projet, ainsi que pour leur accueil lors des caractérisations à Mouzon.

Je tiens également à exprimer ma gratitude envers à Monsieur **Rémy PIRES BRAZUNA** (ICMPE) en France, et Monsieur **Charles Bertrand** (PRAM), Faculté de génie, Université de Sherbrooke au Canada pour leur aide précieuse en imagerie MEB.

Je tiens à exprimer ma gratitude envers tous mes amis qui ont contribué de près ou de loin à la réussite de mon travail et avec qui j'ai partagé de bons moments.

Enfin, du fond de mon coeur, je remercie ma famille, mon père, ma mère, mon petit frère et ma femme pour leur soutien indéfectible, leur patience et leur encouragement au cours de l'élaboration de cette thèse. Il est difficile de lister les noms de toutes les personnes auxquelles j'aimerais exprimer ma reconnaissance. Merci à toutes les personnes côtoyées que je n'ai, hélas, pas pu les mentionner.

Résumé

Cette thèse explore les relations complexes entre microstructures, propriétés acoustiques et processus de fabrication des matériaux fibreux non tissés. Elle étudie deux familles de milieux fibreux composites, issues de fibres textiles recyclées (coton, PET), offrant une diversité de polydispersité. Grâce à la caractérisation microstructurale et à l'homogénéisation numérique, ces travaux ont permis d'identifier les paramètres clés associés aux propriétés de transport et d'absorption sonore. Les diamètres moyens pondérés en volume D_v et en volume inverse D_{iv} se sont révélés être des descripteurs géométriques essentiels. Ils expliquent les comportements acoustiques à différentes fréquences, révélant que les échanges visqueux et thermiques se produisent à travers les canaux les plus larges de la microstructure à basse fréquence, tandis qu'à haute fréquence, la signature acoustique est influencée par l'ensemble de la microstructure, y compris les étranglements les plus petits. Les contributions originales de cette recherche comprennent (1) le développement des Volumes Élémentaires Représentatifs (VERs) pour les milieux fibreux polydisperses ; (2) la résolution d'un problème d'optimisation basé sur le degré de polydispersité ; (3) et la proposition d'une technique expérimentale pour estimer les propriétés de transport à hautes fréquences de milieux fibreux résistifs. En somme, cette thèse offre des perspectives prometteuses pour la compréhension et l'optimisation des propriétés acoustiques des milieux fibreux polydisperses, tout en identifiant les descripteurs microstructuraux cruciaux pour ces matériaux complexes.

Mots-clés : Modèle multi-échelle, milieu fibreux, volume élémentaire représentatif, propriétés de transport, coefficient d'absorption, effet de compression.

Abstract

This thesis explores the complex relationship between the structures, acoustic properties, and manufacturing processes of non-woven materials. Two families of composite fibrous media, derived from recycled textile fibers and recycled PET fibers, were studied, offering a diversity of polydispersity. Through microstructural characterization and numerical homogenization, this research identified key parameters associated with transport and sound absorption properties. The volume-weighted mean diameter D_v and inverse volume weighted mean diameter D_{iv} were found to be essential geometric descriptors. They explain acoustic behaviors at different frequencies, revealing that viscous and thermal exchanges occur through the widest channels of the microstructure at low frequencies ; while at high frequencies, the acoustic signature is influenced by the entire microstructure, including the smallest constrictions. The original contributions of this research include (1) the development of Representative Elementary Volumes (REVs) for polydisperse fibrous media ; (2) solving an optimization problem based on the degree of polydispersity ; (3) and proposing an experimental technique to estimate transport properties at high frequencies. In summary, this thesis offers promising perspectives for understanding and optimizing the acoustic properties of polydisperse fibrous media while identifying crucial microstructural descriptors for these complex materials.

Keywords : Multiscale model, fibrous media, representative elementary volume, transport properties, sound absorption, compression effect.

Table des matières

Table des figures

Liste des tableaux

Liste des Symboles

Symbole	Définition
α_∞	Tortuosité
η	Viscosité dynamique de l'air
∇	Opérateur de gradient
Δ	Opérateur de Laplace
f	Fréquence
γ	Rapport de chaleur spécifiques
k_0	Perméabilité visqueuse statique
k'_0	Perméabilité thermique statique
κ	Paramètre de forme de distribution gamma
Λ	Longueur caractéristique visqueuse
Λ'	Longueur caractéristique thermique
ω	Fréquence angulaire
Ω	Espace occupé par un VER
$\partial\Omega$	Interface solide-fluide
Pr	Nombre de Prandtl
ϕ	Porosité ouverte
$\tilde{q}_{eq}$	Nombre d'onde acoustique
ρ_0	Masse volumique de l'air
$\tilde{\rho}_{eq}$	Equivalent dynamic mass density
$\tilde{K}_{eq}$	Equivalent dynamic bulk modulus
$\langle\cdot\rangle$	Moyenne spatiale
σ	Résistivité statique au passage de l'air
$\mathbf{E}$	Champ électrique
$\mathbf{K}$	Perméabilité globale
i	Unité imaginaire ($\sqrt{-1}$)
θ	Angle zénithal ou vertical
φ	Angle azimutal ou horizontal
$[\mathbf{\Omega}]$	Tenseur d'orientation angulaire
β	Paramètre d'anisotropie
Z_c	Impédance caractéristique du fluide
Z_s	Impédance acoustique de surface
Z_0	Impédance caractéristique de l'air
β	Paramètre d'anisotropie

Liste des acronymes

Acronyme	**Définition**
3D-RF	Three-dimensional random fibrous
CV	Coefficient of variation
D_f	Fiber diameter
D_m	Mean fiber diameter
D_v	Volume-weighted mean diameter
D_{iv}	Inverse volume-weighted mean diameter
DF	Diffuse fields
JCAL	Johnson Champoux Allard Lafarge
L_s	Sample thickness
MEB	Microscopie Électronique à Balayage
NI	Normal incidence
PET	Polyethylene terephthalate
REV	Representative elementary volumes
SAC	Sound absorption coefficient
SAA	Sound absoprtion average
SEM	Scanning Electron Microscope
VER	Volumes élémentaires représentatifs

Chapitre I

Introduction générale

Contenu

I.1 Mise en contexte et problematique

La crise environnementale et énergétique impose aux acteurs industriels en général et à ceux du transport en particulier une réduction de la masse des véhicules et l'usage de matériaux recyclés et recyclables en cohérence avec une stratégie de décarbonation de l'économie (éco-design, iso-performance en réduisant l'usage de matière). Cependant, cette tendance à l'allègement et à l'usage de matériaux recyclés et recyclables s'oppose à priori au contrôle des nuisances sonores. L'allègement suppose en effet une réduction de masse (surfacique, volumique) des matériaux poreux habituellement utilisés pour contrôler le champ réverbéré ou transmis des ondes acoustiques (sous contraintes de place accrue dans les véhicules). Or, l'usage de matériaux recyclés et recyclables introduit une plus grande variabilité dans les matières, ce qui a pour effet d'accroitre le caractère inhomogène et anisotrope des matériaux manufacturés. On parle notamment de polydispersité lorsque la distribution de la taille caractéristique du motif structurant (grain, pore, fibre), résultant du process de fabrication industriel à l'œuvre, est large et se traduit par un coefficient de variation élevé (typiquement plusieurs dizaines de pourcents à cent pour cent ou plus). Pour pallier cette double contrainte d'allègement et d'hétérogénéité locale, le développement d'une compréhension fine des mécanismes gouvernant les propriétés physiques d'intérêt est particulièrement nécessaire (propriétés acoustiques). Parmi les matériaux poreux d'usage, on note que les procédés et structures fibreuses occupent une place privilégiée dans la stratégie d'avenir de décarbonation (fibres plus facilement recyclées et recyclables que leurs homologues cellulaires type polyuréthane).

I.2 Question de recherche

Pour répondre à la problématique scientifique, technique et industrielle, soulevée par le contexte de la décarbonation de l'industrie du transport, on cherchera à identifier les principales caractéristiques microstructurales gouvernant les phénomènes physiques d'intérêt à l'échelle supérieure (acoustique). La question de départ peut alors être formulée de la manière suivante : Quels sont les volumes élémentaires représentatifs (VERs) associés aux propriétés physiques d'intérêt pour un milieu fibreux polydispersé, localement hétérogène et anisotrope ?

I.3 Objectifs du projet de recherche

I.3.1 Hypothèse

L'hypothèse formulée dans ce projet de recherche est qu'il soit possible (1) d'identifier les longueurs caractéristiques locales et mécanismes prépondérants gouvernant les propriétés des ondes acoustiques par un dialogue continu entre simulations multi-échelles, expérimentations fines, processus de fabrication ; (2) pour mieux les contrôler (optimisation) ; (3) et in fine fabriquer les prototypes de non-tissés les plus prometteurs sous contraintes manufacturières (savoir-faire et mutations de l'industrie du textile et des polymères). La réponse méthodologique anticipée s'appuie sur une analyse asymptotique à

échelles multiples, dont les solides résultats de la littérature pavent la démarche. Sous réserve de séparation d'échelle entre tailles caractéristiques du chargement et de la microstructure, la méthode de l'homogénéisation des structures périodiques permet d'établir au premier ordre, les problèmes de cellule gouvernant l'essentiel de la physique d'intérêt. Dès lors, il s'agit de résoudre un nombre limité de problèmes aux limites gouvernant les principaux mécanismes physiques pour un ensemble de microstructures modèles (stochastiques) induites par l'observation (imagerie) et l'expérimentation fine (mesures dédiées) [dialogue et rétroactions] ; dont on rappelle qu'elles doivent être représentatives de microstructures fabricables à échelle industrielle de milieux fibreux polydisperses, localement hétérogènes et anisotropes. La réponse microstructurale anticipée est que les fibres de diamètre élevé gouvernent le comportement asymptotique basses fréquences (fluide visqueux) tandis les plus fines pilotent le comportement asymptotique hautes fréquences (fluide inertiel).

I.3.2 Objectif

L'objectif principal de la recherche est donc (1) d'identifier les volumes élémentaires représentatifs des propriétés acoustiques (hypothèses des petites perturbations) de milieux fibreux (polydisperses, localement hétérogènes, anisotropes) ; (2) d'optimiser les microstructures associées à ces volumes élémentaires représentatifs (optimisation fonctionnelle, sous contraintes, liée aux leviers de fabrication disponibles ou envisageables via une évolution des process) ; (3) de fabriquer les microstructures polydisperses qui apparaissent les plus prometteuses (validation de l'ensemble de la chaîne de modélisation, proposition de stratégies compatibles avec les process existants ou d'évolution des process) ; (4) de valoriser les résultats obtenus (dissémination dans des revues à fort impact et conférences internationales).

I.4 Contributions originales

Les contributions scientifiques originales de ces travaux de recherche sont essentiellement triples :

1. Une identification des volumes élémentaires représentatifs (VERs) de milieux fibreux polydisperses gouvernant les phénomènes de transport en comportements asymptotiques basses et hautes fréquences ; en utilisant uniquement leurs caractéristiques géométriques comme paramètres d'entrées (porosité, distributions de diamètres de fibres et de leurs orientations angulaire).
2. Une mise en évidence sur la base d'un travail exploratoire, exploitant le modèle précédemment développé, que le degré de polydispersité peut être utilisé une fois contrôlé comme nouveau levier d'optimisation des performances acoustiques d'un milieu fibreux.
3. Le développement d'une méthode d'estimation expérimentale des propriétés de transport hautes fréquences d'un milieu fibreux résistif ; c'est-à-dire lorsque les fréquences de transitions visco-inerties et thermique sont relativement élevées (et que la signature acoustique en tube d'impédance comporte essentiellement le comportement basses fréquences du milieu poreux).

I.5 Plan du document

La suite de cette thèse est organisée tel que suit. Au Chapitre II, on introduit brièvement les principaux éléments de l'état de l'art. Au Chapitre III, le modèle polydisperse est formulé pour un milieu fibreux aléatoire tridimensionnel. Au Chapitre IV, le potentiel du modèle polydisperse est étudié sous la forme d'un problème d'optimisation. La méthode de caractérisation acoustique ayant permis de rassembler des données expérimentales sur les échantillons de milieux fibreux étudiés est en partie détaillée au Chapitre III et le Chapitre V contient la conclusion générale.

Chapitre II

Etat de l'art

La détermination des propriétés moyennes ou macroscopiques de matériaux poreux est un problème ancien d'un grand intérêt, par exemple en géophysique en particulier (Adler et Thovert, 1998 [1]), ou en sciences de l'ingénieur en général (Auriault et al.,2010 [2]). Plusieurs méthodes ont été proposées pour le résoudre par une approche rigoureuse.

Le premier problème consiste à idéaliser à l'échelle locale le milieu réel. Le milieu poreux peut être idéalisé par un réseau régulier de formes simplifiées, telles que la sphère ou l'ellipsoïde pour un milieu granulaire, le polyèdre pour une mousse ou un matériau cellulaire, un réseau de cylindres pour un milieu fibreux. Une présentation des formes possibles variées est donnée par Gibson et Ashby (1988) [3] et Adler (1992) [4]. Une distinction relative aux milieux fibreux, plus spécifiquement étudiés dans ce travail, concerne le fait qu'ils soient cohésifs ou non-cohésifs ; il existe des liaisons mécaniques entre les fibres qui confèrent une certaine tenue mécanique au milieu lorsqu'il est cohésif, comme pour une laine minérale ; dans les milieux fibreux non cohésifs, les fibres de petites dimensions sont dispersées dans la phase fluide et ont plutôt pour vocation de modifier ses propriétés rhéologiques. Cette distinction introduit des différences de comportement rhéologique importantes, mais certains outils mathématiques ayant été introduits pour étudier statistiquement les caractéristiques géométriques des milieux non cohésifs s'avèrent utiles pour analyser celles des milieux cohésifs (Avani et Tucker, 1987 [5]).

Le deuxième problème consiste à déterminer les propriétés de transport macroscopiques, telles que la perméabilité. Le nombre de milieux pouvant être traités de manière analytique est très limité, et de nombreuses techniques ont été développées dans la littérature, telles que les modèles auto-cohérents (voir par exemple Berdichevsky et Cai, 1993 [6] ; Boutin et Geindreau, 2010 [7] ; Piegay et al., 2020 [8]). Un autre chemin fructueux a été la détermination de bornes basées sur l'utilisation de moments de la distribution de l'espace poreux (Miller, 1969 [9] ; Milton, 1982 [10] ; Torquato, 1987 [11]). Une méthodologie plus générale, qui sera adaptée dans le cadre de cette thèse, consiste à résoudre les équations aux dérivées partielles qui gouvernent la propriété macroscopique d'intérêt au moyen d'une méthode numérique appropriée (différences finies [12, 13], éléments finis [14], volumes finis [15]), FFT [16], lattice Boltzmann [17]...). Toutes ont leurs avantages et limitations. Les trois problèmes de transport les plus classiques pour l'analyse des propriétés acoustiques des milieux poreux concernent les propriétés de perméabilité visqueuse, de diffusion de la chaleur (perméabilité thermique), d'inertie d'un fluide non visqueux (tortuosité et longueur visqueuse) [18]. Ces problèmes pourront être résolus par des techniques standard telles que la méthode des éléments finis.

Le propos principal de cette thèse consiste à présenter, sous la forme d'un cadre unifié, les techniques pouvant être utilisées pour modéliser les propriétés acoustiques de milieux fibreux réels, en s'inspirant autant que possible des avancées récentes dans ce champ de recherches. Cet état de l'art est en quelque sorte restreint de manière arbitraire aux sujets spécifiques auxquels l'auteur a contribué d'une manière ou d'une autre ; les choix opérés ici permettent de présenter l'état de l'art de manière concise en évitant les répétitions autant que possible avec les revues de la littérature présentées dans les articles 1 (Chapitre III), 2 (Chapitre IV). Bien sûr, les contributions des autres auteurs à ce sujet spécifique sont ici introduites. À ce point, il semble utile d'introduire les principales thèses récentes qui ont été publiées (Talbot, 1993 [19] ; Bergonnier, 2005 [20] ; Peyrega, 2010 [21]) ; Altendorf, 2011 [22] ; Manning, 2012 [23] ; Chapelle, 2016 [24] ; Luu, 2016 [25] ; He, 2018 [26] ; Lei,

2018 [27] ; Piégay, 2019 [28] ; Xue, 2019 [29] ; Hurrell, 2020 [30]).

Ce champ de recherche peut donc être considéré comme étant très actif, d'autant que la liste proposée n'est probablement pas exhaustive. Ces références sont utilisées pour trouver les principaux points de vue et développements qui existent dans le domaine. Parmi ces travaux, on peut distinguer trois catégories générales pour l'étude des propriétés acoustiques de milieux fibreux : (1) par imitation de structure (Talbot, 1993 [19] ; Bergonnier, 2005 [20] ; Peyrega, 2010 [21]) ; Altendorf, 2011 [22] ; Chapelle, 2016 [24] ; (2) par identification de motif structurant (Luu, 2016 [25] ; He, 2018 [26] et Piégay, 2019 [28]) ; (3) descriptive (Manning, 2012 [23], Lei, 2018 [27]), Xue, 2019 [29], Hurrell, 2020 [30]).

(1) Dans la première approche, la morphologie mathématique [31] joue un grand rôle dans l'étude des caractéristiques géométriques du milieu fibreux, les images étant généralement obtenues par tomographie. Néanmoins, la reconstruction du milieu idéalisé est parfois si fine qu'il devient difficile d'identifier quelles sont les caractéristiques géométriques principalement responsables des propriétés de transport. (3) À l'opposé, le point de vue descriptif met l'accent sur la mesure des propriétés géométriques et physiques aux échelles micro et macro, le lien étant généralement assuré par un modèle semi-empirique obtenu par un ajustement sur les données expérimentales collectées. (2) Entre les deux, on recherche un compromis entre l'imitation de la structure et la description des propriétés, où l'on souhaite générer un milieu aléatoire reproduisant statistiquement les principales caractéristiques géométriques saillantes et étudier leurs effets à l'échelle supérieure, sans avoir recours à des paramètres d'ajustement. Cette catégorisation proposée est discutable car les frontières ne sont jamais nettes. Ce travail s'inscrit dans le prolongement des thèses de Luu [25] et He [32] qui ont proposé les étapes principales d'une méthode de reconstruction pour des milieux fibreux aléatoires mono- et polydisperses, respectivement.

Finalement, d'importants travaux ont été menés au cours des deux dernières décennies sur la détermination des propriétés effectives de milieux fibreux aléatoires, en utilisant des techniques d'homogénéisation, mais ils sont généralement restreints à l'examen des propriétés élastiques et thermiques (transferts par conduction) (Vassal et al. [33], Dirrenberger et al. [34], Altendorf et al. [35], Gazzo et al. [36]), voire à des propriétés hydro-thermo-mécaniques (modèle bidimensionnel) gouvernées par la phase solide (Bosco et al. [37]), ou à l'étude de la perméabilité de milieux fibreux (Boutin [38], Thiery and Boutin [39], Ghafour et al. [40]). Néanmoins, à notre connaissance, les effets liés à la polydispersité du milieu fibreux n'ont pas ou peu été étudiés, ou seulement très récemment et restreints à une seule propriété (Tucny et al. [41]). Nous pensons, au contraire, que ces effets doivent être pris en compte et qu'ils pourraient même être utilisés comme un nouveau levier d'optimisation.

Chapitre III

Effect of polydispersity on the transport and sound absorbing properties of three-dimensional random fibrous structures

Contenu

III.1 Avant-propos

Auteurs et affiliations :

— Quang Vu Tran, étudiant doctorant, Université Gustave Eiffel, Univ Paris Est Creteil, CNRS, UMR 8208, MSME, F-77454, Marne-la-Vallée, France. Département de Génie Mécanique, Université de Sherbrooke, J1K 2R1, Québec, Canada. Adler Pelzer Group, Acoustic TechCenter R&D, France

— Camille Perrot, Professeur, Université Gustave Eiffel, Univ Paris Est Creteil, CNRS, UMR 8208, MSME, F-77454, Marne-la-Vallée, France

— Raymond Panneton, Professeur, Département de Génie Mécanique, Université de Sherbrooke, J1K 2R1, Québec, Canada

— Minh Tan Hoang, Ingénieur (Expert Méthodologies et Simulations), Adler Pelzer Group, Acoustic TechCenter R&D, France

— Ludovic Dejaeger, Ingénieur (Leader Acoustique Mouzon), Adler Pelzer Group, Acoustic TechCenter R&D, France

— Valérie Marcel, Ingénieure Matières (Responsable Innovation), Adler Pelzer Group, Acoustic TechCenter R&D, France

— Mathieu Jouve, Ingénieur Matières (Reponsable dév. matières), Adler Pelzer Group, Acoustic TechCenter R&D, France

Date de soumission : 25 Octobre 2023

État de l'acceptation : En révision

Revue : International Journal of Solids and Structures

Référence : [IJSS-D-23-01093]

Titre français : Effet de la polydispersité sur les propriétés de transport et d'absorption acoustique de structures fibreuses aléatoires tridimensionnelles

Contribution au document :

Cet article contribue à la thèse en présentant la méthodologie de modèle de simulation et modélisation numérique, le modèle d'identification des volumes élémentaires représentatifs (VERs) de milieux fibreux polydisperses gouvernant les phénomènes de transport en comportements asymptotiques basses et hautes fréquences ; en utilisant uniquement leurs caractéristiques géométriques comme paramètres d'entrées (porosité, distributions de diamètres de fibres et de leurs orientations angulaire).

Résumé française :

Une technique est proposée, qui utilise une approche multi-échelle pour calculer les propriétés de transport des feutres compressés en utilisant uniquement l'analyse d'images et des calculs numériques. À partir de l'analyse d'images, la distribution du diamètre des fibres et l'orientation des fibres sont déterminées. À partir d'une porosité connue et des deux caractéristiques précédentes, deux volumes élémentaires représentatifs (VER) sont construits : l'un basé sur le diamètre moyen pondéré par le volume et l'autre sur un diamètre moyen pondéré par le volume inverse. Les calculs numériques sur le premier ont montré qu'il estime correctement les perméabilités visqueuses et thermiques, tandis que le second estime correctement la tortuosité et les longueurs caractéristiques visqueuses et thermiques. À partir de ces calculs, des expressions analytiques micro-macro sont développées pour estimer les propriétés de transport des feutres composites polydisperses uniquement en fonction de la porosité ouverte, de la polydiversité des diamètres des

fibres et de l'orientation des fibres. De bons accords sont obtenus entre les prédictions analytiques et les mesures des propriétés de transport. Les propriétés de transport prédites sont également utilisées dans le modèle de fluide équivalent Johnson-Champoux-Allard-Lafarge (JCAL) pour prédire le coefficient d'absorption acoustique des feutres. D'excellents accords sont obtenus avec les mesures en tube d'impédance.

Effect of polydispersity on the transport and sound absorbing properties of three-dimensional random fibrous structures

Q. V. Tran,[1,2,3] C. Perrot,[1] R. Panneton,[2] M. T Hoang,[3] L. Dejaeger,[3] V. Marcel,[3] M. Jouve,[3]

[1] Université Gustave Eiffel, Univ Paris Est Creteil, CNRS, UMR 8208, MSME, F-77454, Marne-la-Vallée, France

[2] Département de Génie Mécanique, Université de Sherbrooke, J1K 2R1, Québec, Canada

[3] Adler Pelzer Group, Acoustic TechCenter R&D, Z.I. François Sommer – BP13, 08210, Mouzon, France

III.2 abstract

A technique is proposed that uses a multi-scale approach to calculate transport properties of compressed felts using only image analysis and numerical calculations. From the image analysis fiber diameter distribution and fiber orientation are determined. From a known porosity and the latter two characteristics, two representative elementary volumes (REV) are constructed : one based on the volume-weighted average diameter and one on an inverse volume-weighted average diameter. Numerical calculations on the former showed that it correctly estimates viscous and thermal permeabilities, while the latter correctly estimates tortuosity and viscous and thermal characteristic lengths. From these calculations, micro-macro analytical expressions are developed to estimate the transport properties of polydisperse composite felts based solely on open porosity, fiber diameter polydiversity, and fiber orientation. Good agreements are obtained between analytical predictions and measurements of transport properties. The predicted transport properties are also used in the Johnson-Champoux-Allard-Lafarge (JCAL) equivalent fluid model to predict the sound absorption coefficient of the felts. Excellent agreements are obtained with impedance tube measurements.

III.3 Introduction

Nonwoven fabrics are some of the most widespread man-made porous materials that are used in many engineering fields including health and medical care, energy or sound proofing applications. The main constituents of nonwoven are fibers that are linked together by cohesive bounds induced by the manufacturing process in the form of fibrous networks with transverse isotropy. Nonwoven fibrous media with a wide diversity of physical and mechanical properties (Dirrenberger et al. [34], Altendorf et al. [42], Bosco et al. [43]) can be manufactured by tailoring the nature of the raw materials and the manufacturing process conditions (e.g., type of geometry, bale opening and weighting of the fibers, fibers web creation, thermal bounding thickness adjustment and cutting). However,

the links between composite nonwoven manufacturing parameters, the resulting fibrous microstructures, and the product performance are still not fully evidenced. For example, the permeability k_0 (Darcy [44]) and the viscous characteristic length Λ (Johnson et al. [45]) of felts often follow a nonlinear evolution with their porosity, the microstructural origins of which are still questioning. Thus, the construction of the aforementioned links constitutes a subject of intense research. In particular, there is still a need for relevant multiscale and multiphysics models that could (1) account for the complexity of composite felt microstructures and related transport and sound absorbing properties and (2) be implemented in numerical simulation tools for computer-aided design of composite felts applications or for monitoring of the composite felts manufacturing process itself.

For that purpose, numerous theoretical studies have been conducted in the last decades. In most cases, composite felts are modeled as aligned fiber bundles (Berdichevsky and Cai [6], Boutin [38], Thiery and Boutin [39], Piegay et al. [8], Tarnow [46, 47, 48], Umnova et al. [49], Semeniuk and Goransson [50], Semeniuk et al. [51]). These approaches often assume that the representative elementary volume of a composite felt can be reduced to the most basic geometric information, that is, porosity ϕ and fiber size, so that it is based on a bicomposite cylindrical pattern made of an internal cylindrical fiber and an external fluid shell that ensures fluid connectivity. The proposed analytical models are interesting because they encapsulate the essential parts of the physics and are easily configurable. However, they do not account for the complexity of the geometry and the combined effect that spatial randomness in the pore space has on flow problems.

To better understand the effects of visco-thermal micro-mechanisms on the values of transport coefficients of composite felts, many fiber scale numerical studies were conducted (Koponen et al. [52], Martys and Garboczi [53], Tomadakis and Robertson [54, 55], Schladitz et al. [56], Umnova et al. [49], Altendorf and Jeulin [57], Peyrega et al. [58], Luu et al. [59, 60], He et al. [32], Soltani et al. [61], Tucny et al. [41]). For example, Luu et al. [59, 60] performed numerical simulations using networks of straight cylindrical fibers to investigate the effect of porosity, fiber radius, and fiber orientation on the in-plane and through-plane transport properties of fibrous media. Using random porous media from two-dimensional models, Martys and Garboczi [53] demonstrated the important effect that spatial randomness in the pore space has on flow problems. This analysis showed that, in a random pore structure with a distribution of pore sizes, the viscous fluid flow will tend to go through the largest pore necks, decreasing the importance of the narrowest necks. They also highlighted that the sizes of the dynamically connected pore regions were not exactly the same for the electric and fluid flow cases (Martys and Garboczi [53]). In particular, for a fibrous material made of wood fibers with an open porosity $\phi = 0.64$, Peyrega and Jeulin [62] and Peyrega et al. [58] showed that the volume-weighted average radius r_v was an appropriate size of the fiber radii to quantitatively predict its sound absorbing properties at normal incidence. This approach assumed a two-dimensional Boolean model of random cylinders composed of overlapping fibers, where the locations of the centers of the discs were determined according to a random Poisson point process. This analysis was extended to three-dimensional models for glass wool samples obtained with various processing parameters by He et al. [32].

Keeping in mind that at fixed porosity, fewer fibers are introduced into a given volume when the fiber radius is volume-weighted, these results highlight that the r_v length scale

provides an effective way to reconstruct pore space. This space encompasses the largest pores, forming a continuous path for the flow of viscous fluids in actual fibrous media. These numerical results confirm the trends reported in several complementary experimental and semi-empirical studies (Delany and Bazley [63], Bies and Hansen [64], Miki [65], Garai and Pompoli [66], Manning and Panneton [67], Kerdudou et al. [68], Xue et al. [69], Pelegrinis et al. [70]). Briefly, they highlight (i) the central role of fiber distributions (in size and orientation) and (ii) the need for a proper characterization of the geometry and transport processes in polydisperse fiber structures. This is particularly true for nonwovens that exhibit a wide distribution of fiber diameters and lengths [58, 32].

On the one hand, noticeable progress has been achieved in the purpose of characterizing the transport parameters of porous materials thanks to dedicated testing devices (Stinson and Daigle [71], Leclaire et al. [72], Ayrault et al. [73]). These tests are interesting but still remain difficult to carry out, as they require permeable porous media to enable the propagation of ultrasonic waves through the thickness of the material. On the other hand, significant progress has also been achieved to characterize finely the microstructures of nonwoven fibrous media with imaging techniques such as scanning electron microscope images (Luu et al. [59]) and optical granulomorphometry (He et al. [32]) or X-ray microtomography coupled with advanced image analysis procedures (Lux [74], Peyrega et al. [75], Depriester et al. [76]). For instance, He et al. investigated the effect of fiber distributions (orientation, length, diameter) on several transport parameters of low density glass wools from optical granulomorphometry (length, diameter) and scanning electron microscope images (orientation) for ten products provided with two different classes of surface densities. Angular orientation and volume averaging of fiber diameters were used to reconstruct virtual geometries and quantitatively predict the viscous permeabilities k_0 of the corresponding samples. However, they did not fully capture the overall transport properties, in particular with respect to the high frequency parameters (viscous Λ and thermal Λ' characteristic lengths).

In light of the above, the objective of this study is to propose a multiscale model for the overall transport and long-wavelength sound-absorbing properties of composite felts, taking into account the appropriate descriptors of the polydisperse microstructure that can be obtained using images. For this purpose, two types of composite nonwovens with several compression ratios were manufactured and thermobonded. Their microstructures were characterized using scanning electron microscope images. We also characterized their transport and sound-absorbing properties. The combination of these data makes it possible to formulate relevant hypotheses for the architecture of fiber networks and their transport processes on the fiber scale. These features were then upscaled using homogenization with multiple scale asymptotic expansions for periodic structures (Sanchez-Palencia [77], Bensoussan et al. [78], Auriault et al. [79]). This method proposes a rigorous framework to deduce the effective coefficients of importance and the effective equations that govern the macro-fields of the equivalent continuum media of composite felts. It also provides well-posed boundary value problems to be solved on representative elementary volumes (REVs) to estimate their macroscale properties. These problems are first solved numerically using the finite element method. Then, a second semi-analytical multiscale model is proposed, approximating the numerical results obtained by curve fitting and yielding unified models which assume the effective coefficients of importance as a function of porosity, fiber orien-

tations, and effective fiber radii. Predictions of the numerical and semi-analytical models are compared with experimental data and discussed.

III.4 Materials and experimental methods

III.4.1 Felts

Two nonwoven materials are investigated (Fig. III.1) : namely “cotton felt" and “PET felt". Raw materials entering into the initial composition (Tab. III.1) together with the corresponding manufacturing process are discussed in the following. Note that in the textile industry, the fineness (t) of the fibers is specified by dtex, which enables a linear density estimate of the fiber size. To calculate the diameter of the fiber from the fineness t (dtex) and the mass given by unit volume of the fiber material ρ_f, the following formula is used : $D_f = \sqrt{4t/\pi\rho_f}$.

III.4.1.1 Cotton felt

The fabrication of the cotton felt uses an airlay process, where the aerodynamic web forming is a dry procedure to form a web out of a wide variety of staple fibers. The fibers leave from a rotating drum into a turbulent air flow. Suctioning into a perforated moving conveyor belt or a perforated drum leads to the formation of a random three-dimensional web structure (Handbook of nonwovens, Chap. 4 [80] ; Gramsch et al. [81]).
The input fiber material is a mixture of 75% shoddy fibers and 25% bicomponent fibers in mass. The core of the bicomponent is made of PET, and its surface is made of coPET in a 1 :1 ratio. The bicomponent fibers are homogeneous with circular cross sections, whereas the shoddy fibers obtained after tearing of textile waste are not homogeneous. This shoddy is made from a mixture of 55% cotton and 45% PET. In post-processing, the nonwoven material called felt is reinforced by thermobonding with a chosen compression ratio. Here, the bicomponent fibers have an adhesive effect.

III.4.1.2 PET felt

The input fiber material is a mixture of 60% PET fibers and 40% bicomponent fibers in mass. The same bicomponent fibers are used as for cotton felts. The fibers are homogeneous with circular cross sections and regular lengths. In web forming, the web is formed by a roller card. Fiber tufts and bundles are disentangled to form a parallel layer of fibers. The fibers in the card web have a lengthwise orientation. Then, this card web is laid in several layers on a take-off belt via a conveyor belt system with an oscillating carriage movement. This take-off belt moves 90 degrees to the cross-lapper. The fiber web is mechanically bonded by needling through the use of barbed needles. A portion of horizontal fibers are reoriented into the vertical plane in the form of fiber tufts. This nonwoven material is called needlefelt (Handbook of nonwovens, Chap. 8 [82] ; Nonwoven Fabric, Chap. 6 [83]). Finally, thermobonding reinforcement is also applied along with the chosen compression ratio.

FIGURE III.1 – Felt samples thermobonded at different thicknesses (sample diameter, $45mm$).

Cotton felt	Thickness (mm)	Compression ratio	Density (kg/m^3)	Mass composition	
				Bicomponent	Shoddy
F1	20.3 ± 0.3	1.0 ± 0.00	56.9 ± 5.5	25%	75%
F2	16.1 ± 0.6	1.3 ± 0.05	72.4 ± 10.6	25%	75%
F3	11.2 ± 0.2	1.8 ± 0.04	103.5 ± 10.8	25%	75%
F4	5.9 ± 0.2	3.4 ± 0.10	184.8 ± 27.9	25%	75%
PET felt	Thickness (mm)	Compression ratio	Density (kg/m^3)	Mass composition		
				Bicomponent $4.4dtex$	PET $6.7dtex$	PET $17dtex$
B1	10.3 ± 0.5	1.0 ± 0.00	141.0 ± 8.4	40%	30%	30%
B2	4.3 ± 0.1	2.4 ± 0.17	344.9 ± 15.5	40%	30%	30%

TABLE III.1 – Information of the cotton felts and PET felts

III.4.2 Characterization of the microstructure

The microstructure of the non-woven fibrous media was first characterized using Scanning Electron Microscope (SEM) images (Fig. III.2). The reader is referred to A for a detailed description of the preparation and cutting of samples prior to acquisition of SEM images. Based on these two-dimensional images, typical fiber diameters were measured manually (Figs. III.2a). To determine the in-plane [respectively out-of-plane] orientation distributions of the fibers, we superimposed straight segments on the fibers on the surface of the fibrous materials and extracted the in-plane orientation angle φ (Fig. III.2b) [respectively out-of-plane orientation angle θ (Fig. III.2c)] for each segment of all identified fibers on orthogonal sections of the materials.

III.4.3 Characterization of transport and acoustic properties

The open porosity ϕ and true mass density ρ were determined using the pressure / mass method (Salissou and Panneton [84]). This method makes it possible to precisely determine the uncertainty in porosity depending on the volume of samples tested. This is

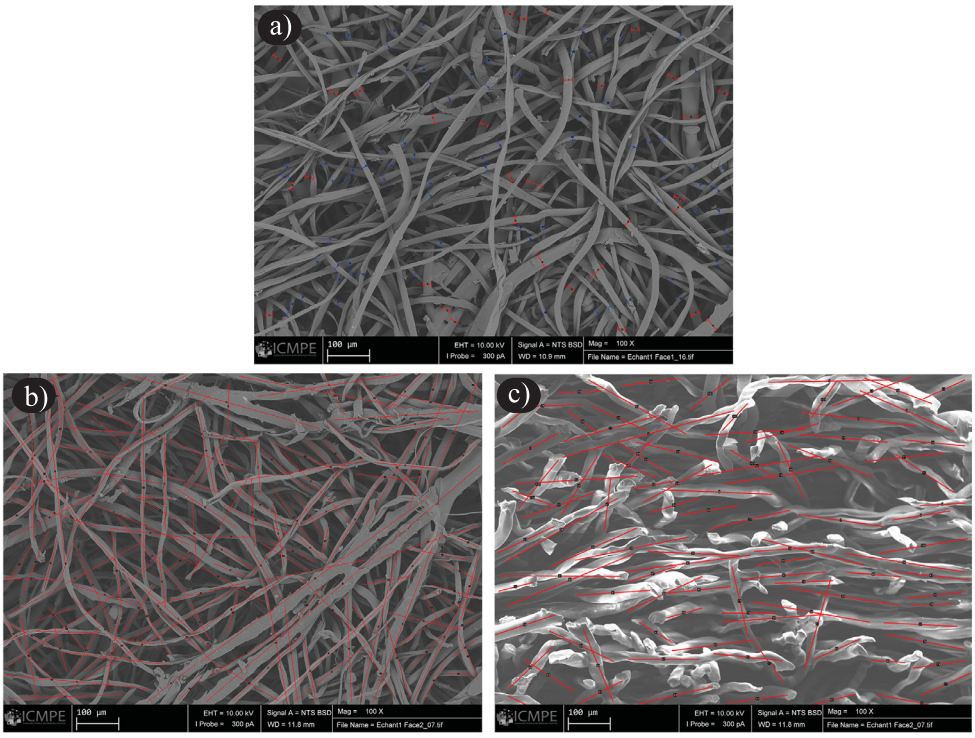

FIGURE III.2 – Example of SEM images of cotton felt F2 and dimensional measurements of fibers (Fiji software). Measurement of : (a) fiber diameters (blue is cotton fibers, red is bicomponent fiber) in the xy-plane ; (b) azimuthal or horizontal angle (φ) in the xy-plane, and (c) zenithal or vertical angle measurements (θ) in the xz-plane.

important since open porosity will be a fundamental property for the proposed multiscale model to work properly. For each felt family (cotton and PET) and each fibrous material in a family (F1, F2, F3, F4, B1, B2), the density and porosity were measured. To ensure sufficient precision of measurements, for each fibrous material within a family, measurements were performed in batches of 12 specimens of cylindrical samples with a diameter of 45 mm (repeated three times per batch).

The airflow resistivity σ was measured at a flow velocity of 0.5 mm/s following the static airflow method described in the ISO 9053-1 :2018 standard. For each fibrous material, three cylindrical samples with a diameter of 45 mm were cut and all leaks were carefully avoided by adding petroleum jelly to the circumference of the sample.

The torturosity α_∞ was measured using the high-frequency ultrasound transmission technique (Allard et al. [85]). Three samples with a diameter of 100 mm for each fibrous material were measured in air.

The viscous Λ and thermal Λ' characteristic lengths could not be validly measured with the two-gas ultrasound transmission technique (air and argon, Kino [86]). It was also impossible for us to obtain valid results with the acoustic method of Panneton and Olny ([87], [88]). Indeed, due to acoustic measurements limited to 4000 Hz and to vibration effects, the stationarity criterion of these methods was not respected over the characteristic lengths. The same was true for thermal static permeability k'_0. Consequently, the Kozeny-

Carman formula approach, as described in Henry et al. [89], was used to estimate the two characteristic lengths Λ and Λ'. This approach involves using the directly measured values for porosity ϕ, resistivity σ, and tortuosity α_∞, as detailed in D.

For the same reason, only an estimate of the static thermal permeability k_0' could be obtained. It used the following relation between Λ' and k_0' [88] :

$$k_0' = M' \frac{\phi \Lambda'^2}{8}. \tag{III.1}$$

The coefficient M' is the dimensionless thermal shape factor. It differs from unity when the shape of the porous medium does not consist of circular cylindrical pores arranged in a parallel formation. From an educated guess based on the mean value of the results found for fibers in Tab. II of [88], it was set to $M' = 2.09$. Therefore, an estimate of k_0' was obtained from this equation using the measured porosity and the estimated thermal characteristic length.

Finally, the sound absorption coefficient (hard-backed) of each felt was measured at normal incidence in an acoustic impedance tube of 44.44 mm in diameter. The incident acoustic plane wave traveled along the z-axis and excited the front (or rear) face of the felt in the xy-plane (refer to Fig. III.2). The three-microphone method described in the ISO 10534-2 :2023 standard was used. The microphone spacing and tube diameter allowed valid measurements in the frequency range 45 to 4300 Hz. Three samples per felt were measured on both faces to capture variations from one specimen to another and to verify how symmetric the felts were in thickness. The side of the specimen that is not facing the sound excitation is in contact with a hard reflective backing. To prevent air leakage between the tube wall and the specimens, a thin layer of Teflon was applied around the sample.

III.5 Experimental results and discussion

III.5.1 Characterization of the microstructure

The SEM images shown in Fig. III.2 give typical features of the studied nonwoven fibrous media, fibers and fiber connections. From these images and the corresponding measurements, several important remarks can be made.

III.5.1.1 Fiber network

Figure III.2 shows that the nonwoven fibrous medium consisted of a more or less densely connected fibrous network through the heat bonding process. It shows a generally uniform fiber orientation distribution φ in the xy-plane (Fig. III.3c). The standard deviation on the out-of-plane angle θ decreases as the compression ratio increases (Fig. III.3d, Tab. III.2). For all compression ratios (from F1 to F4 and B1 to B2), the average value of θ remains close to 90^o. These features reveal a transversely isotropic fiber orientation (see the corresponding second-order fiber orientation tensor in Advani and Tucker [5]), which could be obtained using the numerical generation process parameterized with a preferred fiber alignment along the Oz direction. Moreover, the observation regarding

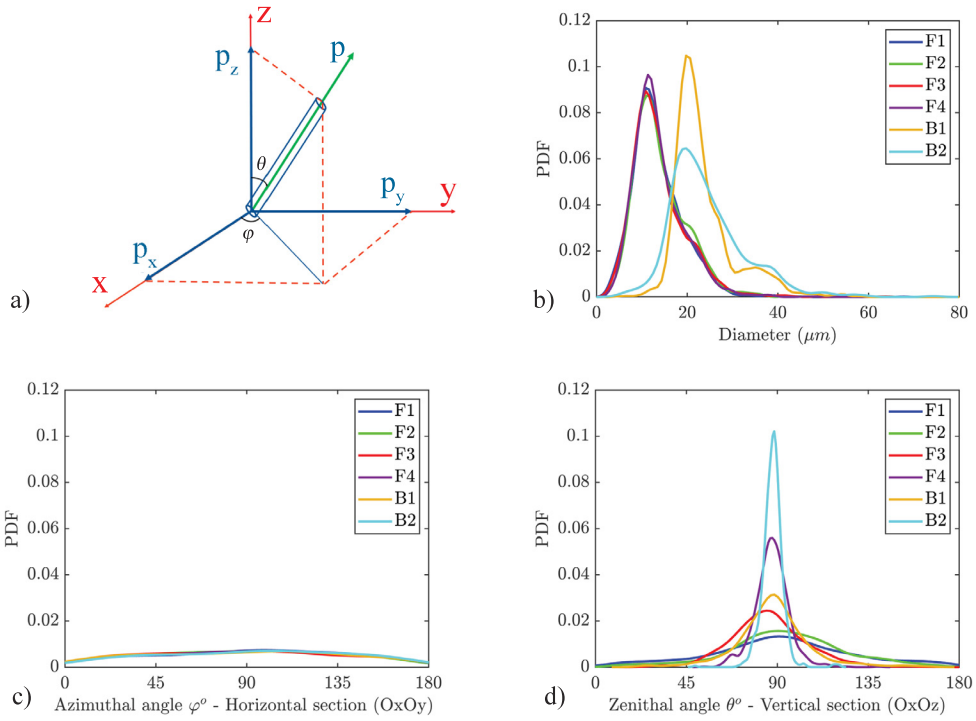

FIGURE III.3 – (a) The orientation of a fiber in three-dimensional space in spherical coordinates. The estimated probability density functions of (b) the fiber diameter; (c) the azimuthal angle φ; (d) the zenithal angle θ as plotted using a non-parametric kenel method.

fiber connections tends to show that fibers can intersect; which could be considered in further simulations.

III.5.1.2 Fibers

Figure III.2 reveals that the fibers exhibited a rather small radius of curvature at the scale of a few hundred micrometers so that each fiber i could generally be ascribed a mean tangent unit vector $\overrightarrow{p_i}$ to characterize its orientation (Fig. III.3a). Furthermore, the fibers exhibited a more or less cylindrical shape with possible intersections due to the manufacturing process (Fig. III.2c). The fibers had a mean diameter $D_m = 13.78$ μm for the cotton felts (F1-F4) and $D_m = 23.95$ μm for the PET felts (B1-B2), see Tab. III.2. For each family of felts, these parameters were practically constant regardless of the compression ratio. In addition, the fiber diameter distributions were nearly the same for the cotton felt family (F1-F4), Fig. III.3b. Finally, a small peak can be distinguished at $D_m = 20.1$ μm that corresponds to the bicomponent fibers and a second peak at $D_m = 39.5$ μm that corresponds to the second population of PET fibers (17 *dtex*). The first population of PET fibers (6.7 *dtex*) does not appear clearly due to the fact that it is embedded in the central peak of PET felts.

It should be mentioned that the thermocompression process on PET fibers had the effect of spreading the distributions of fiber diameter populations (Fig. III.3b, B1, and

	Diameter		Zenith angle θ^o	
Samples	Number of measurements	$D_m(\mu m)$	Nb of measurements	θ^o
F1	2386	13.5 ± 5.6	823	91.9 ± 36.2
F2	2086	14.1 ± 5.8	850	94.1 ± 28.9
F3	2389	13.8 ± 6.2	803	85.9 ± 18.9
F4	2214	13.7 ± 5.6	864	87.3 ± 8.6
B1	2131	23.6 ± 6.9	727	87.9 ± 18.6
B2	1780	24.3 ± 8.4	644	87.7 ± 5.3

TABLE III.2 – Statistics related to fiber diameters and angular orientation of fibers as experimentally determined from SEM images

B2). This was not expected. This may be because B1 was not heat-bonded, unlike B2, and the fibers were deformed in B2 after heat-bonding. Also, additional inaccuracy can be attributed to the manual measurement procedure. However, the two fiber diameter distributions were relatively similar at the end.

III.5.2 Characterization of the transport properties

The transport properties, including the open porosity ϕ, static airflow resistivity σ (or alternatively static viscous permeability $k_0 = \eta/\sigma$, where η is the dynamic viscosity of the air), tortuosity α_∞, viscous Λ and thermal Λ' characteristic lengths, and static thermal permeability k'_0, are expected to be predicted using analytical expressions as a function of the morphological parameters. For example, Tarnow [46] proposed an equation to determine the airflow resistivity for 2D cylinders of equal radii distributed in a square or random lattice. Modifications of Tarnow's equations were suggested by Xue et al. [69] for situations in which a fibrous medium comprises more than one fiber component and when the radius of each fiber component varies within a certain range. Furthermore, Tamayol and Bahrami [90] used a scale analysis technique (or semi-empirical approach) to determine the transverse permeability of various fibrous matrices, including square, staggered and hexagonal arrangements of aligned fibers, as well as simple two-directional mats and simple cubic structures. Umnova et al. [49] proposed an analytical method to predict the tortuosity, the characteristic lengths, and the static thermal permeability of a regular array of rigid parallel cylinders parallel or perpendicular to the flow direction. Pompoli and Bonfiglio [91] provided a modification of existing formulations of transport parameters based on numerical simulations for two-dimensional random structures considering fiber diameters with symmetric and asymmetric distribution. Luu et al. [60] proposed a microstructural model for the transport parameters of three-dimensional networks of rectilinear fiber with constant diameter allowing for possible intersections. The equations were derived from rationalized numerical simulations in the form of master curves expressed as functions of porosity ϕ, mean fiber radius r_m, and Ω_{zz} an effective parameter that parameterizes the angular orientation of the fibers.

For fibrous materials manufactured by thermo-compression with different thicknesses, Lei et al. [92] assumed that the transport parameters can be separated into two groups, depending (ϕ, Λ', k'_0) or not (σ, α_∞, Λ) on the orientation of the fibers. In their approach,

porosity depends on the compression rate n according to Castagnède et al. [93] formula ; and Λ' and k_0' are determined as analytical functions of porosity ϕ (Umnova et al. [49]) as predicted by the Castagnède et al. [93] formula. Then, the model allowing prediction of σ is an extension of the Tarnow [46] model by considering averaging over an angular distribution function. The same principle is used to predict α_∞ and Λ, where this time the Umnova formula [49] is used before performing the angular averaging. We note, however, that Lei et al. [92] model requires prior knowledge of the transport properties value before compression, which supposes available initial experimental measurements.

To compare the prediction of these models with our experimental data as a function of the compression ratio for cotton felts (F1-F4), we propose a standard dimensionless representation. Here, the average fiber diameter D_m is used to make all the dimensions of the transport properties dimensionless. When fibrous materials are characterized by a wide distribution of fiber diameters (here the cotton-felt family, F1-F4), Fig. III.4 shows that the aforementioned models do not provide a relevant prediction for the transport parameters of the nonwoven fibrous materials studied. The model of Lei et al. [92] predicts the correct evolution of the transport parameters with the compression ratio when the experimental data are known at $n = 1$. Hence, Fig. III.4 suggests that the transport behavior of the considered polydisperse fibrous media is ruled by representative volume elements different from those often assumed in previous models. In particular, we formulate the hypothesis that these models do not adequately account for the contribution of the polydispersity of fiber diameters and the particular physics induced by these geometries (Fig. III.3b).

III.6 New microstructural model focusing on fiber characteristic sizes

The experimental data collected in the previous section and the comparisons with literature models showed the difficulty of classical analytical microstructural models in predicting the transport properties of nonwoven fibrous media with large fiber diameter polydiversity. Furthermore, these models do not always succeed in predicting transport properties as a function of the compression ratio. Consequently, this section presents the development of two three-dimensional (3D) microstructural models in the porosity range $0.65 \leq \phi \leq 0.99$. These models take into account, in particular, the polydispersity of the fiber diameter and the fiber angular orientation. They are built on several assumptions related both to the fibrous microstructures and to fiber-scale thermoviscous dissipation mechanisms of locally heterogeneous fibrous materials in the long-wavelength regime. The approach assumes that the local characteristic sizes governing the transport phenomena within a polydisperse random fibrous microstructure depends on the time scale range of interest. This leads to the introduction of two specific diameters into the reconstruction procedure of two idealized 3D microstructures from which an upscaling technique is applied, namely the numerical homogenization method in the low- and high- frequency asymptotic regimes. Finally, additional equations are proposed to rationalize the results into compact analytical estimates for the dimensionless transport parameters of polydisperse fibrous structures.

III.6.1 Idealized microstructures

The typical Representative Elementary Volume (REV) of the nonwoven fibrous materials studied is seen as a 3D random fibrous network with N straight cylindrical fibers. A fiber i in the REV is of diameter D_i and defined by its center location M_i and its orientation vector $\overrightarrow{p_i}$. The fibrous medium studied exhibits a structure with transverse isotropy. Compressing the medium causes anisotropy. Following Schladitz et al. [56], this anisotropy can be described by a density function of the directional distribution $p_\beta(\theta, \varphi)$ (Stoyanet al. [94]). For the materials studied, with isotropy in the xy-plane, the function is :

$$p_\beta(\theta, \varphi) = \frac{1}{4\pi} \frac{\beta sin(\theta)}{(1 + (\beta^2 - 1)cos^2\theta)^{\frac{3}{2}}}, \tag{III.2}$$

where $\beta > 0$ is the anisotropy parameter.

Furthermore, it is assumed that there is a good scale separation between the size L of the reconstructed domain (REV size) and the smallest size between the macroscopic size of the nonwoven fibrous test samples (cylindrical samples with a diameter of 45 mm) and the macroscopic size of the acoustic compression wave $\mathcal{L} = \lambda 2\pi$ (of wavelength λ). Note that the order of magnitude of size L is given by the ratio L/D_m. This magnitude is chosen so that the porosity of the REV is equal to the experimental value within 0.1% of the relative difference. In addition, for the sake of simplicity, fibers are allowed to intersect during construction of a REV, which is consistent with the bounds visible on SEM images due to the thermo-compression process.

Samples	$CV(\%)$	$D_v(\mu m)$	$D_{iv}(\mu m)$	β	Ω_{zz}
F1	40.3	19.5 ± 0.3	8.9 ± 0.4	1.4	0.22
F2	39.8	18.7 ± 0.2	9.1 ± 0.3	1.7	0.21
F3	41.9	19.1 ± 0.2	9.3 ± 0.2	3	0.12
F4	38.9	18.5 ± 0.2	9.5 ± 0.2	6.5	0.04
B1	26.6	26.7 ± 0.2	19.8 ± 0.3	3.5	0.09
B2	33.1	31.2 ± 0.2	18.6 ± 0.3	12	0.01

TABLE III.3 – Estimated microstructural descriptors of the studied materials. Ω_{zz} is the angular orientation parameter [60].

III.6.2 Idealized transport phenomena

In order to accurately upscale the transport and sound absorption phenomena of the fibrous media being studied, the diameters of the fibers are weighted according to their volume at low frequencies and inversely weighted according to their volume at high frequencies. These weighted diameters are given, respectively, by :

$$D_v = \frac{1}{\sum_{i=1}^{N_f} V_i} \sum_{i=1}^{N_f} V_i D_i, \tag{III.3}$$

and

$$D_{iv} = \frac{1}{\sum_{i=1}^{N_f} \frac{1}{V_i}} \sum_{i=1}^{N_f} \frac{1}{V_i} D_i, \tag{III.4}$$

where V_i is the volume of fiber i. For the samples studied, these diameters are given in Tab. III.3.

This apparently strong assumption is supported by the fact that the viscous boundary layer δ_v scales as $\sqrt{\eta/(\omega\rho_0)}$, in which η is the dynamic viscosity of the fluid, ρ_0 is its density at rest and ω is the angular frequency of the sound wave. Indeed, due to the large viscous boundary layer δ_v at low frequencies and the local heterogeneities in the fiber network, the flow will tend to pass more through the largest pore necks. On the other hand, at high frequencies, inertial forces associated with fluid density dominate fluid motion, increasing the importance of the narrowest necks. The reader is also referred to Martys and Garboczi [53] for a basic description of these transport phenomena supplemented by computer simulation studies. Consequently, when the considered nonwoven fibrous materials are subjected to a macroscopic long-wavelength plane compressional wave, the elementary transport parameters corresponding to the propagation of the sound wave through the materials are mostly influenced by the largest fibers at low frequencies and the smallest fibers at high frequencies. Note that more small-volume fibers can be introduced into a REV of fixed volume and porosity than large-volume fibers. Therefore, REV containing small-volume fibers will contain narrower constrictions than REV filled with large-volume fibers.

It should be noted that a volume-weighted average diameter was previously introduced by Peyrega et al. [58] and He et al. [32] to predict with success the permeability of heterogeneous fibrous materials. Here, we extend this idea to the inverse volume-weigthed average diameter. Physically, D_{iv} is thought to be the counterpart of D_v to create the pore space that contains the smallest pores that form a continuous pathway through the fibrous polydisperse material in the high-frequency regime. It is easy to see that these arguments can be generalized to thermal effects.

III.6.3 Theoretical upscaling

Under an harmonic excitation, at angular frequency ω, the local fluid velocity is governed by the linearized Navier-Stokes equations. At low frequencies, the viscous drag forces dominate, and the Navier-Stokes equations simplify to the Stokes equations where the fluid is incompressible. At high frequencies, inertial forces dominate, and there is a strong analogy between the inertial flow problem and the electrical conduction problem (Brown [95], Johnson et al. [45]). In this case, the Navier-Stokes equations can be replaced by the electric conduction problem. In this high-frequency analogy, the solid phase acts as an insulator and the fluid phase as a conductor (Johnson et al. [96], Zhou and Sheng [97]).

Therefore, using this analogy together with theoretical developments (Auriault et al. [79], Lévy [98]), from the homogenization method for periodic structures with multiscale asymptotic expansions (Bensoussan et al. [99], Sanchez-Palencia [100]), several interesting results can be mentioned. Among them, it is possible to show that the macroscopic

transport properties of interest $(k_0; \alpha_\infty, \Lambda)$ derive from generic boundary value problems (Stokes problem ; electric conduction problem). Furthermore, an approximate but robust function $k(\omega)$ can be provided that predicts the dependence of visco-inertial effects using the low (k_0) and high (α_∞, Λ) frequency properties as input to the model. Finally, an analog frequency-dependent description $k'(\omega)$ of the thermal exchanges between the frame and the saturating fluid involving two macroscopic transport properties $(k'_0; \Lambda')$ can also be introduced (Lafarge et al. [101]).

III.6.4 Estimates of the transport properties

III.6.4.1 Numerical homogenization

Taking advantage of the analogy mentioned above and theoretical developments, the transport properties of the random fibrous microstructures of the model were determined using a finite element method to solve Stokes, Laplace, and Poisson equations in the pore space. The transport properties of the nonwoven fibrous materials are then calculated by (i) generating for each studied nonwoven fibrous material two REVs, one for each asymptotic regime ; (ii) solving the local partial differential equations which govern the phenomena at low and high frequencies, and (iii) computing the resulting transport parameters thanks to spatial averaging of the resulting fields.

For step (i), two series of numerical REVs, one with a mean volume-weighted diameter D_v and one with a mean inverse volume-weighted fiber diameter D_{iv}, were generated to mimic the fibrous microstructures of the manufactured nonwoven seen by the sound wave in the low- and high-frequency regimes, respectively. Briefly, for each series, N straight fibers i of diameter D_i, with orientation vector $\overrightarrow{p_i}$, were generated within many REVs of volume L^3. Following Schladitz et al. [56], Altendorf and Jeulin [57], Chapelle et al. [102], a stationary Poisson line process is defined with a one-parametric directional distribution $p_\beta(\theta, \varphi)$. This parameter captures the degree to which the nonwoven is pressed. Practically, the values of L were set such that the relative difference between the porosity of the geometric model and the measured porosity of the corresponding nonwoven fibrous material is less than 0.1% ; for 100 realizations of the geometrical model. Figure III.5 presents a convergence study on L, for the materials studied, in terms of ratio L/D_m. One can note that a ratio greater than 20 meets this porosity requirement.

Thus, fiber networks were generated in REVs with various porosities ϕ, ranging from 0.76 to 0.948, a fiber diameter distribution based on Gamma law, and a density function of directional distribution $p_\beta(\theta, \varphi)$, see Eq.III.2. The Gamma law and the parameter β were determined by fitting the experimental results obtained from the SEM images. An example for material F2 is shown in Fig. III.6. The figure shows the best-fit Gamma law and directional distribution. The figure also shows that the generation procedure allowed fibrous networks to be obtained with fiber diameter and orientation distributions close to those measured experimentally. The best-fit β values for each material samples are given in Tab.III.3. Figure III.7 shows six examples of idealized monodisperse fibrous networks with isotropic (or un-compressed) ($\beta = 1$), strechted ($\beta = 0$) and compressed ($\beta > 1$) structures to show the influence of the parameter β.

For step (ii), periodic boundary conditions were ascribed to solve the boundary value

problems on a REV. For a given fiber in contact with a couple of bounding surfaces, a point of the fiber was randomly determined along its length. The fiber was cut at this point so that one segment of the fiber could be translated to maintain continuity at the boundaries. A visual description of this process is given in Appendix C.

Figure III.8 shows the periodic microstructural models reconstructed for material F2. Figure III.8a shows detailed information on the polydispersity of the fiber diameters and the directional distribution that accounts for the compression ratio. Three monodisperse models of the same medium are also presented : one with a mean fiber diameter D_m (Fig. III.8b), one with a volume-weighted average diameter D_v (Fig. III.8c)), and one with an inverse volume-weighted average diameter D_{iv} (Fig. III.8d).

Assuming that all diameters follow a Gamma law, the polydispersity is easily quantified by the coefficient of variation CV. This coefficient is defined as the ratio of the standard deviation on the fiber diameters to the mean value D_m. For the materials studied, the values of CV are given in Tab. III.3. Figure III.8 underlines the inequality $D_v \geq D_m \geq D_{iv}$ and the interest in using the two different microstructural descriptors D_v and D_{iv} to predict the transport properties corresponding to, respectively, low-frequency (k_0, k_0') and high-frequency (Λ, Λ', α_∞) transport phenomena at known porosity.

III.6.4.2 Semi-analytical model

To build compact analytical expressions for the transport properties of nonwoven fibrous materials with relevant microstructural parameters, additional assumptions were stated on both the fibrous microstructures and the expected structures of the laws. Their relevance was checked using the microstructure generator and finite element simulations in the next section. The assumptions and main expressions of the semi-analytical model are detailed in the following.

1. The Gamma distribution offers a proper description of the distribution of fiber diameters. One characteristic of this fiber diameter polydiversity is the coefficient of variation CV.
2. A stationary Poisson line process with a one-parametric directional distribution $p_\beta(\theta, \varphi)$ captures the angular orientation of a transversely isotropic fibrous medium and the degree to which the nonwoven was pressed.
3. The model should capture the geometry of the samples for a wide range of possible porosities ($0.65 \leq \phi \leq 0.99$) and anisotropic parameters ($0 \leq \beta \leq 20$).
4. A systematic mapping can be found by simulations in realizations of the geometric model. On the one hand, this mapping allows us to define r_v and r_{iv} as functions of r_m and CV, which are easily measurable microstructure descriptors. Here r stands for radius. On the other hand, there is a mapping between the anisotropy parameter β and the orientation tensor governed by Ω_{zz} (Tab. III.4).
5. The fibers could intersect so that Λ'/r_{iv}, the dimensionless ratio of two times the pore volume V_p to pore surface area S_p divided by inverse volume-weigthed average radius, can be written as given by Luu et al. [60] :

$$\frac{\Lambda'}{r_{iv}} = \frac{\phi}{1 - \phi + c}, \tag{III.5}$$

where c is a constant accounting for the effects of fiber intersections on this high-frequency property.

6. Archie's law [103] that relates porosity to tortuosity holds. This law is given by :

$$\alpha_\infty = (1/\phi)^\gamma, \tag{III.6}$$

where γ is a constant that can vary between porous materials. This relation is defined for a series of materials from the same formation or manufacturing process. The detailed information on the pore structure is contained in the exponent γ. Theoretical studies have shown that γ depends on the shape of the structuring element. When the microstructure is modeled as being built up of straight cylinders with mainly different orientations, a variable exponent could be used to handle the details of the pore space taken as a function of the angular orientation (β or Ω_{zz})

$$\alpha_{\infty z} = (\frac{1}{\phi})^{Q(\Omega_{zz})}, \tag{III.7}$$

where $Q(\Omega_{zz})$ is function of angular orientation (β or Ω_{zz}).

7. The relation between the characteristic lengths derived by Johnson et al. [45] holds. This relation can be written as

$$\frac{\Lambda'}{\Lambda} = 1 - \frac{\ln(\alpha_\infty)}{\ln(\phi)}, \tag{III.8}$$

This relation holds for the felts studied in which the porosity decreases by uniform growth of the insulating (solid) phase into the pore space. With Eq.III.7, the previous relation becomes

$$\frac{\Lambda'}{\Lambda} = 1 + P(\Omega_{zz}). \tag{III.9}$$

In principle, the function of angular orientation is the same as the one of Eq.III.7 but its fitted values could fluctuate to try to compensate for the oversimplifications of Eqs. III.6 and III.8. This is why $Q(\Omega_{zz})$ is replaced by a new function $P(\Omega_{zz})$.

8. Several classical models aim to represent the dependence of permeability on the geometric characteristics of the fiber network. The most classical model is the Kozeny-Carman equation (see Eq. (16) of [104]) given by :

$$\frac{k_0}{r_v^2} = \zeta \frac{\phi^3}{(1-\phi)^2}, \tag{III.10}$$

where ζ is the Kozeny "constant" which depends on the particle shape and size forming the solid skeleton. It can be shown that the through-plane normalized permeability k_0/r_v^2 also depends on the fiber orientations (β or Ω_{zz}). Indeed, the ratio k_0/r_v^2 increases significantly for larger fiber alignment in the direction of the macroscopic pressure gradient. It is assumed that a simple expression to estimate the normalized permeability k_0/r_v^2 as a function of $\phi^3/(1-\phi+m)^2$ and fiber orientation (Ω_{zz}) can take the form

$$\log_{10}\left(\frac{k_{0z}}{r_v^2}\right) = A \log_{10}\left(\frac{\phi^3}{(1-\phi+m)^2}\right) + S(\Omega_{zz}), \tag{III.11}$$

where A and $S(\Omega_{zz})$ are parameters to be calibrated by simulation for obtaining a general form.

9. Because diffusion of heat does not provide any preferred direction (spatially uniform heating), static thermal permeability k_0', normalized by the square of the volume-weighted fiber radius r_v^2, can generally be written as a function independent of fiber orientation. In addition, the relation between k_0' and Λ' was introduced in Eq. III.1. Then, combining Eqs.III.1 and III.5, the normalized thermal permeability as a function of the open porosity can be expressed as

$$\frac{k_0'}{r_v^2} = m_1 \frac{\phi^3}{(1-\phi+m_2)^2}, \tag{III.12}$$

where m_1 and m_2 are calibration constants. It should be noted that this relation is normalized by the volume-weighted fiber radius r_v, as k_0' is a low-frequency parameter. The value of m_1 accounts for the shape of the porous network, while m_2 may be different from c as the effects of the fiber intersections may be different at low frequencies.

Equations III.5, III.7, III.9, III.11 and III.12 form the semi-analytical model (or micro-macro relationships) for transversely isotropic polydisperse nonwoven fibrous media. They depend only on the open porosity ϕ, the angular orientation (β or Ω_{zz}), and the coefficient of variation CV. The main equations of the semi-analytical model are summarized in Tab. III.4, where the constants and polynomials were determined with the numerical results presented in the following section.

Parameter	Equation	R-squared
(a) Thermal length	$\frac{\Lambda'}{r_{iv}} = \frac{\phi}{1-\phi+0.00073}$	0.999
(b) Viscous length	$\frac{\Lambda'}{\Lambda} = 1 + P(\Omega_{zz})$	0.996
(c) Tortuosity	$\alpha_\infty = (\frac{1}{\phi})^{Q(\Omega_{zz})}$	0.977
(d) Viscous permeability	$\log_{10}(\frac{k_0}{r_v^2}) = 0.7501 \log_{10}(\frac{\phi^3}{(1-\phi+0.0038)^2}) + S(\Omega_{zz})$	0.996
(e) Thermal permeability	$\frac{k_0'}{r_v^2} = 0.08 \frac{\phi^3}{(1-\phi+0.0173)^2}$	0.988
(f) Coefficient Ω_{zz}	$\Omega_{zz} = 0.8564 e^{-0.8927\beta} + 0.02163$	0.981
(g) Weighted radii	$\frac{r_v}{r_m} = 0.0002CV^2 - 0.00014CV + 1.003$	0.999
	$\frac{r_{iv}}{r_m} = 0.909 e^{-\left(\frac{CV-4.742}{31.97}\right)^2} + 0.417 e^{-\left(\frac{CV-42.37}{25.92}\right)^2}$	0.999
(h) Polynomials	$P(\Omega_{zz}) = -0.158\Omega_{zz}^2 - 0.666\Omega_{zz} + 0.925$	
	$Q(\Omega_{zz}) = -0.0914\Omega_{zz}^2 - 0.341\Omega_{zz} + 0.495$	
	$S(\Omega_{zz}) = 0.1313\Omega_{zz}^2 + 0.1755\Omega_{zz} - 1.13$	

TABLE III.4 – Semi-analytical model equations to predict the transport properties of a fibrous material.

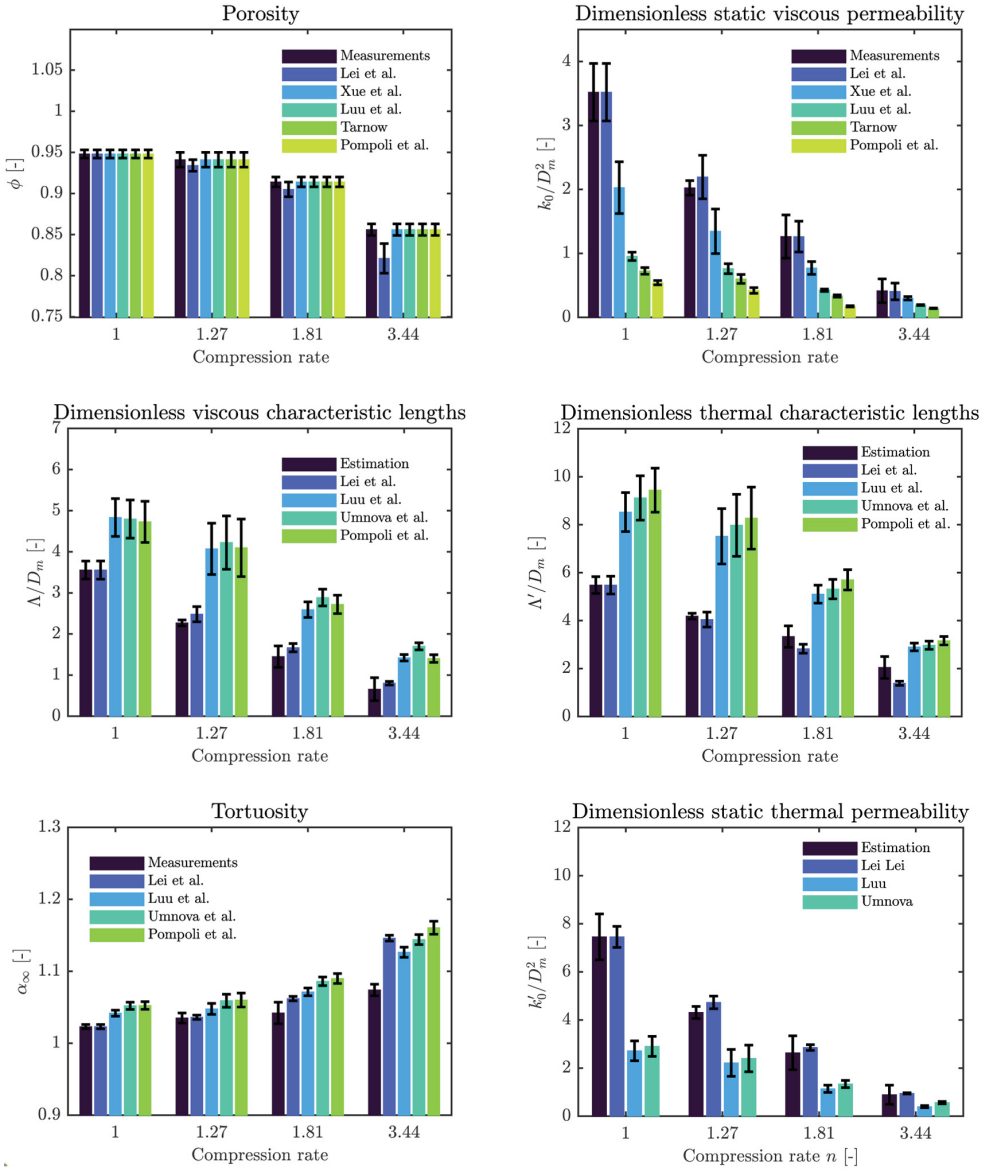

FIGURE III.4 – Comparison between experimental estimates of the transport parameters on cotton felts F1 to F4 and the corresponding predictions with literature models (Lei et al. [92], Xue et al. [69], Luu et al. [59], Umnova et al. [49], Tarnow [46], Pompoli and Bonfiglio [91]). Note that the compression ratio of 1 refers to F1.

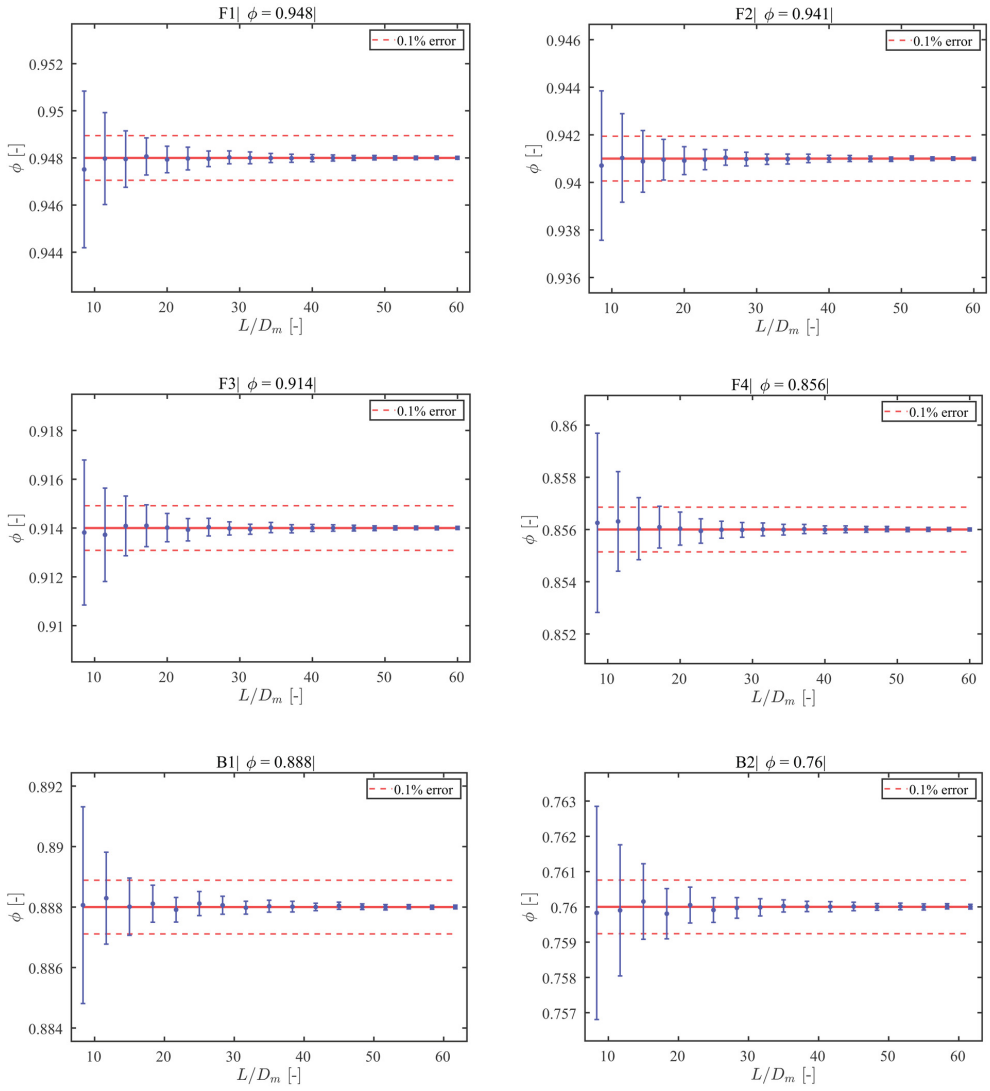

FIGURE III.5 – Evolution of porosity ϕ of the simulated three-dimensional random fibrous microstructures as a function of the size of the cubic box L/D_m, and comparison with the characterized value of porosity.

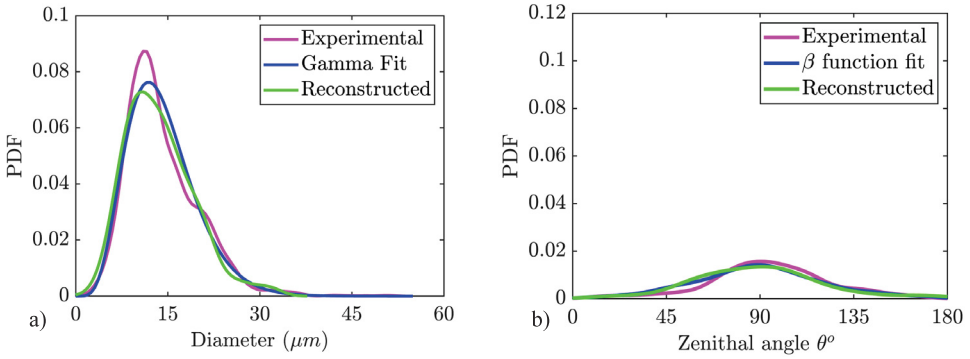

FIGURE III.6 – Illustration of a comparison between the distributions of fiber diameters and orientations as determined experimentally and from the corresponding models, also shown are the distributions after reconstruction.

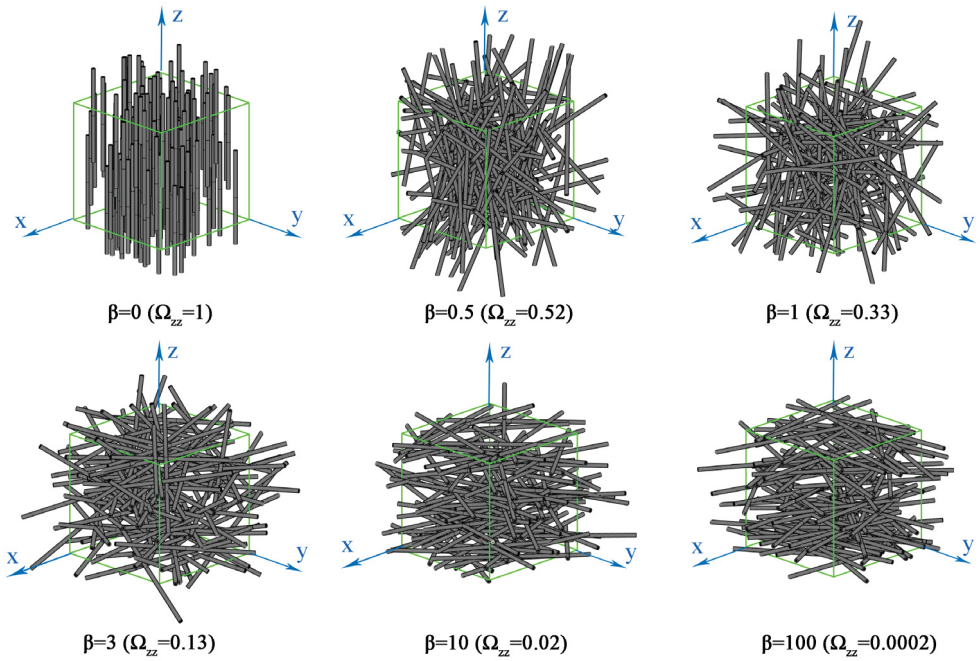

FIGURE III.7 – Various configurations corresponding to the variation of fiber orientation states with β ranging from 0 to 100, respectively.

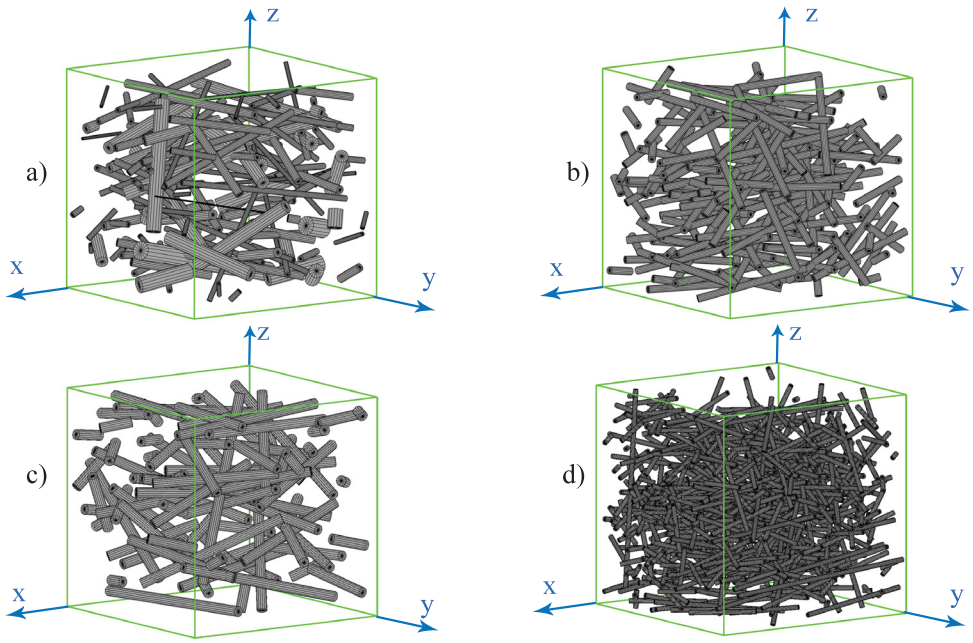

FIGURE III.8 – Randomly overlapping fiber periodic structures of cotton felt F2 ; (a) polydisperse fibrous media ; (b) monodisperse fibrous media with mean fiber diameter, D_m ; (c) monodisperse fibrous media with volume-weighted mean diameter, D_v ; (d) monodisperse fibrous media with inverse volume-weighted mean diameter, D_{iv}.

III.7 Model prediction and discussion

III.7.1 Numerical results

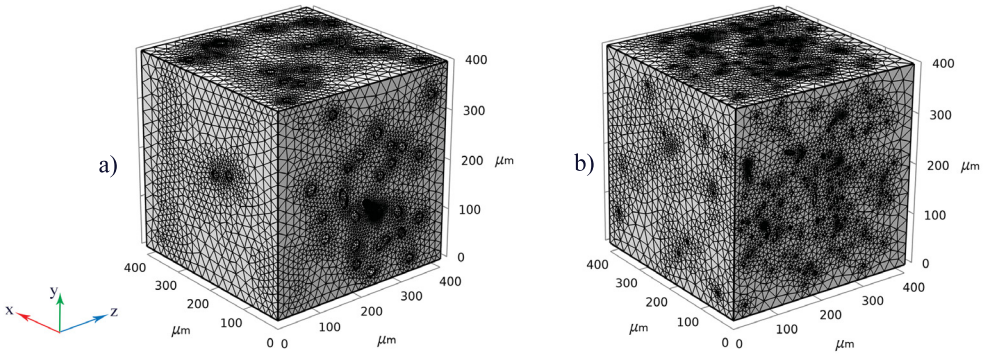

FIGURE III.9 – Typical meshes of the fluid phase in a periodic REV of fibrous medium F2. The meshes are used to perform finite element simulations on : a) structure with inverse volume-weighted diameter with 947,011 tetrahedral elements, and b) structure with volume-weighted diameter with 1,042,941 tetrahedral elements.

By taking advantage of two specific weighted fiber diameters, we have proposed that the studied polydisperse fibrous microstructures subjected to several compression rates and thermo-mechanical bounding could be modeled by two different REVs (i.e., volume weighted r_v and inverse volume weighted r_{iv} fiber radii) corresponding to the transport phenomena than can be simulated in the low and high frequency regimes. Therefore, it was possible to extract from three elementary boundary value problems (Stokes, Laplace, Poisson), and from the computation of the corresponding solution fields (Figs. III.9 and III.10), the expressions of the through-plane static viscous k_0 and thermal k_0' permeabilities of the nonwoven fibrous medium, as well as their through-plane viscous characteristic length Λ and tortuosity α_∞. For its part, the thermal characteristic length Λ' was calculated directly by twice the ratio of pore volume to surface area in each REV mesh. Figure III.11 shows the evolution of k_0/r_v^2, k_0'/r_v^2, Λ/r_{iv}, Λ'/r_{iv}, and α_∞ with the porosity ϕ, for nonwovens with transverse isotropy and with a preferred orientation (Fig. III.7). These predictions were obtained with a domain size L/D allowing for convergence on porosity by taking five realizations for each porosity. From this figure, several remarks can be drawn :

— The through-plane viscous permeability k_0/r_v^2 increases non-linearly with the porosity and diverges as the porosity ϕ is approaching unity ($\sim \phi^3/(1-\phi)^2$). At high porosities, the effect of preferred fiber orientation (induced by compression or manufacturing process) is strong and cannot be ignored. Lower viscous permeabilities are observed for in-plane fiber orientations than for out-of-plane fiber orientations, in agreement with previous results (Tarnow [46]) . In contrast, the static thermal permeability k_0'/r_v is independent of fiber orientation at a constant porosity. It is noteworthy that, as shown by the results of Fig. III.11a, the formal inequality $k_0' \geq k_0$ is also clearly apparent (Avellaneda and Torquato [105]).

— Similarly, the viscous Λ and thermal Λ' characteristic lengths also increase non-

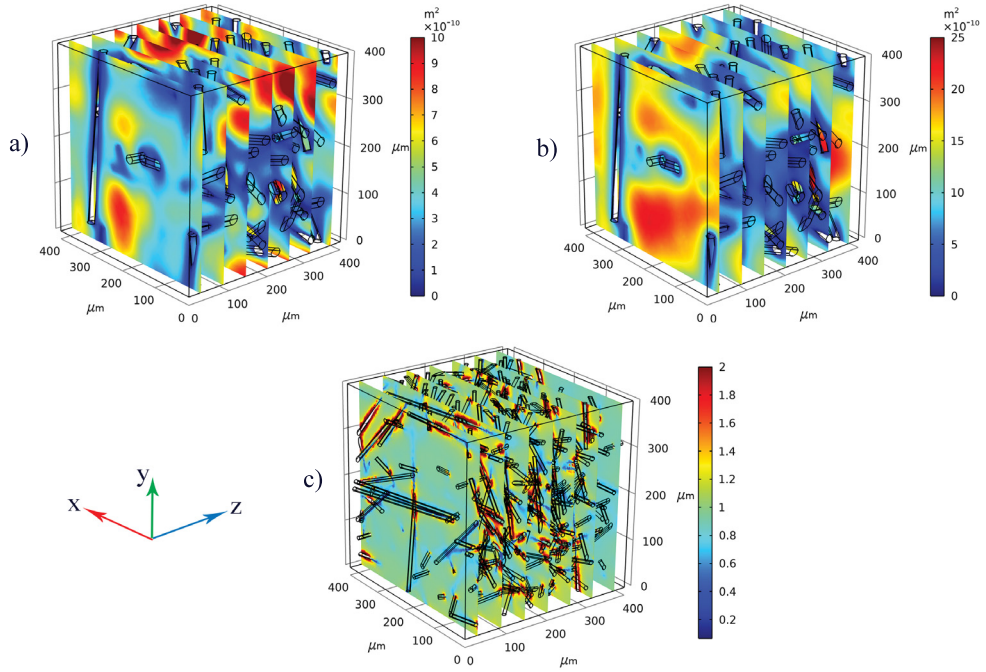

FIGURE III.10 – Asymptotic fields of velocity and temperature computed on the discretized REVs of Fig.III.9 for material F2 : (a) scaled velocity field expressed as local permeability (k_0) [m^2] corresponding to Stokes flow in the z direction with the REV reconstructed by volume-weighted diameter ; (b) scaled heat diffusion field expressed as local static thermal permeability (k_0') [m^2] with the REV reconstructed by volume-weighted diameter, and (c) scaled velocity field expressed as tortuosity α_∞ [$-$] corresponding to potential flow in the z direction with the REV reconstructed by volume inverse weighted diameter.

linearly with the porosity ($\sim \phi/(1-\phi)$) [Fig. III.11c-d] but to a lesser content than for the viscous k_0 and thermal k_0' permeabilities ($\sim \phi^3/(1-\phi)^2$) [Fig. III.11a-b]. We also checked the following inequality, $1 \leq \Lambda'/\Lambda \leq 2$, available for fibrous media in the dilute limit ($\phi \to 1$) [106] ; with $\Lambda'/\Lambda = 1$ in the limit of in-plane orientation distributions of fibers and $\Lambda'/\Lambda = 2$ for fully aligned fibers (Fig. III.11e). This observation implies that the ratio Λ'/Λ increases with the compression rate. The results of Λ'/Λ were relatively independent of porosity [Eq. III.9]. Increasing the fiber alignment significantly increases the viscous characteristic length [Fig. III.11c], the effect is larger for high porosities ($\Lambda' \sim \phi/(1-\phi)$ and $\Lambda'/\Lambda = 1 + P(\Omega_{zz})$) which occurs physically because Λ is weighted by the scalar product of the local electric field solution $\mathbf{E} \cdot \mathbf{E}$ (in plane orientation of fibers creates smaller channels for the preferential fluid flow).

— The tortuosity α_∞ decreases with increasing porosity (Archie's law ; $\alpha_\infty \to 1$ when $\phi \to 1$). However, apart from this limit $\phi \to 1$), the tortuosity α_∞ was shown to increase at constant porosity when the fibers are perpendicular to the potential flow direction. This situation corresponds to a more tortuous path (Fig. III.11f) for which a larger dispersion of the microscopic velocities is obtained (Eq. D.9).

III.7.2 Comparison between finite element simulations and the semi-analytical model

Fig. III.11 shows the five correlation functions k_0/r_v^2 (ϕ, Ω_{zz}), $k_0'/r_v^2(\phi)$, Λ/r_{iv} (ϕ, Ω_{zz}), Λ'/r_{iv} (ϕ), α_∞ (ϕ, Ω_{zz}) with porosity, over a wide range of porosities $(0.65 \leq \phi \leq 0.99)$. The dashed lines in Fig. III.11 are drawn from the results of curve fitting to the simulation data ; the analytical expressions are those of Eqs. (III.5, III.7, III.9, III.11, III.12) and the fitted coefficients reported throughout Tab. III.4. Good agreement with the simulation data is seen in all five cases, confirming the above initial law derivations. The square of the correlation coefficient gives R-squared ≥ 0.977. The fact that R-squared is less than one indicates that at some porosities, there is a small proportion of Sum of Squared Errors (SSE) that is not accounted for by the regression. The coefficient of determination (R-squared) of the fit was 0.999 for the thermal characteristic length, 0.977 for the tortuosity, 0.996 for the ratio of the thermal over viscous characteristic lengths, 0.996 for the viscous permeability and 0.988 for the thermal permeability. The proportionate amount of variation in the response variable (dimensionless transport parameter) that is explained by the independent variables (porosity ϕ and orientation of fibers Ω_{zz}) was therefore always very close to one.

The residual analysis enables a local quantitative appreciation of the adequacy of the fitted model (Fig. III.12). The residuals from a fitted model are defined as the differences between the response data (simulations) and the fitting to the response data (model) at each predictor value. The largest differences are obtained for the tortuosity α_∞, as $\phi \to 0.65$ and $\Omega_{zz} \to 1$. In this situation, the tortuosity values should correspond to the upper bound [Eqs. III.6 and III.7] of a solid fibrous network with lower porosities. But if simulations are performed in opposite fiber orientations, from $\Omega_{zz} = 0$ for in-plane fibers to $\Omega_{zz} = 1$ for unidirectionally aligned fibers, a large variation of tortuosity values should be observed which is somehow contradictory with the initial choice of an Archie's law [Eq. III.6]. The presence of these contradictory behaviors (α_∞ increases with decreasing ϕ, α_∞ decreases with increasing Ω_{zz}) can be used to explain the higher sensitivity of the model to geometrical parameters and the larger proportion of numerical results not entirely present in the model. Similar arguments can be given to quantify the differences between the finite element simulations and the analytical model for the static thermal permeability k_0' : as $\phi \to 1$, the value of k_0' diverges as $(\sim \phi^3/(1-\phi)^2)$ [Eq. III.5] which statistically increases the proportion of SSE that is not completely explained by the regression.

Our results suggest that a better fit would require an increase in the domain size L/D_m, which is important to ensure a lower relative difference between the porosities of the generated microstructures and the porosity that serves as the target, as ϕ approaches one. i.e., if ϕ target $= 0.99$ with err $= 0.01\%$, $L/D_m = 55$; if ϕ target $= 0.99$ with err $= 0.001\%$, $L/D_m = 140$ (see Figs. C.2 and III.5).

Finally, in this section, we presented a comparison between the analytical result and the numerical finite element solution. We saw, through a detailed analysis of the residues, that the comparison between finite element simulations and the analytical model (Figs. III.11 and III.12, Tab. III.4) revealed that the analytical expressions [Eqs. III.5, III.7, III.9 III.11, III.12] fit well with the trends gained from the finite element simulation when the same microstructure parameters are used as input. Hence, analytical estimates can

be considered to be accurate enough predictors of the transport properties of nonwoven fibrous materials.

III.7.3 Comparisons with experimental results

Two different types of comparisons are presented to validate the semi-analytic model in Tab. III.4. The first type of comparisons, shown in Fig. III.13, concerns the transport properties predicted by the model and their experimental measurements or estimates, presented in Section III.5.2. The second type of comparisons, shown in Fig. III.14, concerns the sound absorption coefficient predicted by the model for each felt and its impedance tube measurement obtained from the method presented in Section III.4.3. From these comparisons, several important results can be drawn. They are listed below.

— From the comparisons shown in Fig. III.13, one can conclude that the proposed semi-analytical model allows nice quantitative predictions of the measured transport properties k_0, k_0', Λ, Λ', and α_∞. The comparison is good for a wide range of open porosities ($0.760 \leq \phi \leq 0.948$) [Tab. III.5] and for different fiber orientation distributions ($0.01 \leq \Omega_{zz} \leq 0.22$) [Tab. III.3]. It is recalled that fiber orientation is related to the compression ratio that varies in the range ($1 \leq n \leq 3.4$) for the two families of composite nonwoven fibrous materials (F and B, Tab. III.1). These two families have a different fiber diameter polydispersity content ($CV \sim 40\%$ for F and $CV \sim 30\%$ for B, Fig. III.3b and Tab. III.3). Consequently, the overall agreement between the analytical and experimental results supports the validity of the semi-analytical model within, at least, the degrees of fiber diameter polydiversity and orientation studied. Moreover, this proves that the fiber diameter polydispersity and, to a lesser extent, the orientation of fibers play a leading role in the transport properties of these fibrous composites.

— Despite a relatively good overall comparison, a few differences are worth discussing. First, for k_0', we recall here that it was not possible to have a direct measurement of k_0'. Its value is estimated from the identification of Λ' (Eq. III.1), which is in turn estimated from other measured properties thanks to the Kozeny-Carman formula (Eq. : B.2). Consequently, we must look at the trend of its evolution more than its values. The same holds for Λ' and Λ. Second, the predicted value of k_0 for F1 departs from the measurement. As explained previously (Section 5.2), the model diverge for high porosity values approaching.

— We next explored the sound absorbing behavior at normal incidence in an analytical way using the predicted transport parameters in a JCAL model (D) that allowed us to generate the sound absorption coefficient that could be compared directly with experiments (Fig. III.14). This analysis shows that the sound absorption coefficients at normal incidence that are predicted are comparable to those measured experimentally. Together with a close match between the transport parameter values in the experiments and in the models, this and the above results confirm the accuracy of the numerical models and indicate that they capture the essential physics of the viscous fluid-flow, excess temperature, and potential flow velocity field in a polydisperse nonwoven composite and the corresponding transport and sound absorbing properties.

	Results	ϕ	$\sigma(N.s.m^{-4})$	α_∞	$\Lambda(\mu m)$	$\Lambda'(\mu m)$	$k'_0 \times 10^{-10}(m^2)$
F1	Model	0.948 ± 0.005	38358 ± 1612	1.022 ± 0.002	48 ± 5	84 ± 8	12.1 ± 1.6
	Exp	0.948 ± 0.005	28684 ± 3664	1.023 ± 0.003	46 ± 3	74 ± 5	13.6 ± 1.7
F2	Model	0.941 ± 0.009	47235 ± 3191	1.026 ± 0.004	42 ± 7	74 ± 12	9.9 ± 2.1
	Exp	0.941 ± 0.009	45716 ± 2553	1.035 ± 0.007	35 ± 1	59 ± 2	8.6 ± 0.4
F3	Model	0.914 ± 0.006	87776 ± 2818	1.042 ± 0.003	25 ± 2	47 ± 4	5.1 ± 0.5
	Exp	0.914 ± 0.006	76479 ± 20416	1.042 ± 0.015	27 ± 4	46 ± 6	5.1 ± 1.3
F4	Model	0.856 ± 0.007	242696 ± 5784	1.078 ± 0.005	15 ± 1	28 ± 2	1.6 ± 0.1
	Exp	0.856 ± 0.007	235845 ± 105324	1.074 ± 0.008	17 ± 4	28 ± 6	1.7 ± 0.8
B1	Model	0.887 ± 0.001	65456 ± 2770	1.057 ± 0.006	42 ± 4	79 ± 8	6.3 ± 0.8
	Exp	0.888 ± 0.001	52018 ± 4732	1.089 ± 0.005	34 ± 2	57 ± 3	7.5 ± 0.6
B2	Model	0.764 ± 0.022	246602 ± 12283	1.144 ± 0.021	15 ± 2	29 ± 4	1.18 ± 0.1
	Exp	0.760 ± 0.022	213834 ± 44998	1.175 ± 0.02	22 ± 2	32 ± 4	1.1 ± 0.2

TABLE III.5 – Comparison of semi-analytical (Model) and experimental (Exp) estimates of the transport parameters of cotton and PET felts

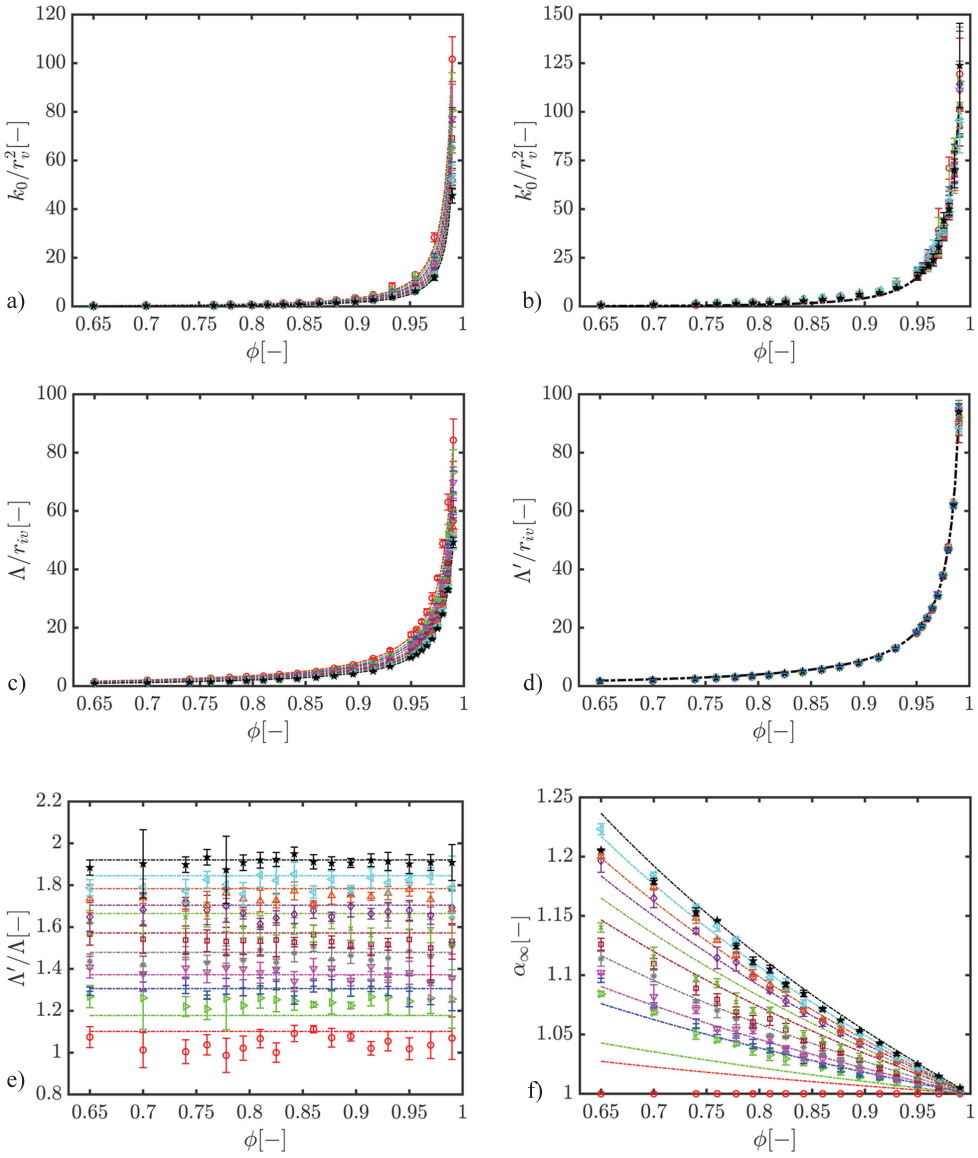

FIGURE III.11 – Normalized transport parameters as a function of porosity ϕ. The symbols indicate the statistically averaged orientation of fibers as determined by value of β or Ω_{zz} : $\Omega_{zz} = 0$ ($\star$), $\Omega_{zz} = 0.11$ ($\triangleleft$), $\Omega_{zz} = 0.19$ ($\triangle$), $\Omega_{zz} = 0.30$ ($\diamond$), $\Omega_{zz} = 0.39$ ($\times$), $\Omega_{zz} = 0.49$ ($\square$), $\Omega_{zz} = 0.61$ ($*$), $\Omega_{zz} = 0.71$ ($\triangledown$), $\Omega_{zz} = 0.81$ ($+$), $\Omega_{zz} = 0.91$ ($\triangleright$), $\Omega_{zz} = 1$ ($\circ$). The dashed lines are estimates obtained by the semi-analytical model derived from the numerical simulations (Tab. III.4).

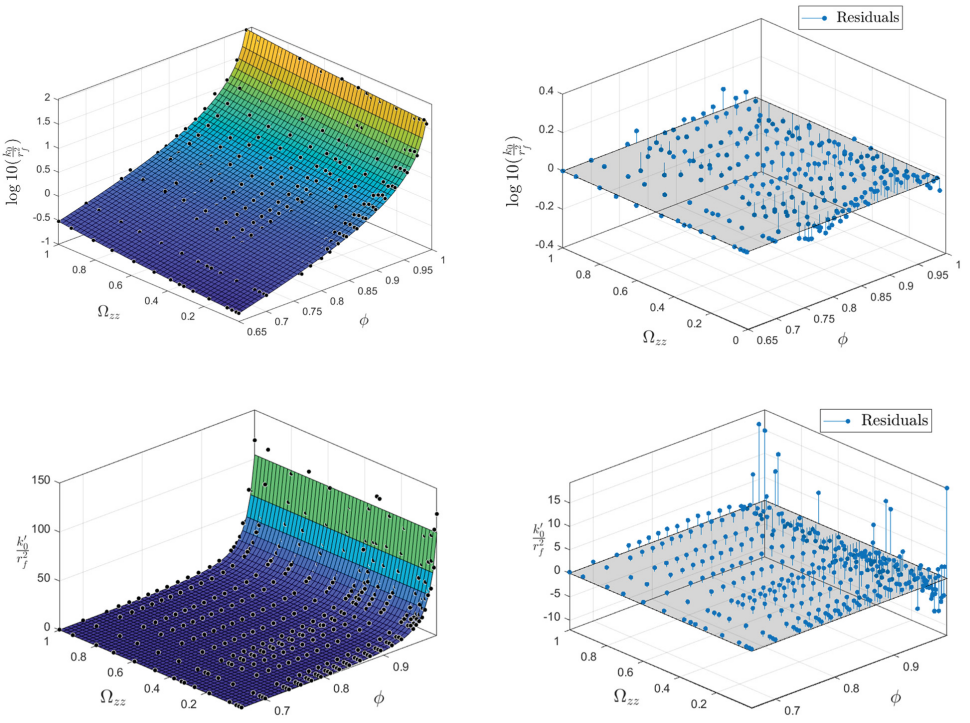
log 10($\frac{k_0}{\tau_f}$)
Ω_{zz}
ϕ
Residuals
$\frac{K}{\tau_f^2 R_s}$

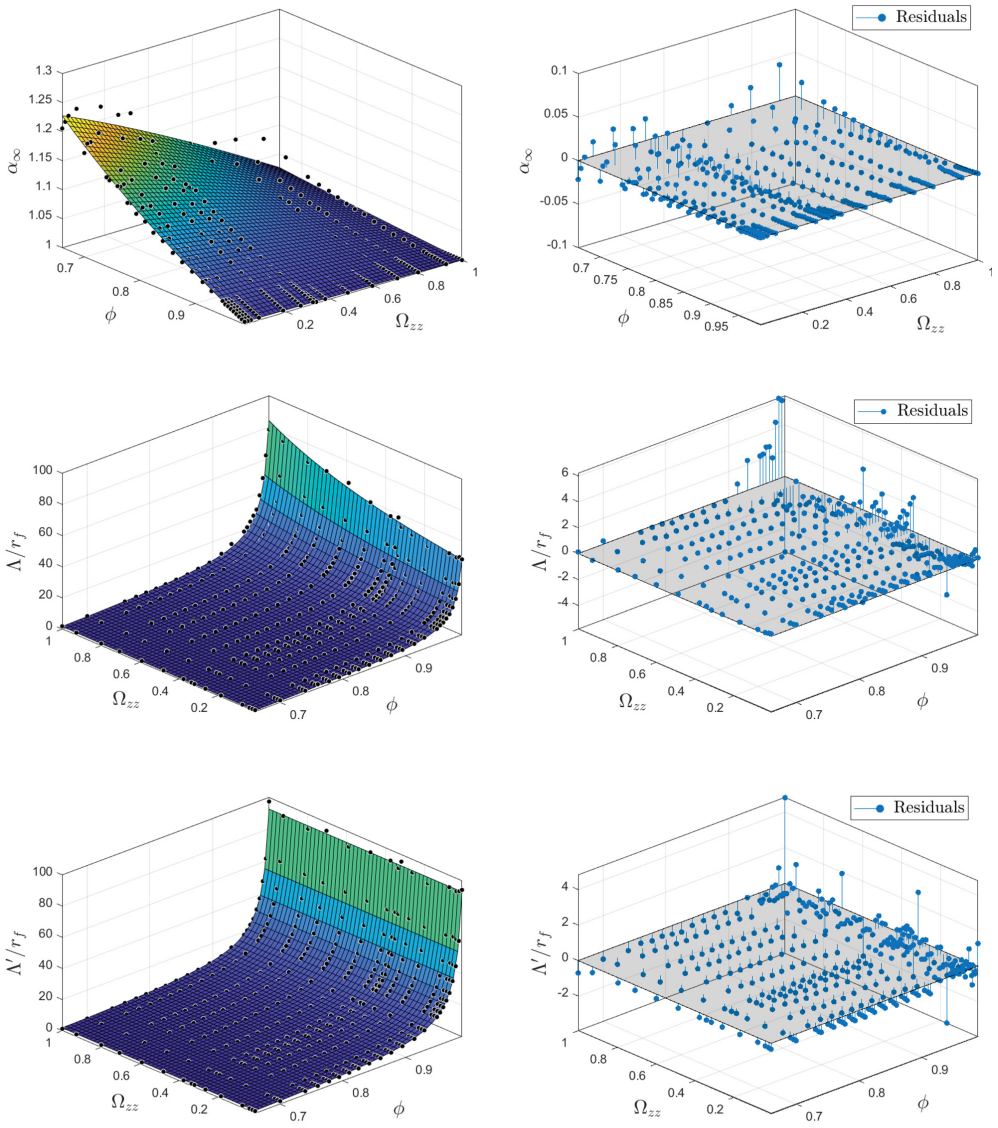

FIGURE III.12 – Map fittings and residual plots of dimensionless transport parameters (semi-analytical model derived from the numerical simulations).

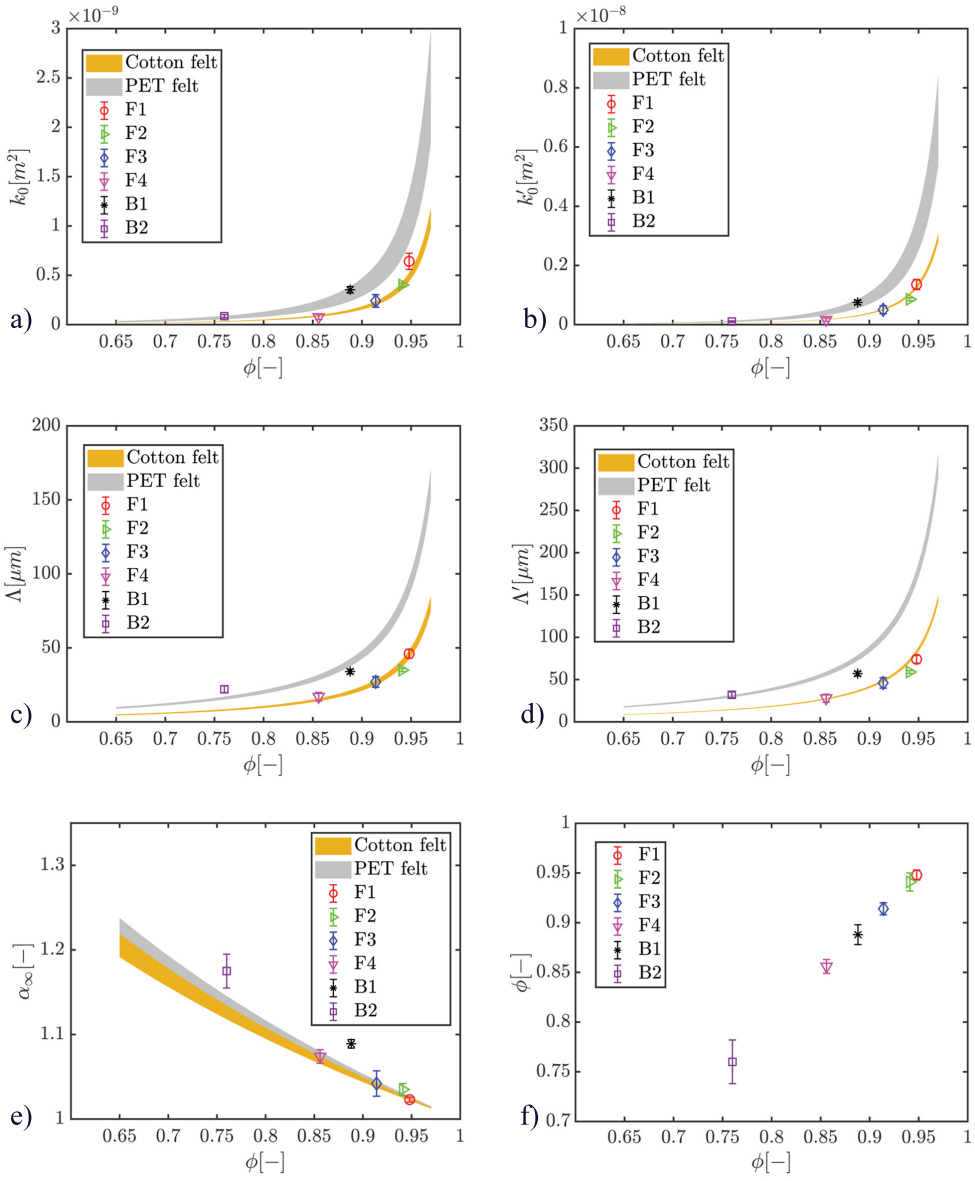

FIGURE III.13 – Evolution of the transport patameters k_0, k_0', Λ, Λ', α_∞ with the porosity ϕ for three-dimensional random fibrous materials with transversely isotropic structure and a preferred angular orientation Ω_{zz} depending on the compression rate n. Comparison between the predictions of the semi-analytical models Tab. III.4 and the data obtained from experiments (symbols). These predictions are obtained using the average microstructurals descriptors in Tab. III.3 for the cotton felts ($D_v = 18.95 \pm 0.5\mu m$; $D_{iv} = 9.20 \pm 0.26\mu m$; $\Omega_{zz} = 0.15 \pm 0.09$; $CV = 40.2 \pm 1.2\%$) and for the PET felts ($D_v = 28.95 \pm 3.25\mu m$; $D_{iv} = 19.20 \pm 0.85\mu m$; $\Omega_{zz} = 0.05 \pm 0.05$; $CV = 29.9 \pm 4.6\%$) The thick lines correspond to the deviation of either cotton felts (orange) or PET felts (grey).

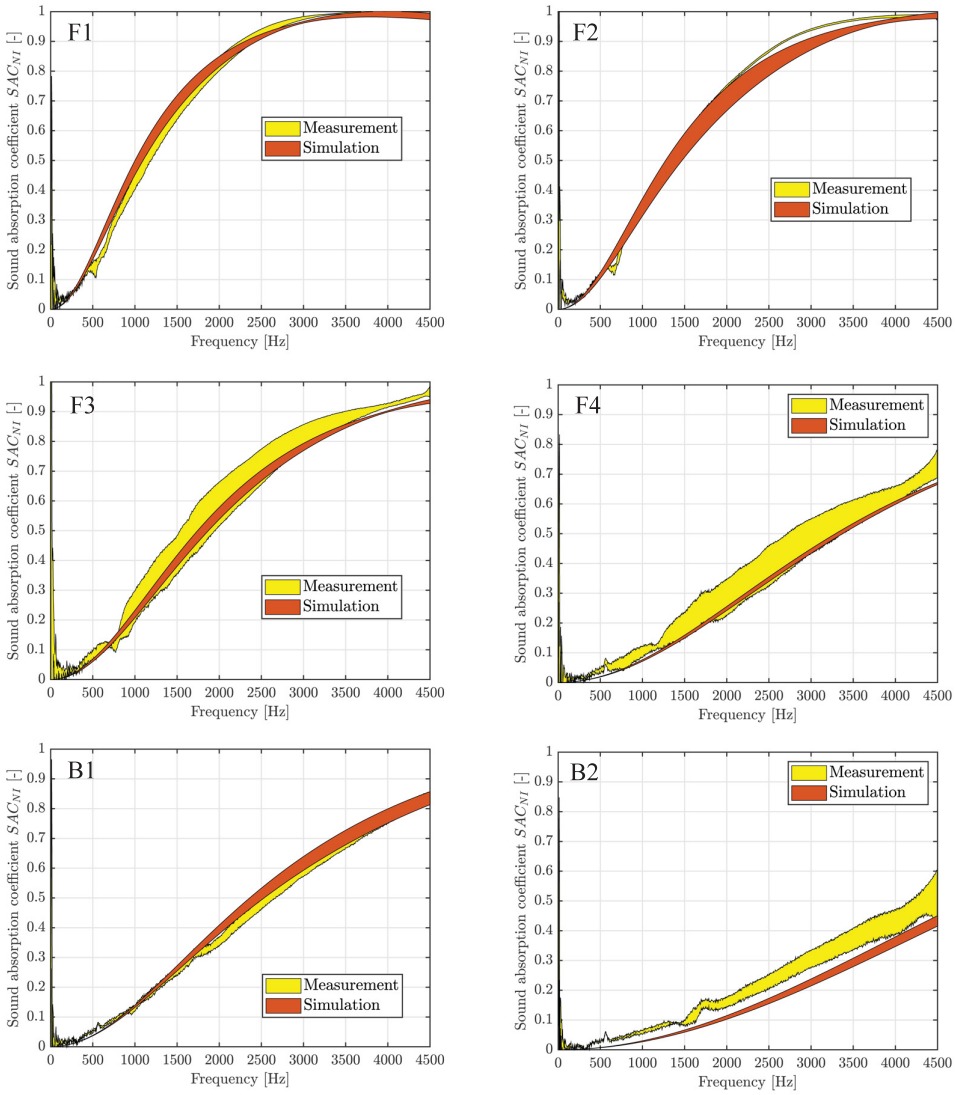

FIGURE III.14 – Comparison between measurements and predictions of the sound absorption coefficient at normal incidence. Sample thickness : F1 - 20.3 mm ; F2 - 16.1 mm ; F3 - 11.2 mm ; F4 - 5.9 mm ; B1 - 10.3 mm ; B2 - 4.3 mm.

III.8 Conclusions

The objective of this study was to link the macroscale transport and sound absorbing properties of nonwoven fibrous composites with their polydisperse fibrous microstructures and the related visco-thermal dissipation mechanisms. For that purpose, two families of composite nonwovens were manufactured using a thermo-compression process, from either recycled cotton and co-PET fibers or a mix of recycled PET and Co-PET fibers with different classes of fineness, and further compacted with several compression rates. SEM images showed that their random fibrous microstructures exhibited well known transverse isotropy with a preferential orientation of fibers that depended on the compression rate. In addition, regardless of the family of the composite nonwovens, the fibers originating from a recycling process were characterized by a wide distribution of diameters which could be modeled as a Gamma-law, a trend already observed for glass and stone wools. From the fiber scale images of their microstructures, we also saw that the radius of curvature of the fibers was large when compared to the fiber radii, so that the individual fibers could be considered as straight cylinders. The connectivity between two adjacent fibers due to the thermo-compression bounded co-PET process was also visible so as to reasonably assume that fibers could intersect.
From these experimental data obtained at fiber scale, fiber network models were proposed to predict the through-plane transport properties of the considered polydieperse nonwoven composites. Two microscale models were established. The first one used volume weighted fiber diameter and the second inverse volume weighting as mean diameters to perform finite element simulations. The results were rationalized in the form of analytical laws that can be easily used for engineering purposes, e. g., to optimize polydisperse fibrous media. The modeling approach emphasised the leading roles of the fiber content, polydispersity and orientation on the macroscale transport and sound absorbing properties of the considered nonwovens. The modeling approach quantitatively well predicted the transport and sound absorbing properties characterized at macro-scale. If the porosity and distributions of fiber diameters and orientations are provided as inputs, we have shown that the predictions of the numerical and analytical models can nicely estimate the transport and sound absorbing properties at normal incidence of random and transversely isotropic polydisperse fibrous media for a large range of porosities and without any adjusted parameter. The identified micro-structural descriptor of the low frequency behavior is in accordance with literature data, i. e., at low polydispersity content, only one fiber diameter is necessary to derive the overall transport parameters characterizing both low and high frequency behaviors, thus suggesting a switch from mono disperse to poly disperse fiber distribution as a new lever to understand and optimize transport and sound absorbing properties. The developed model should be tested accordingly for fiber diameter distributions characterized by very large coefficient of variations.

Acknowledgments

This work was part of a project supported by ANRT and Adler Pelzer Group, Acoustic TechCenter R&D under convention CIFRE No. 2020/0122. The MSME laboratory is part

of the LabEx MMCD (Investisements d'Avenir : grant agreement no. ANR-11-MABX-022-01). Partial support for this work was also provided by Université Paris-Est Sup (mobility grant from the ED SIE). The authors also acknowledge the support of the Natural Sciences and Engineering Research Council of Canada (NSERC) [funding with ref. number RGPIN-2018-06113]. We acknowledge Rémy Pires-Brazuna (ICMPE UMR 7189 CNRS) for SEM imaging of the fibrous samples.

Chapitre IV

Utilizing polydispersity in three-dimensional random fibrous based sound absorbing materials

Contenu

IV.1 Avant-propos

Auteurs et affiliations :

— Quang Vu Tran, étudiant doctorant, Université Gustave Eiffel, Univ Paris Est Creteil, CNRS, UMR 8208, MSME, F-77454, Marne-la-Vallée, France. Département de Génie Mécanique, Université de Sherbrooke, J1K 2R1, Québec, Canada. Adler Pelzer Group, Acoustic TechCenter R&D, France

— Camille Perrot, Professeur, Université Gustave Eiffel, Univ Paris Est Creteil, CNRS, UMR 8208, MSME, F-77454, Marne-la-Vallée, France

— Raymond Panneton, Professeur, Département de Génie Mécanique, Université de Sherbrooke, J1K 2R1, Québec, Canada

— Minh Tan Hoang, Ingénieur (Expert Méthodologies et Simulations), Adler Pelzer Group, Acoustic TechCenter R&D, France

— Ludovic Dejaeger, Ingénieur (Leader Acoustique Mouzon), Adler Pelzer Group, Acoustic TechCenter R&D, France

— Valérie Marcel, Ingénieure Matières (Responsable Innovation), Adler Pelzer Group, Acoustic TechCenter R&D, France

— Mathieu Jouve, Ingénieur Matières (Reponsable dév. matières), Adler Pelzer Group, Acoustic TechCenter R&D, France

Date de soumission : 12 Novembre 2023
État de l'acceptation : En révision
Revue : Physics of Fluids
Référence : [POF23-AR-09056]

Titre français : Utilisation de la polydispersité dans des milieux fibreux aléatoires tridimensionnels à base de matériaux insonorisants

Contribution au document :

Cet article contribue à la thèse une mise en évidence sur la base d'un travail exploratoire, exploitant le modèle précédemment développé, que le degré de polydispersité peut être utilisé une fois contrôlé comme nouveau levier d'optimisation des performances acoustiques d'un milieu fibreux.

Résumé française :

La distribution des diamètres des fibres joue un rôle crucial dans les propriétés de transport et d'absorption acoustique d'un milieu fibreux tridimensionnel aléatoire (3D-RF). Traditionnellement, la moyenne pondérée par le volume des diamètres des fibres a été utilisée comme un descripteur microstructural approprié pour prédire la perméabilité visqueuse statique des milieux 3D-RF. Cependant, les propriétés acoustiques à longue longueur d'onde d'un milieu 3D-RF sont également sensibles aux plus petites fibres, ce qui est particulièrement vrai dans le régime haute fréquence. Dans nos recherches récentes, nous avons démontré qu'une moyenne pondérée par le volume inverse des diamètres des fibres peut efficacement servir de descripteur microstructural complémentaire pour capturer le comportement en haute fréquence des milieux fibreux polydisperses. Dans le présent travail, nous passons en revue l'identification de deux volumes élémentaires représentatifs (VER) qui repose sur la reconstruction de microstructures 3D-RF ayant des diamètres de fibres moyennés par le volume et inverses, respectivement, dans les régimes de basse fréquence et haute fréquence. Nous examinons les implications d'une

telle procédure de pondération sur les propriétés de transport et d'absorption acoustique des milieux fibreux polydisperses, mettant en évidence leurs avantages potentiels. De plus, nous discutons des défis associés à ce domaine de recherche. Enfin, nous donnons un bref aperçu des orientations futures et des opportunités pour faire progresser ce domaine d'étude, dans le but de relever les défis et d'étendre les avantages de l'utilisation de la polydispersité comme nouveau levier pour l'optimisation des microstructures 3D-RF dans les dispositifs d'absorption acoustique.

Utilizing polydispersity in three-dimensional random fibrous based sound absorbing materials

Q. V. Tran,[1,2,3] C. Perrot,[1] R. Panneton,[2] M. T Hoang,[3] L. Dejaeger,[3] V. Marcel,[3] M. Jouve,[3]

[1] Université Gustave Eiffel, Univ Paris Est Creteil, CNRS, UMR 8208, MSME, F-77454, Marne-la-Vallée, France

[2] Département de Génie Mécanique, Université de Sherbrooke, J1K 2R1, Québec, Canada

[3] Adler Pelzer Group, Acoustic TechCenter R&D, Z.I. François Sommer – BP13, 08210, Mouzon, France

IV.2 Abstract

The distribution of fiber diameters plays a crucial role in the transport and sound absorbing properties of a three-dimensional random fibrous (3D-RF) medium. Conventionally, volume-weighted averaging of fiber diameters has been utilized as an appropriate microstructural descriptor to predict the static viscous permeability of 3D-RF media. However, the long wavelength acoustical properties of a 3D-RF medium are also sensitive to the smallest fibers, this is particularly true in the high-frequency regime. In our recent research, we demonstrated that an inverse volume-weighted averaging of fiber diameters can effectively serve as a complementary microstructural descriptor to capture the high-frequency behavior of polydisperse fibrous media. In the present work, we review the identification of two representative volume elements (RVEs) which relies on the reconstruction of 3D-RF microstructures having volume-weighted and inverse-volume weighted averaged fiber diameters, respectively in the low-frequency and high frequency regimes. We examine the implication of such a weighting procedure on the transport and sound absorbing properties of polydisperse fibrous media, highlighting their potential advantages. Furthermore, we discuss the challenges associated with this research field. Finally, we provide a brief perspective of the future directions and opportunities for advancing this area of study, aiming to overcome challenges and extend the benefits of employing polydispersity as a new lever for the optimization of 3D-RF microstructures in sound-absorbing materials.

IV.3 Introduction

Three-dimensional random fibrous (3D-RF) structures have become one of the most widespread technologies in large-scale manufacturing of sound-absorbing materials known as nonwovens or felts, employing various types of fibers to achieve their acoustical constraints. Some commonly used manufacturing processes include the airlay process [80, 81] and the carding, cross-lapping, and needing process [82, 83]. Traditional thermobonded airlaid

nonwoven typically incorporates a mixture of non-homogeneous shoddy fibers (75%) and bicomponent fibers (25%) in the airlay process.

The bicomponent fibers have a core made from PET and a surface made from coPET. On the other hand, to facilitate recycling, needlefelt nonwoven use a mixture of PET fibers (60%) and bicomponent fibers (40%). In both cases, in post-processing, the nonwoven materials are reinforced by thermobonding (with a chosen compression ratio), where the bicomponent fibers have an adhesive effect. However, the use of non-homogeneous fibers in the manufacturing process comes with some drawbacks. One of the disadvantages is that the transport mechanisms can be significantly impacted by the fiber size variations induced by the manufacturing process. For example, shoddy fibers are obtained after the tearing of textile waste from a mixture of 55% cotton and 45% PET, and cotton fibers can introduce fiber dust particles, which affect the distribution of fiber diameters. The manufacturing process of nonwoven leads to a wide distribution of fiber diameters and fiber orientations, which affects the frequency-dependent response of the fluid within the corresponding 3D-RF structure. Moreover, mixing fibers of different sizes is generally recommended. The largest fibers ensure the rigidity and mechanical stability of the nonwoven material, while the smallest fibers provide sound absorbing capabilities to the fibrous materials. Therefore, an important research direction in this field is the study of various distributions of fiber diameters and orientations and the development of models that account for the corresponding frequency-dependent response functions. Several approaches have been explored to achieve this goal. Perhaps the most direct method is to conduct a series of laboratory measurements on samples of varying fiber size and orientation (semi-empirical models) [92, 107, 108]. Alternatively, in the quest for theoretical understanding, one may seek to better understand the mathematical (analytical derivations) [109, 110, 46, 111, 50, 112] or physical (semi-phenomenological description) [96, 101, 113, 114] basis of the generalized (dynamic) Darcy-scaled equations for macroscopic transport. Lastly, one can consider studies based on numerical simulations [115, 53, 52]. Notably, Peyrega and Jeulin [62] used a volume-weighted average diameter to successfully predict the static viscous permeability of heterogeneous fibrous materials and our group has recently demonstrated that an inverse volume weighted average diameter can serve as a complementary microstructural descriptor to predict the characteristic lengths and tortuosity of these polydisperse 3D random fibrous materials.

In this paper, we aim to provide a comprehensive overview of research advancements in employing 3D polydisperse RF microstructures, with a particular emphasis on using polydispersity as a new lever of optimization. Starting from existing specimens of nonwoven fibrous materials, we focus specifically on three different types of studies : (i) a parametric study, using the coefficient of variation of the fiber diameters (polydispersity degree, P_d) as input parameter ; (ii) optimizing the sound absorption average at normal incidence over a wide frequency range of a given nonwoven specimen by controlling the degree of polydispersity of the fiber diameters ; (iii) achieving targets of industrial interest consisting of lowering the lower frequency from which the sound absorption in a diffuse field is greater than 80%.

The paper is organized in the following sequences. In the first section, we delve into the fundamental transport properties of 3D-RF microstructures used as sound-absorbing materials that are characterized by a wide distribution of their fiber diameters. We dis-

cuss the unique transport properties and microstructural descriptors derived from the polydispersity of these materials, highlighting their potential advantages over traditional fibrous materials. This section serves as a foundation for understanding the subsequent discussions. Building upon the understanding of 3D microstructure based RF materials, we dedicate the second section to exploring the advantages offered by employing specific polydispersity degree as a microstructural optimization lever. We discuss the benefits associated with tuning the polydispersity degree of 3D-RF microstructures in terms of their transport properties, sound absorption average at normal incidence, sound absorption targets in diffuse field. By doing so, we highlight our contribution to the field, showing the advancements we have made in leveraging these materials for polydisperse fiber diameters. Finally, we conclude the article with a brief perspective and outlook on current challenges and the future of research in this area. We discuss emerging challenges, potential directions for further explorations, and the significance of continued investigations into 3D-RF microstructured materials as a microstructural optimization lever of their physical properties. By summarizing the current state of the field and presenting potential avenues for future research, we aim to inspire and guide researchers in this exciting area of study. of this work.

IV.4 Nonwoven fibrous media characterized by local heterogeneity

IV.4.1 Predicting transport properties

Martys and Garboczi [53] demonstrated through numerical computations the important effect spatial randomness in the pore space has on flow problems. In particular, they established a crucial distinction between the electric fields and the fluid-flow fields for a given pore structure. Leveraging this distinction, they identified that in a random pore structure with a distribution of pore sizes, the fluid-flow will tend to go more through the largest pore necks ; while the electrical current-flow rate was comparatively less sensitive to the width of narrow necks. As a result, the fluid velocity fields and the electric fields can sample the pore space quite differently. Subsequently, Peyrega and Jeulin [62] made substantial advances in this area, particularly in identifying the volume-weighted average radius as a key microstructural descriptor for the determination of the representative volume element of a random fibrous medium. Moreover, Tran [116] and collaborators delved into the associated microscopic basis of macroscopic viscous permeability, shedding further light on how macroscopic viscous permeability depends on the largest pore sizes of a locally heterogeneous 3D-RF microstructure. The volume-weighed average diameter D_v of a wide distribution of fiber diameters is larger than non-weighted average diameter D_m, and the number of introduced fibers in a cubic box of size L/D_m is therefore lower in the volume-weighted average diameter case than in the non-weighted average diameter one – while the porosity is known and given by measurements in both cases. As a result, the reconstructed pore sizes of 3D-RF structures having a volume-weighted average diameter match with the largest pore necks through which the viscous fluid-flow will tend to go in the corresponding nonwoven specimen. This reconstruction procedure enables the

identification of a REV having D_v as the average diameter and the computed viscous permeability k_0 to be consistent with the measured values [$S_D = 45mm$, $L/D_m \approx 25(-)$, $L = 400\mu m$] in real samples whose sample diameters are much larger than those of the RVE [116].

The combined presence of a wide distribution of fiber diameters and random microstructure promotes pore-size local heterogeneity, leading to the identification of the volume-weighted average diameter, as being an appropriate microstructural descriptor for the prediction of the static viscous permeability. The use of the finite element method revealed that velocity fields are consistent with experimental measurements of viscous permeability using volume-weighted average diameter D_v, as shown in Fig. IV.1(a)-IV.1(d) and IV.1(j). However, the electric current paths are clearly less concentrated and tortuous than do the fluid-flow paths, so there are significantly fewer stagnant areas for the electrical current flow than for the fluid flow. Λ is defined [45] by the following ratio of integrals : $\Lambda = 2\int \mid \mathbf{E}(\mathbf{r}) \mid^2 dV_p / \int \mid \mathbf{E}(\mathbf{r}) \mid^2 dS$, where $\mathbf{E}(\mathbf{r})$ is the magnitude of the electrical field in the pore space, dV_p is the volume element in the pore space, and dS is the surface element on the pore solid interface. Therefore, Λ can be thought of as a dynamically weighted hydraulic radius [96], where the weighting procedure substantially favors the smaller pores because of current conservation. Fig. IV.1(c) shows a 3D-RF microstructure where inverse volume-weighted average diameter is used as the appropriate microstructural descriptor for the prediction of the viscous characteristic length Λ. The geometrical reconstruction method is given in our previous work [116]. The smaller pores of the nonwoven polydisperse fibrous materials were probed by measuring the experimental value of the Λ parameter, a value captured by using inverse volume-weighted average diameter D_{iv} during the reconstruction procedure, as shown in Figs. IV.1(i) and IV.1(k). The change in pore size reconstruction induced by fiber diameter polydispersity and volume-based fiber diameter weighting is shown in Fig. IV.1(a)-IV.1(c). At the scale of the reconstructed unit-cell, the non-weighted average diameter D_m was neither an appropriate microstructural descriptor for describing the largest pores connected with viscous fluid flow nor a correct one to identify the smallest dynamically connected pore sizes probed by electrical current flow ; Fig. IV.1(b), IV.1(e) and IV.1(h). D_v based and D_{iv} based REVs predictions all showed excellent agreement respectively with static viscous permeability k_0 and characteristic length Λ measurements over a large range of porosities ϕ ; Fig. IV.1(j) and IV.1(k).

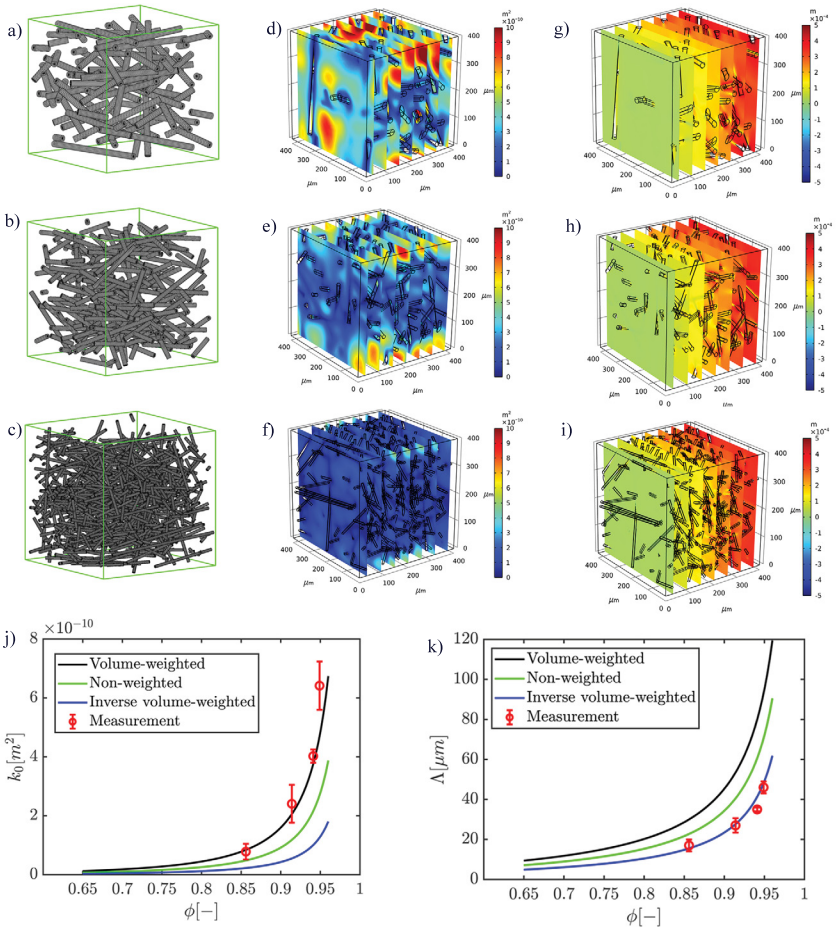

FIGURE IV.1 – Effect of polydispersity on the transport properties. (a)-(c) Three-dimensional random fibrous microstructures corresponding to the sample denoted F2 using volume-weighted, non-weighted, inverse volume-weighted average diameters, respectively. (d)-(f) Velocity fields expressed as local permeability ($k_{0zz}[m^2]$) corresponding to Stokes flow in the z direction with the REV reconstructed using (a) volume weighted, (b) non-weighted and (c) inverse volume-weighted average diameter. (g)-(i) Scaled potential field ($\varphi[m]$ corresponding to potential flow in the z direction [-] with the REV reconstructed using (a) volume weighted, (b) non-weighted and (c) inverse volume-weighted average diameter. (j) The static viscous permeability $k_0(m^2)$ of nonwoven fibrous materials (F1, F2, F3, F4) as a function of porosity ϕ(-). (k) The viscous characteristic length $\Lambda(\mu m)$ of nonwoven fibrous materials (F1, F2, F3, F4) as a function of porosity ϕ(-).

IV.4.2 Polydispersity effect on the transport properties of three-dimensional random fibrous microstructures

Polydispersity effect occurs when particles of varied sizes in the dispersed phase modifies the expected behavior of the corresponding system. The wide distribution of fiber diameters changes the transport parameters of a 3D-RF microstructure characterized by a sharply peaked distribution of fiber diameters, resulting is a non-conventional REV. Our previous works describe the Gamma-based distribution of fiber diameter configuration and confirms this effect in glass wool, cotton felts and PET felts' composites.[32, 116] Figure IV.2(a) illustrates the Gamma distribution shape of fiber diameters according to the equation

$$f(D;a,b) = \frac{1}{\Gamma(a)b^a} D^{a-1} e^{-\frac{D}{b}}, \tag{IV.1}$$

where D is the fiber diameter of the probability distribution function parameterized with the shape a ($a > 0$) and scale b ($b > 0$) parameters. Fig. IV.2(b) shows the geometry of 3D-RF structures with an increasing coefficient of variation $CV = 1/\sqrt{a}$ used as a measure of dispersion ; at $CV = 20\%$, $CV = 50\%$, and $CV = 100\%$. The corresponding porosity is equal to $\phi = 94.1\%$ and the mean fiber diameter is given by $D_m = ab = 14\mu m$. The REVs based on D_v and based on D_{iv} are presented in Fig. IV.2(c) and IV.2(d), respectively. Coefficient of variation was around 40% in the cotton felts case (F1-F4) and

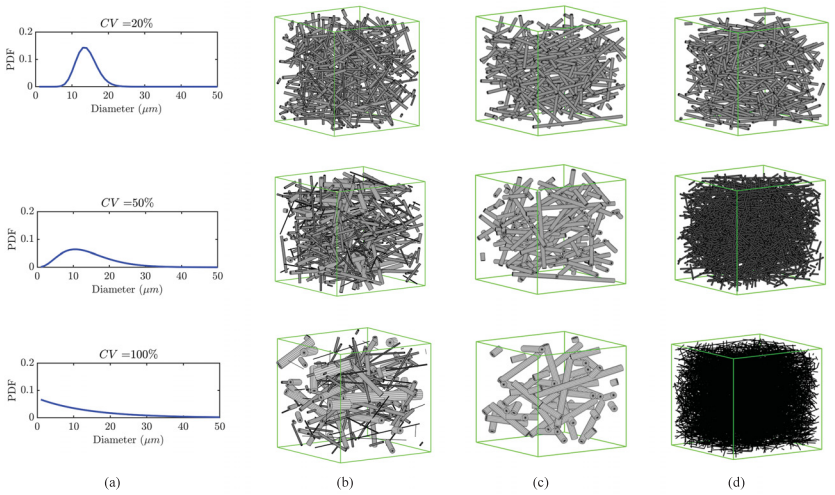

FIGURE IV.2 – Polydispersity effect on the representative elementary volumes of three-dimensional random fibrous microstructures. (a) The probability distribution function of Gamma-based fiber diameters ($D_m = 14\mu m$) for increasing coefficients of variation CV of fiber diameters ($CV = 20\%$, $CV = 50\%$, $CV = 100\%$). (b) Geometric reconstruction of corresponding three-dimensional random fibrous microstructures ($\phi = 94.1\%$). Geometric reconstructions of (c) D_v-based and (d) D_{iv}-based representative elementary volumes used to predict the viscous fluid flow and electrical current flow effective transport properties of polydisperse fibrous media.

30% in the PET felts one, and the orientation of fibers of the 3D-RF microstructures was

parameterized according to an additionally needed parameter Ω_{zz} ($0 \leq \Omega_{zz} \leq 1$) [5]. Therefore, assuming a Gamma-based distribution of fiber diameters, geometrical parameters of the model include porosity ϕ, mean fiber diameter D_m, coefficient of variation of the fiber diameters CV and angular orientation of fibers Ω_{zz}. There exist a strong analogy between the visco-inertial frequency-dependent response function of a Newtonian fluid-filled rigid porous medium [96], and its frequency-dependent thermal counterpart [106, 101]. Therefore, the D_v-based cell was simultaneously utilized as the REV to compute the static viscous permeability k_0 and the static thermal permeability k'_0. On the other hand, on the asymptotic high frequency range, the D_{iv}-based cell was used as the REV for the calculation of the viscous Λ and thermal Λ' characteristic lengths together with the tortuosity α_∞. The fiber diameters' dispersion effects for the D_v-based cell and D_{iv}-based cell is shown in Fig. IV.3. Figure IV.3 demonstrates a significant increase of the volume-weighted average diameter, D_v, with respect to the corresponding mean diameter D_m, for an increasing coefficient of variation CV of the Gamma-based law. This increase of D_v/D_m can be characterized by a polynominal function of second order with respect to CV. Meanwhile, the inverse volume-weighted diameter D_{iv} undergoes an exponential decrease as the coefficient of variation CV of the fiber diameters increases, due to the increasing amount of small fibers present in the probability distribution function for high levels of CV (Fig. IV.2a). This indicates that polydisperse 3D-RF microstructures having D_v and D_{iv} based cells as REVs can introduce drastic contrasts in the local characteristic sizes (D_v ; D_{iv}) and the corresponding asymptotic transport parameters (k_0, k'_0 ; Λ, Λ', α_∞) owing to their strong and different sensitivities to the extreme values of the distribution. These findings suggest that the polydisperse-based RF microstructures effectively exhibit a tuning effect for the design of sound absorbing fibrous materials.

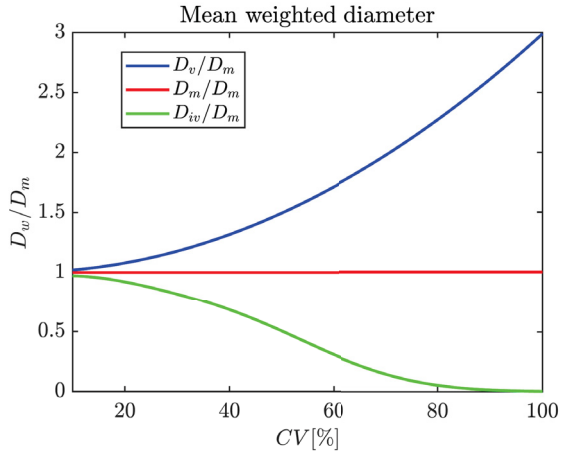

FIGURE IV.3 – Evolution of the volume-weighted average diameter D_v and the inverse volume-weighted average diameter D_{iv} as a function of the polydispersity degree P_d of a fiber diameters' distribution quantified through the coefficient of variation CV of a Gamma-based law at constant mean diameter D_m.

IV.4.3 Advantages

Replacing the monodisperse fiber diameters with polydisperse 3D materials can significantly enhance the viscous k_0 and thermal k_0' static permeabilities. It can also reduce the viscous Λ and thermal Λ' characteristic lengths, increase the sound absorption average (SAA), and creates subwavelength sound absorbers.

IV.4.3.1 Tuning transport parameters

In this study, we analyze the evolution of transport properties as a function of the coefficient of variation CV for two different families of composite microstructures : composite felts (F1-F4) and PET felts (B1-B2). Figure IV.4 illustrates the transport parameters of these 3D-RF microstructures when increasing the coefficient of variation CV of the fiber diameters (at unchanged porosities ϕ and orientation of fibers Ω_{zz}). We observe a non-linear increase in the dimensionless static viscous k_0/r_m^2 and thermal k_0'/r_m^2 permeabilities (with $r_m = D_m/2$), while the dimensionless viscous Λ/r_m and thermal Λ/r_m characteristic lengths show a non-linear decrease with CV, and both the ratio Λ'/Λ and the tortuosity α_∞ remain independent of the polydispersity (α_∞ is independent of the length scale of the microstructure). This suggests that controlling the polydispersity of fiber diameters through the coefficient of variation CV with the manufacturing process provides a new lever for optimizing sound-absorbing fibrous materials.

IV.4.3.2 Increasing sound absorption average

The sound absorption average at normal incidence (SAA_{NI}) of a material is computed with its sound absorption coefficients at normal incidence (SAC_{NI}) at 16 one-third octave bands f_i from 125 to 4500 Hz with

$$SAA_{NI}^{125-4000} = \frac{1}{16} \sum_{f_i=125}^{4500} SAC_{NI}(f_i), \tag{IV.2}$$

Here, the SAC_{NI} is calculated with the material of thickness L_s placed on a hard reflecting backing. Consequently, SAA_{NI} is a measure of the energy dissipated by visco-thermal losses in the material for a unit incident acoustic power. This single number rating is an important coefficient that can be used for characterizing the sound absorbing properties of porous materials in a large frequency range, including low frequencies. We have previously shown that using polydispersity can significantly modify the transport properties of 3D-RF microstructures at constant porosity ϕ and angular orientation Ω_{zz}. Figure IV.5 shows how the sound absorption average at normal incidence $SAA_{NI}^{125-4000}$ can be maximized by optimization of the CV from the initial set of studied materials (F1-F4 ; B1-B2). The increase in $SAA_{NI}^{125-4000}$ in 3D-RF microstructures is due to a larger fiber diameter polydispersity ($CV \simeq 75\%$) that allows for a strong contrast between the largest fibers that dominate transport phenomena in the low frequency regime (k_0 ; k_0') and the smallest fibers that govern transport phenomena in the high frequency regime (Λ, α_∞ ; Λ') ; see Tab. IV.1. Here, the optimization was based on a differential evolution algorithm as proposed elsewhere [117, 118]. The results show that the optimized 3D-RF materials (controlled

by polydispersity) exhibit lower viscous f_v and thermal f_t transition frequencies than the initial materials – which allowed visco-thermal dissipation mechanisms to occur in a lower frequency range.

In the previous calculations, the sound absorbing coefficient at normal incidence, SAC_{NI}, derives from the knowledge of the intrinsic transport parameters of the 3D-RF materials (k_0, k_0', Λ, Λ', α_∞). The frequency-dependent response functions, $\tilde{\rho}_{eq}(\omega)$ and $\tilde{K}_{eq}(\omega)$ are described as [96, 106, 101]

$$\tilde{\rho}_{eq}(\omega) = \frac{\alpha_\infty \rho_0}{\phi}\left[1 + \frac{\phi\eta}{i\omega k_0 \alpha_\infty \rho_0}\sqrt{1 + i\frac{4\alpha_\infty^2 k_0^2 \rho_0 \omega}{\eta \Lambda^2 \phi^2}}\right], \tag{IV.3}$$

and

$$\tilde{K}_{eq}(\omega) = \frac{\gamma P_0/\phi}{\gamma - (\gamma-1)\left[1 - i\frac{\phi\kappa}{k_0' C_p \rho_0 \omega}\sqrt{1 + i\frac{4k_0'^2 C_p \rho_0 \omega}{\kappa \Lambda'^2 \phi^2}}\right]^{-1}}, \tag{IV.4}$$

where $\tilde{\rho}_{eq}(\omega)$ is the equivalent dynamic density, $\tilde{K}_{eq}(\omega)$ is the equivalent bulk modulus, $\omega = 2\pi f$ is the angular frequency, i is the imaginary unit, ρ_0 is the mass density of air, η is the dynamic viscosity of air, P_0 is the atmosphere pressure, $\gamma = C_p/C_v$ is the ratio of heat capacities at constant pressure and volume, and κ is the heat conductivity of air.

By knowing the visco-inertial $\tilde{\rho}_{eq}(\omega)$ and thermal $\tilde{K}_{eq}(\omega)$ response functions of the equivalent fluid of the porous medium, we can determine the wave number $\tilde{q}_{eq}(\omega)$ and the characteristic impedance $\tilde{Z}_{eq}(\omega)$ of the material,

$$\tilde{q}_{eq}(\omega) = \omega\sqrt{\tilde{\rho}_{eq}(\omega)/\tilde{K}_{eq}(\omega)}, \tag{IV.5}$$

$$\tilde{Z}_{eq}(\omega) = \sqrt{\tilde{\rho}_{eq}(\omega)\tilde{K}_{eq}(\omega)}. \tag{IV.6}$$

At normal incidence, the surface impedance $\tilde{Z}_s(\omega)$ and sound absorption coefficient $SAC_{NI(\omega)}$ of a porous material of thickness L_s, backed by a rigid and impervious wall, for any angular frequency ω, are provided by

$$\tilde{Z}_s(\omega) = -i\tilde{Z}_{eq}\cot(\tilde{q}_{eq}L_s), \tag{IV.7}$$

$$SAC_{NI} = 1 - \left|\frac{\tilde{Z}_s - Z_0}{\tilde{Z}_s + Z_0}\right|^2, \tag{IV.8}$$

where $Z_0 = \rho_0 c_0$ is the impedance of the air and c_0 is the sound speed in air.

In Fig. IV.5, it can be observed that there is a significant change in the thickness-to-wavelength ratio L_s/λ_0, where $\lambda_0 = \omega_0/c_0$, and ω_0 is the angular frequency at the first peak absorption. In fact, optimized polydispersed-based 3D-RF microstructures show ratios L_s/λ_0 that can achieve values lower than 1/32 (F4 and B2) - note that the typical ratio of

conventional porous materials is around 1/4. This result can be seen as the signature of a certain class of metamaterials called subwavelength material (or slow-sound material). In fact, the optimized properties increase $\tilde{\rho}_{eq}$ and decrease $\tilde{K}_{eq}$. Consequently, the sound speed in the equivalent medium is reduced. These results demonstrate that the use of controlled fiber diameter polydispersity, such as that provided with a gamma distribution shape and characterized with a $CV \sim 80\%$, has the potential to enhance the performance of sound-absorbing nonwoven materials.

		CV (%)	ϕ (−)	k_0 ($\times 10^{-10} m^2$)	k'_0 ($\times 10^{-10} m^2$)	α_∞ (−)	Λ (μm)	Λ' (μm)	f_v (Hz)	f_t (Hz)	$SAA_{NI}^{125-4500}$ (%)
F1	Init.	40.3	0.948	4.5	12.1	1.022	48	84	4668	2557	42
	Opt.	73.3	0.948	11.1	27.8	1.022	6.9	12	2018	1112	48
F2	Init.	39.8	0.941	3.9	9.9	1.026	42	74	5684	3103	35
	Opt.	74.6	0.941	10.0	27.1	1.026	5.3	9.4	2213	1209	43
F3	Init.	41.9	0.914	2.1	5.1	1.042	25	47	10102	5850	27
	Opt.	72.1	0.914	4.7	13.1	1.042	3.3	6.1	4533	2631	34
F4	Init.	38.9	0.856	0.7	1.6	1.077	15	28	25286	17463	14
	Opt.	73.8	0.856	1.9	5.1	1.077	1.3	2.4	9998	7073	21
B1	Init.	26.6	0.888	2.7	6.3	1.056	42	79	7215	4601	20
	Opt.	75.5	0.888	9.6	23.1	1.056	3.3	6.1	2116	1356	32
B2	Init.	33.1	0.76	0.7	1.2	1.144	15	29	21495	21023	7
	Opt.	77.6	0.76	2.4	4.3	1.144	0.8	1.6	6690	6518	15

TABLE IV.1 – Transport parameters evolution (ϕ, k_0, k'_0, Λ, Λ', α_∞) before (Init.) and after (Opt.) optimization of polydispersity (CV) in the three-dimensional random fibrous microstructures of cotton felts (F1-F4) and PET felts (B1-B2). f_v and f_t represent the visco-inertial and thermal transition frequencies which have been significantly reduced after optimization, which consists in maximizing the sound absorption average at normal incidence across the 16 one-third octave bands (f_i) ranging from 125 to 4500 Hz, $SAA_{NI}^{125-4000}$ [relative increase : F1(14%), F2(23%), F3(26%), F4(50%), B1(60%), B2(114%)].

IV.4.3.3 Enhancing diffuse field sound absorption

Sound absorbing targets present in the industry for a porous material generally corresponds to a diffuse field (DF) acoustical excitation, satisfying $SAA_{DF} \geq 0.8$, for $f_i \geq f_t$, where f_t is a given one-third octave band. Lowering f_t can lead to various issues in designing sound absorbing materials, as absorbing low frequencies is a challenge that suggests targets of increasing difficulty : $f_t = 1600Hz$ (Target 1), $f_t = 1250Hz$ (Target 2), $f_t = 1000Hz$ (Target 3), $f_t = 800Hz$ (Target 4) and $f_t = 630Hz$ (Target 5). These targets are defined without air gap behind the materials (hard-backed configuration), and the recommended or targeted thickness and mass are usually not mentioned, suggesting that the targets need to be reached with the lowest weight and cost. The sound absorption coefficient in diffuse field, SAC_{DF}, is described as :

$$SAC_{DF} = \frac{\int_{\theta_{min}}^{\theta_{max}} SAC(\omega,\theta)\cos\theta\sin\theta d\theta}{\int_{\theta_{min}}^{\theta_{max}} \cos\theta\sin\theta d\theta}, \tag{IV.9}$$

where $\theta_{min} = 0^o$ and $\theta_{max} = 90^o$ are the selected diffuse field integration limits.
$SAC(\omega,\theta) = 1 - \left|\frac{\tilde{Z}_s(\omega,\theta)\cos\theta - Z_0}{\tilde{Z}_s(\omega,\theta)\cos\theta + Z_0}\right|^2$ is the sound absorption coefficient at oblique incidence,

$\tilde{Z}_s(\omega,\theta) = -i\tilde{Z}_{eq}(\tilde{q}_{eq}/\tilde{q}_x)\cot(\tilde{q}_{eq}L_s)$ is the surface impedance at oblique incidence with $\tilde{q}_x = \sqrt{\tilde{q}_{eq}^2 - q_t^2}$ the longitudinal wave number and $q_t = q_0 \sin\theta$ the transverse wave number.

Our research demonstrates that 3D-RF materials, specifically polydisperse with controlled $CV \sim 75\% - 79\%$ can serve as effective sound-absorbing materials in diffuse field to achieve the required industrial targets. By simulating the SAC_{DF} from the initial felts (F1-F4 ; B1-B2), we identified the optimal coefficient of variation CV allowing us to reach the targets of increasing level of difficulty with the minimal thickness. The results, shown in Fig. IV.6a for the case of cotton felt F1, revealed that none of the targets can be reached from the initial microstructure ($CV = 40.3\%$) and the thickness of the sample ($L_s = 20$ mm). Fig. IV.6b demonstrated an achievement of Target 1 by using a CV of 78% with a significant reduction of the sample thickness ($L_s = 11$ mm). We obtained similar polydispersity results for the other targets of increasing difficulty (Target 2, $CV = 79\%$, Fig. IV.6c ; Target 3, $CV = 78\%$, Fig. IV.6d ; Target 4, $CV = 77\%$, Fig. IV.6e ; Target 5, $CV = 75\%$, Fig. IV.6f). However, the sample thicknesses had to be increased (Target 2, $L_s = 13$ mm, Fig. IV.6c ; Target 3, $L_s = 16$ mm, Fig. IV.6d ; Target 4, $L_s = 20$ mm, Fig. IV.6e ; Target 5 $L_s = 27$ mm, Fig. IV.6f. To better appreciate the performance that has been obtained by increasing and controlling the degree of polydispersity P_d through the coefficient of variation CV of the Gamma law, the results can be plotted in terms of the thickness-to-wavelength ratio, L_s/λ_0. Using a controlled degree of polydispersity allowed us to reach sub-wavelength sound absorption in the diffuse field by lowering the maximum sound absorption peak below the quarter-wavelength resonance frequency ($L_s/\lambda_0 = \frac{1}{4}$), indicating a greater ability to absorb low-frequency sound. Therefore, using 3D-RF materials with controlled polydispersity to efficiently absorb low-frequency sound is an important approach as it *a priori* does not require substantial modifications of the manufacturing processes.

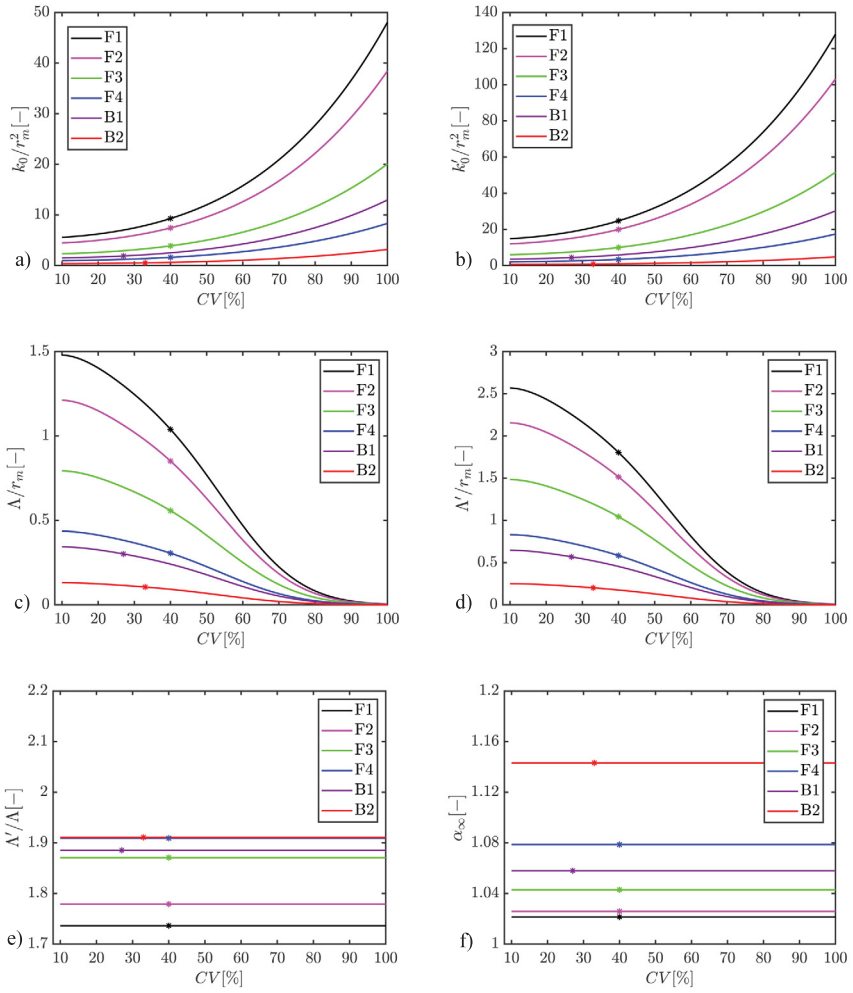

FIGURE IV.4 – Dimensionless transport parameters as a function of the coefficient of variation CV of fiber diameters for cotton felts (F1-F4) and PET felts (B1-B2). The porosities ϕ and orientation of fibers Ω_{zz} of each felt are unchanged with CV and taken from measurement.[116] The dots correspond to the experimentally determined values of CV in the initial state of polydispersity.

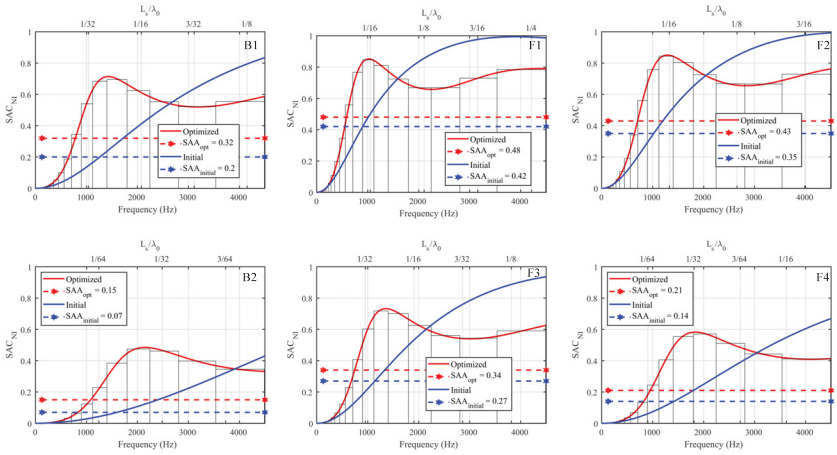

FIGURE IV.5 – The sound absorbing coefficient at normal incidence, SAA_{NI} as a function of frequency for the two families of felts studied in this work : Cotton felts (F1-F4) and PET felts (B1-B2). The SAA_{NI} responses obtained prior to modification of the polydispersity (coefficient of variation CV) are shown with a blue line. The red line represents the SAA_{NI} abtained after optimization of the polydispersity by maximizing the SAA_{NI} between the third octave bands from 125 to 4500 Hz. The two dotted lines correspond to the associated single number ratings before (blue) and after (red) optimization.

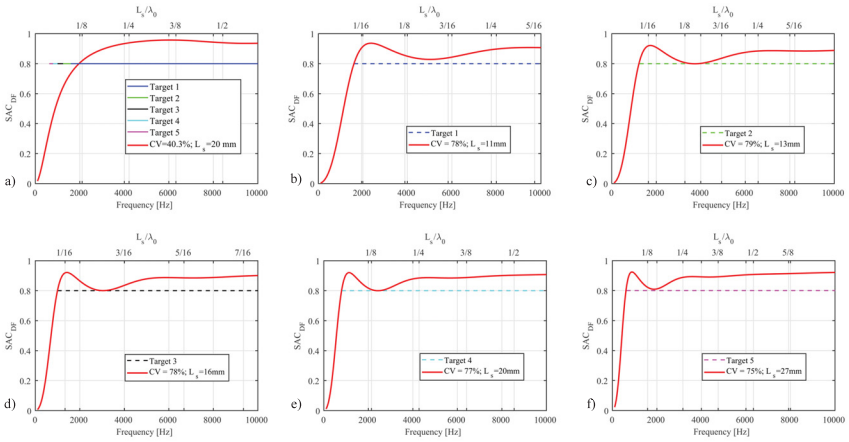

FIGURE IV.6 – Diffuse field sound absorbtion coefficient SAC_{DF} as a function of frequency for cotton felt F1 : (a) initial configuration with $CV = 40.3\%$ and $L_s = 20mm$. The next panels (b) to (f) represent the optimized configurations satisfying targets of increasing difficulty when the polydispersity degree (CV) is allowed to be increased as a microstructural optimization lever, for the targets listed in the legend.

IV.5 Outlook and perspective

In this section, we discuss the challenges of this research area and a possible roadmap for a future work.

IV.5.1 Challenges from the manufacturing process

3D-RF microstructures, including cotton felts and PET felts, are commonly manufactured by techniques coming from the textile industry. After their selection, the recycled (shoddy, PET) or noble (bicomponent) fibers are provided within different fineness specified by the *dtex* unit which enables a linear density estimates of fiber size, such that a corresponding fiber diameter can be determined. However, the model we developed from which we have evidenced a strong potential of optimization is not without drawbacks, as it relies on continuous distribution of fiber diameters. Fig. IV.7 provides the distribution of fiber diameters obtained through SEM images that corresponds to the F1 cotton felt sample and compares this distribution with the one required to reach Target 4 ($CV = 77\%$, same sample thickness). On the left side of the distribution, the fibrous material presents a relatively high number of very thin fibers. The asymmetry of the probability distribution function suggests a mix of at least three or four initial families of fibers of different linear densities ($dtex$) with lower CV ($20\% - 30\%$) to achieve the required distribution. However, the fiber distribution of the corresponding manufactured material may exhibit discontinuity compared to the targeted Gamma law. This discontinuity is not necessarily problematic if, as expected, the microstructural descriptors governing the physics of the transport parameters are D_v and D_{iv}. Also, the experimental validation of the model is still incomplete, since it relies on samples already manufactured which do not correspond to the expected optimal behavior ($CV \sim 30\% \neq CV \sim 77\%$).

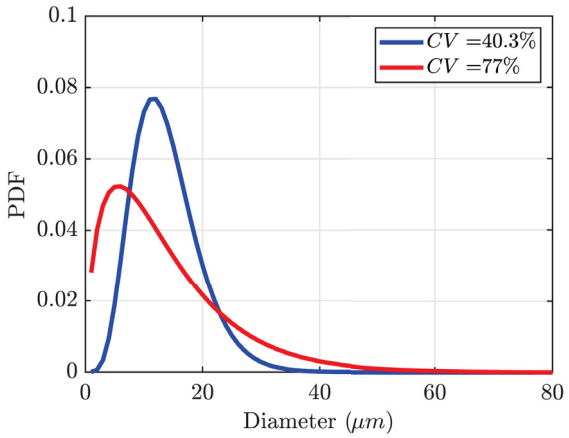

FIGURE IV.7 – Comparison of the Gamma distribution of fiber diameters obtained through SEM images ($CV = 40.3\%$), cotton felt F1 and the Gamma distribution of fiber diameters required to reach Target 4 ($CV = 77\%$)

IV.5.2 Future roadmap

In order to address the challenges associated with discontinuity and validation of the model in highly polydispersed 3D-RF microstructures, a crucial aspect of our future roadmap involves the development of a manufacturing method that enables the precise and controlled elaboration of a relatively continuous distribution of polydisperse fiber diameters with $CV \sim 77\%$ from a chosen reduced set of fiber families with $CV \sim 30\%$.

Another promising method for achieving continuous fiber diameter distribution with a high degree of polydispersity is Melt-Spun Fibers (MSF) [119]. The melt spinning technique is a mature method for manufacturing polymer fibers from thick filaments $\sim 100\mu m$ to submicrometric fibers. The method is inexpensive and can offer the scalable production of 3D-RF microstructures as a chosen polydispersity degree P_d. In our forthcoming work, we aim to leverage MSF-methods on a chosen basis of polydisperse fiber diameters in our experiments to achieve improved 3D-RF structures with controlled distribution of fiber diameters.

IV.6 Summary

In summary, this article highlights the potential of using three-dimentional random fibrous microstructures with various distributions of fiber diameters as a way to control visco-thermal dissipation mechanisms in sound absorbing materials. This approach offers numerous advantages including tuning transport parameters across a broad range of values, enhancing the sound absorption average, achieving targets of sound absorption in diffuse field with increasing levels of difficulty, and sub-wavelength sound absorption. However, challenges persist, such as manufacturing a continuous distribution of fiber diameters with prescribed properties. To overcome this challenge, we suggest reconstructing the prescribed distribution with a limited set of three or four families of fibers carefully selected, or exploring the synthesis of a distribution of fiber diameters through the melt spinning technique. These perspectives offer promising avenues for further advancements in the field of utilizing 3D-RF microstructures for subwavelength sound absorbing materials.

Acknowledgments

This work was supported by the Association Nationale de la Recherche et de la Technologie and Adler Pelzer Group under convention Cifre No. 2020/0122 and the Natural Sciences and Engineering Research Council of Canada (Ref. RGPIN-2018-06113). We greatly acknowledge the fruitful discussions with Jean-Yves Curien during the course of this work.

Chapitre V

Conclusion générale

Les travaux réalisés dans cette thèse ont porté sur la mise en relation entre structures, propriétés acoustiques et processus de fabrication de matériaux fibreux non tissés. Pour mener à bien cette étude, deux familles de milieux fibreux composites ont été étudiées. La première est issue de fibres textiles recyclées, mélangées à des fibres dites bicomposants (feutres coton) tandis que la seconde est constituée de fibres issues du recyclage de PET, elles-mêmes mélangées à des fibres bicomposants (feutre PET). L'ensemble de ces fibres contribue à la polydispersité du milieu. Un renforcement de la tenue mécanique des feutres est obtenu par chauffage, à différents taux de compression, la partie extérieure des fibres bicomposants fondant à plus basse température. Ces matériaux composites sont ensuite caractérisés aux échelles micro au moyen d'images MEB (distributions de diamètres et d'orientations angulaires) et macro (propriétés de transport et d'absorption sonore). Les données collectées à l'échelle micro permettent de construire des modèles de microstructures idéalisées, qui reproduisent les caractéristiques géométriques observées, sur la base desquels les propriétés macroscopiques sont déterminées par homogénéisation numérique. La comparaison entre les paramètres de transport mesurés et calculés est satisfaisante lorsque (1) les diamètres sont pondérés en volume pour la prédiction des paramètres à basses fréquences (perméabilité visqueuse k_0 et thermique k_0') ; (2) les diamètres sont pondérés en volume inverse pour la détermination des paramètres à hautes fréquences (longueurs visqueuses Λ et thermiques Λ', ainsi que la tortuosité α_∞). Il en résulte que les descripteurs microstructuraux appropriés sont le diamètre moyen pondéré en volume D_v et le diamètre moyen pondéré en volume inverse D_{iv}, respectivement pour les comportements asymptotiques à basses et hautes fréquences. Lorsqu'ils sont combinés aux distributions d'orientation angulaire des fibres et à la porosité, ces indicateurs géométriques permettent de prédire les propriétés de transport et le coefficient d'absorption sonore de ces non tissés sans paramètre d'ajustement. Cela permet de répondre à la question de recherche de cette thèse en identifiant les VERs associées aux propriétés physiques d'intérêt pour un milieu fibreux polydisperse et localement hétérogène. Il s'agit du résultat central de cette thèse. Sur le plan physique, cela s'interprète de la manière suivante : en basses fréquences, les épaisseurs des couches limites visqueuse et thermique sont importantes, les échanges visqueux et thermiques se font par l'intermédiaire des canaux les plus larges de la microstructure. En hautes fréquences, les épaisseurs des couches limites visqueuse et thermique sont plus fines, la signature acoustique est sensible à l'ensemble de

la microstructure, en particulier aux étranglements les plus petits. Une reconstruction de VERs avec D_v et D_{iv} comme diamètres moyens des fibres permet de bien rendre compte de ces phénomènes ; car à une porosité donnée, $D_v \geq D_m$ et $D_{iv} \leq D_m$ ce qui implique l'introduction d'un faible nombre de fibres de grand diamètre à basse fréquence et d'un grand nombre de fibres de petit diamètre à haute fréquence pour expliquer les signatures acoustiques mesurées sur des échantillons localement hétérogènes (où D_m est le diamètre moyen sans pondération). À partir de ce résultat, il a effectivement été possible d'étendre les prédictions du modèle à une large gamme de porosités, d'orientations et surtout de polydispersités, ce qui a permis de disposer d'un outil d'optimisation.

Il est clair que les contributions originales annoncées en introduction ont été réalisées. La première contribution originale consiste au développement et à la vérification des VERs de milieux fibreux polydisperses. La deuxième contribution originale avait pour but de résoudre un problème d'optimisation en utilisant le degré de polydispersité comme variable.

Cette approche s'est avéré donner des résultats très encourageants, en menant à des gains significatifs en absorption sonore et en permettant de mettre en évidence des comportements en absorption sublongueur d'onde. La troisième contribution est d'ordre expérimentale et méthodologique. Il s'agit de proposer une technique permettant de fournir une estimation expérimentale des propriétés de transport à hautes fréquences, pour les milieux fibreux très résistifs. En s'appuyant sur des conjectures théoriques approchées mais robustes, et sur des informations induites par la morphologie des systèmes étudiés, la technique proposée s'est avéré fructueuse et a permis d'étendre les méthodes de caractérisation indirectes à une gamme de valeurs pour lesquelles des hypothèses de validité habituelles n'étaient pas respectées.

Il est également clair qu'il reste encore beaucoup à faire. Nous avons proposé un modèle polydisperse et validé son utilisation pour une gamme restreinte de coefficients de variation ; mais une validation systématique pour des coefficients de variation élevés reste à mener. Différentes voies devraient aussi être explorées à l'avenir ; les études multiphysiques sont encore assez peu développées et une généralisation de l'approche menée dans cette thèse aux propriétés thermiques (conduction, convection, rayonnement) et élastiques reste à faire. Cela implique la mise en place de bancs de mesure dédiés et de caractérisations morphologiques où les techniques d'imagerie avancées puissent être utilisées pour alimenter les modèles numériques. Il s'agit d'un champ de recherches fascinant, où dialoguent théorie, expérimentations fines, et méthodes numériques.

Annexes

Annexe A

Protocol of preparation and cutting of samples prior to the acquisition of SEM images

For non-conductive materials like cotton and PET felts, a high performance metallizer by cathode sputtering was used, coupled with a magnetron source (Cressington sputter coater 208HR) ; which made it possible to deposit a conductive film of a few nanometers (controlled by a quartz probe, here a Cressington MTM 20) on the surface of the samples. To verify the homogeneity of the microstructure, specifically in terms of fiber diameters, two cubic specimens with dimensions of 10 mm were taken randomly from different locations of the studied panels (provided with dimensions of 210 mm x 297 mm). On each extracted cubic specimen, SEM images were then acquired to fully scan two horizontal and two vertical planes (situated on opposite faces of the cubic specimens), using a magnification factor of 100 times. For each plane (four planes of interest on each cubic sample), 10 sub-images were randomly extracted to directly measure the morphological parameters of interest in the fibrous network, using the FiJi software [120] with a resolution of 0.56 μm per pixel. These parameters include the diameters of the fibers and their orientation angles in the horizontal and vertical planes, as shown in Fig. III.2.

Annexe B

Experimental approach used to estimate the viscous and thermal characteristic lengths

The so-called Kozeny-Carman resistivity formula, introduced by Henry et al. [89] in their Eq. (15), is given by :

$$\sigma_{KC} = \frac{8\alpha_\infty \eta}{\phi \Lambda'^2_{est}}, \tag{B.1}$$

where Λ'_{est} is a characteristic dimension. Typically, we can assume that the value of Λ'_{est} is between Λ and Λ', and that σ_{KC} is an estimate of σ. From the Kozeny-Carman formula, a value of Λ'_{est} could be obtained using experimental measurements of ϕ, σ, and α_∞. Therefore, Λ'_{est} corresponds to the following equation :

$$\Lambda'_{est} = \sqrt{\frac{8\alpha_\infty \eta}{\phi \sigma}}. \tag{B.2}$$

For a typical porous material, assuming macroscopic homogeneity, the following inequality $\Lambda \leq \Lambda'_{est} \leq \Lambda'$ is expected. As a first approximation, the simulated ratio $r = \Lambda'/\Lambda$ can be used to deduce Λ'_{est} from Λ_{est}. The following formula is applied :

$$\Lambda_{est} = \frac{\Lambda'_{est}}{r}, \tag{B.3}$$

Here, we used r = 1.61, 1.69, 1.70, 1.65, 1.68 and 1.45 corresponding to the simulated values for F1, F2, F3, F4, B1, and B2, respectively.

Annexe C

Geometrical reconstruction

Based on the results of microstructure characterization, a random fibrous network is reconstructed as follows :

1. A random point is chosen in a unit cube of known size L (the unit cell).
2. From this random point M_i, a vector $\overrightarrow{p}$ is determined, which passes through this random point (having as zenithal θ and azimuthal φ angles, randomly selected values from the measured probability density functions).
3. Based on the knowledge of $\overrightarrow{p}$, the coordinate of the intersecting points P_1P_2 with the unit cube are derived.
4. Next, the segment P_1P_2 is cut at M_i, from which one can obtain continuity of the solid phase on the opposite faces of the unit cube. This is done by translation of a sub-segment M_iP_2. For instance, Fig. C.1a illustrates this procedure. Here, M_iP_2 is translated to ensure continuity of P_1 and P_2 (by horizontal translation of the unit cube).
5. Knowing the fiber diameter distribution obtained from measurements, a fiber radius is then randomly drawn from the corresponding Gamma fit distribution (Fig. C.1b).

The algorithm which is reported in Fig. C.2 allows iterative alteration of the fiber number N_f and the domain size L_i until porosity is converged towards the experimentally determined value. By applying the algorithm with 100 iterations for each domain size L/D_m, the result displayed in Fig. III.5 shows that it is possible to control both the average porosity and the standard deviation of a reconstructued three-dimensional fibrous structure. L_i was chosen to ensure that the ratio ϵ of the standard deviation over the mean value of the targeted porosity is less than 0.1%.

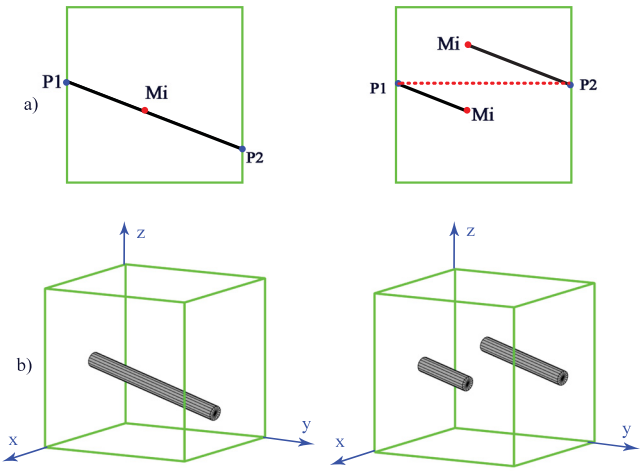

FIGURE C.1 – Illustration of some important steps by which a representative volume element with periodic boundaries can be constructed.

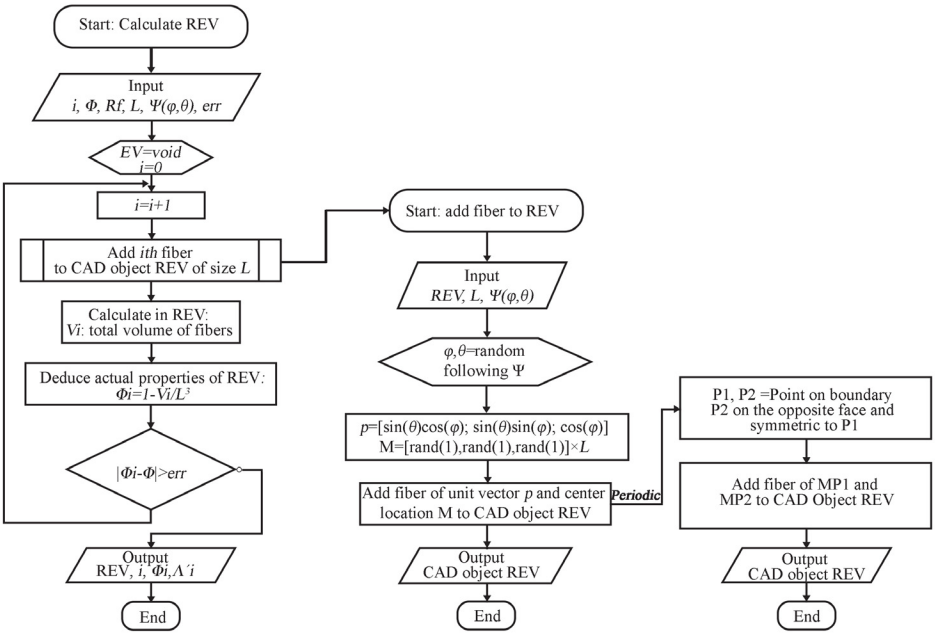

FIGURE C.2 – Algorithm used to calculate the domain size in order to reconstruct microstructures of the random fibrous materials under study with periodic boundary conditions.

Annexe D

Elementary transport processes and acoustical macro-behavior

In this section, we focus on identifying macroscopic transport properties by addressing local equations with adequate boundary conditions. These equations are classically derived from an asymptotic analysis.
Note that, the open porosity ϕ and the thermal characteristic length Λ' are purely geometric parameters that can be directly calculated from the microstructure and determined by integration :

$$\phi = \frac{\int_{\Omega_f} dV}{\int_{\Omega} dV}, \tag{D.1}$$

$$\Lambda' = 2\frac{\int_{\Omega_f} dV}{\int_{\partial\Omega} dS}, \tag{D.2}$$

where Ω is the volume element (VE), Ω_f is the fluid volume and $\partial\Omega$ denotes the solid border of a solid element.
The remaining transport parameters are determined numerically by applying spatial averaging to the solution fields corresponding to the problems mentioned below.

1. Viscous permeability
   At low frequencies, also known as the static regime, viscous forces are dominant. The low Reynold's number flow of an incompressible Newtonian fluid in this regime is governed by the steady-state Stokes equation :

$$\begin{aligned} \eta\Delta\mathbf{v} - \nabla p = -\nabla p^m \quad &\text{in} \quad \Omega_f, \\ \nabla\cdot\mathbf{v} = 0 \quad &\text{in} \quad \Omega_f, \\ \mathbf{v} = 0 \quad &\text{on} \quad \partial\Omega, \\ \mathbf{v} \quad &\text{and}\, p \,\text{are}\, \Omega-\text{periodic}; \end{aligned} \tag{D.3}$$

   where $\mathbf{v}, p$, and η are the velocity, pressure, and viscosity of the fluid, respectively. The term ∇p^m is a macroscopic pressure gradient acting as a driving force, $\partial\Omega$ is the fluid-solid interface. The macroscopic pressure gradient is specified in the form,

$$\nabla p^m = |\nabla p^m|\mathbf{e}. \tag{D.4}$$

Since the Eq. D.3 is linear, it can be shown that

$$\phi \langle \mathbf{v} \rangle = -\frac{\mathbf{K}}{\eta} \cdot \nabla p^m, \tag{D.5}$$

where $\mathbf{K}$ is a positive-definite symmetric tensor, the symbol $\langle \bullet \rangle$ indicates a fluid-phase averaging, that is

$$\langle \bullet \rangle = \frac{1}{\Omega_f} \int_{\Omega_f} \bullet \, dV.$$

The static permeability k_0 along the direction specified by the unit vector is calculated as,

$$k_0 = (\mathbf{K} \cdot \mathbf{e}) \cdot \mathbf{e} = -\frac{\eta\phi}{|\nabla p^m|} \langle \mathbf{v} \rangle \cdot \mathbf{e}. \tag{D.6}$$

2. Viscous characteristic length and tortuosity
At high frequencies, when ω is large enough, inertial forces dominate over viscous forces. The fluid tends to behave as an ideal fluid, having no viscosity. In this case, the inertial flow problem is analogue to the problem of electric conduction of a conducting fluid saturating an insulating porous structure :

$$\begin{aligned} \mathbf{E} = \mathbf{e} - \nabla\varphi \quad &\text{in} \quad \Omega_f, \\ \nabla \cdot \mathbf{E} = 0 \quad &\text{in} \quad \Omega_f, \\ \mathbf{E} \cdot \mathbf{n} = 0 \quad &\text{on} \quad \partial\Omega, \\ \varphi \text{ is } \Omega - \text{periodic}, & \end{aligned} \tag{D.7}$$

where $\mathbf{e}$ is a global unit electric field, while $\mathbf{E}$ is the electric field solution of the boundary problem, $-\nabla\varphi$ is the scalar electrostatic potential and $\mathbf{n}$ is local unit normal vector directed into the pore space.
Then, the components of the high frequency tortuosity tensor $\alpha_{\infty ij}$ can be obtained from

$$e_i = \alpha_{\infty ij} \langle E_j \rangle . \tag{D.8}$$

In the case of isotropy, the components of the tensor simplify to the diagonal form $\alpha_{\infty ij} = \alpha_\infty \delta_{ij}$. The tortuosity can also be determined by calculating the mean square value of the local electric field through

$$\alpha_\infty = \frac{\langle \mathbf{E} \cdot \mathbf{E} \rangle}{\langle \mathbf{E} \rangle \cdot \langle \mathbf{E} \rangle}. \tag{D.9}$$

The viscous characteristic length Λ can also be determined (for an isotropic medium) by

$$\Lambda = 2\frac{\int_{\Omega_f} \mathbf{E} \cdot \mathbf{E} \, dV}{\int_{\partial\Omega} \mathbf{E} \cdot \mathbf{E} \, dS}. \tag{D.10}$$

3. Thermal permeability
   Under the excitation of an external, harmonic source, with perfect absorbing conditions at the fluid-solid interface, the static thermal permeability is obtained from the equation

$$k_0' = \phi \langle u \rangle , \tag{D.11}$$

   where the scaled, Ω-periodic temperature field u, is the solution to the Poisson equation

$$\begin{aligned} \Delta u &= -1 \quad \text{in} \quad \Omega_f, \\ u &= 0 \quad \text{on} \quad \partial\Omega. \end{aligned} \tag{D.12}$$

   Here u is presumed to be periodic with a period L_i across the three spatial directions. The parameter k_0' is a positive definite scalar that is solely dependent on the geometry of the medium.

D.1 Acoustical macro-behavior

Significant semi-phenomenological models with visco-thermal dissipation mechanisms were developed by Johnson et al. [96] and Lafarge et al. [101]. In these works, the assumption of a rigid solid skeleton was made *apriori*. Johnson et al. and Lafarge et al. proposed that two general expressions for the frequency-dependence of the visco-inertial and thermal exchanges between the frame and the saturating fluid can be established with two sets of parameters (Λ, k_0, α_∞, ϕ) and (Λ', k_0', ϕ). The model is consistent with the frequency dependence of the first two leading terms of the exact result for high frequencies, but only one term for low frequencies. Both numerical simulations and experiments have demonstrated that the model by Johnson et al. and Lafarge et al., known as the JCAL model, is very robust (although not exact). In this section, we provide a summary of the JCAL model, as a mean of prediction of the sound absorption of polydisperse fibrous media.
For porous materials having a rigid and motionless skeleton, the equivalent dynamic mass density $\tilde{\rho}_{eq}(\omega)$ and the equivalent dynamic bulk modulus $\tilde{K}_{eq}(\omega)$ of the material are computed as

$$\tilde{\rho}(\omega) = \frac{\alpha_\infty \rho_0}{\phi} \left[1 + \frac{\phi\sigma}{i\omega\alpha_\infty\rho_0} \sqrt{1 + i\frac{4\alpha_\infty^2 \eta \rho_0 \omega}{\sigma^2 \Lambda^2 \phi^2}} \right], \tag{D.13}$$

and

$$\tilde{K}_{eq}(\omega) = \frac{\gamma P_0/\phi}{\gamma - (\gamma-1)\left[1 - i\frac{\phi\kappa}{k_0' C_p \rho_0 \omega}\sqrt{1 + i\frac{4k_0'^2 C_p \rho_0 \omega}{\kappa \Lambda'^2 \phi^2}}\right]^{-1}}. \tag{D.14}$$

In these equations, $\sigma = \mu/k_0$ is the (through plane) airflow resistivity, ρ_0 is the density of air, P_0 the atmospheric pressure, $\gamma = C_p/C_v$ the ratio of heat capacities at constant pressure and volume, i the imaginary unit and $\omega = 2\pi f$ the angular frequency. The wave number $\tilde{q}_{eq}(\omega)$ and the characteristic impedance $\tilde{Z}_{eq}(\omega)$ are then given by :

$$\tilde{q}_{eq}(\omega) = \omega\sqrt{\tilde{\rho}_{eq}(\omega)/\tilde{K}_{eq}(\omega)}, \tag{D.15}$$

$$\tilde{Z}_{eq}(\omega) = \sqrt{\tilde{\rho}_{eq}(\omega)\tilde{K}_{eq}(\omega)}. \tag{D.16}$$

The normal incidence surface impedance is expressed by

$$\tilde{Z}_s = -i\tilde{Z}_{eq}\cot\left(\tilde{q}_{eq}L_s\right). \tag{D.17}$$

The sound absorption coefficient at normal incidence of thickness L_s follows :

$$SAC_{NI} = 1 - \left|\frac{\tilde{Z}_s - Z_0}{\tilde{Z}_s + Z_0}\right|^2, \tag{D.18}$$

where $Z_0 = \rho_0 c_0$ is the impedance of the air, c_0 is the sound speed in air.

Annexe E

Characteristic transition frequencies

The viscous transition frequency f_v characterises the transition between the high and low frequency limits of the dynamic viscous permeability $k_{(\omega)}$ (Johnson et al. [45]). One could estimate f_v using the following simple formula

$$f_v = \frac{\phi\sigma}{2\pi\rho_0\alpha_\infty}, \tag{E.1}$$

where $\rho_0 = 1.213 \times 10^3 (kg/m^3)$ is the density of air at rest and normal conditions. Here, low frequency means $f \ll f_v$, whereas high frequency corresponds to $f \gg f_v$.
As a thermal counterpart of f_v, thermal transition frequency f_t characterises the transition between high and low frequency limits of the dynamic thermal permeability $k'(\omega)$ (Lafarge et al. [101]) :

$$f_t = \frac{\phi\kappa}{2\pi k'_0 C_p}, \tag{E.2}$$

where $\kappa = 2.5 \times 10^{-2} (W/m \cdot K)$ is the air heat conductivity, $C_p = 1.219 \times 10^3 (J/K)$ is the Isobaric heat capacity of air.
Low frequencies refers to $f \ll f_t$ whereas high frequencies must be understood as $f \gg f_t$. From these simple equations [Eqs. (E.2)-(E.1)] and the results in Tab. III.5, the characteristic transition frequencies of the materials studied are calculated and reported throughout Tab. E.1. These values are useful to show that the high frequency behavior is barely measurable with a standard impedance tube.

Samples	$f_v(Hz)$	$f_t(Hz)$
F1	3488 ± 446	4761 ± 610
F2	5454 ± 312	7491 ± 439
F3	8802 ± 2353	12431 ± 333
F4	24664 ± 11018	34925 ± 11908
B1	5565 ± 510	8051 ± 750
B2	18147 ± 3867	49614 ± 10766

TABLE E.1 – Estimation of the characteristic transition frequencies of cotton felts and PET felts.

Bibliography

[1] P. Adler, J.-F. Thovert, S. Békri, and F. Yousefian. "Real Porous Media: Local Geometry and Transports". In: *Journal of Engineering Mechanics-asce - J ENG MECH-ASCE* 128 (Aug. 2002).

[2] J.-L. Auriault, C. Boutin, and C. Geindreau. *Homogenization of coupled phenomena in heterogenous media*. Vol. 149. John Wiley & Sons, 2010.

[3] L. Gibson and M. Ashby. "Cellular Solids: Structure and Properties Pergamon Press". In: *New York, USA* (1988).

[4] P. Adler. *Porous media: geometry and transports*. Elsevier, 2013.

[5] S. G. Advani and C. L. Tucker III. "The use of tensors to describe and predict fiber orientation in short fiber composites". In: *Journal of Rheology* 31.8 (1987), pp. 751–784.

[6] A. L. Berdichevsky and Z. Cai. "Preform permeability predictions by self-consistent method and finite element simulation". In: *Polymer Composites* 14.2 (1993), pp. 132–143.

[7] C. Boutin and C. Geindreau. "Periodic homogenization and consistent estimates of transport parameters through sphere and polyhedron packings in the whole porosity range". In: *Physical Review E* 82.3 (2010), p. 036313.

[8] C. Piegay, P. Gle, E. Gourlay, E. Gourdon, and S. Marceau. "A self-consistent approach for the acoustical modeling of vegetal wools". In: *Journal of Sound and Vibration* 495 (2021), p. 115911.

[9] M. N. Miller. "Bounds for effective bulk modulus of heterogeneous materials". In: *Journal of Mathematical Physics* 10.11 (1969), pp. 2005–2013.

[10] G. Milton. "Bounds on the elastic and transport properties of two-component composites". In: *Journal of The Mechanics and Physics of Solids - J MECH PHYS SOLIDS* 30 (June 1982), pp. 177–191.

[11] S. Torquato. "Characterization of the microstructure of disordered media: a unified approach". In: *Physical Review B* 35.10 (1987), p. 5385.

[12] R. Lemaitre and P. Adler. "Fractal porous media IV: three-dimensional stokes flow through random media and regular fractals". In: *Transport in Porous Media* 5 (1990), pp. 325–340.

[13] X. Du and M. Ostoja-Starzewski. "On the size of representative volume element for Darcy law in random media". In: *Proceedings of the Royal Society A: Mathematical, Physical and Engineering Sciences* 462.2074 (2006), pp. 2949–2963.

[14] C. Sandström and F. Larsson. "On bounded approximations of periodicity for computational homogenization of Stokes flow in porous media". In: *International Journal for Numerical Methods in Engineering* 109.3 (2017), pp. 307–325.

[15] M.-A. Chadil, S. Vincent, and J.-L. Estivalezes. "Accurate estimate of drag forces using particle-resolved direct numerical simulations". In: *Acta Mechanica* 230 (2019), pp. 569–595.

[16] S. Mezhoud, V. Monchiet, M. Bornert, and D. Grande. "Computation of macroscopic permeability of doubly porous media with FFT based numerical homogenization method". In: *European Journal of Mechanics - B/Fluids* 83 (2020), pp. 141–155.

[17] B. Ferreol and D. H. Rothman. "Lattice-Boltzmann simulations of flow through Fontainebleau sandstone". In: *Multiphase Flow in Porous Media* (1995), pp. 3–20.

[18] T. G. Zieliński, R. Venegas, C. Perrot, M. Červenka, F. Chevillotte, and K. Attenborough. "Benchmarks for microstructure-based modelling of sound absorbing rigid-frame porous media". In: *Journal of Sound and Vibration* 483 (2020), p. 115441.

[19] H. Talbot. "Analyse morphologique de fibres minérales d'isolation". In: *These Ecole des Mines de Paris* (1993).

[20] S. Bergonnier. "Relations entre microstructure et propriétés mécaniques de matériaux enchevêtrés". Theses. Université Pierre et Marie Curie - Paris VI, Dec. 2005.

[21] C. Peyrega. "Prediction des proprietes acoustiques de materiaux fibreux heterogenes a partir de leur microstructure 3d". PhD thesis. École Nationale Supérieure des Mines de Paris, 2010.

[22] H. Altendorf. "3D Morphological analysis and modeling of random fiber networks: applied on glass fiber reinforced composites". PhD thesis. École Nationale Supérieure des Mines de Paris; Technische Universität ..., 2011.

[23] J. P. Manning, S. ELKOUN, and O. DOUTRES. *Modèle Acoustique D'une Couche Absorbante Composée de Fibres Shoddy: Acoustical Model of a Shoddy Fibre Absorber*. Université de Sherbrooke, 2012.

[24] L. Chapelle. "Characterization and modelling of the mechanical properties of mineral wool". PhD thesis. Technitical University of Denmark Kongens Lyngby, Denmark, 2016.

[25] H. T. Luu. "Modélisation multi-échelle de la dissipation acoustique dans des textiles techniques faits de fibres naturelles". Theses. Université Paris-Est, Dec. 2016.

[26] M. He. "Multiscale prediction of acoustic properties for glass wools: Computational study and experimental validation". PhD thesis. Université Paris-Est, 2018.

[27] L. Lei. "Étude des matériaux poreux thermo compressés pour la modélisation des écrans acoustiques automobiles". PhD thesis. Compiègne, 2018.

[28] C. Piegay. "Approche conjointe acoustique et thermique pour l'optimisation des laines végétales du bâtiment". Theses. Université de Lyon, Nov. 2019.

[29] Y. Xue. "Modeling and design methodologies for sound absorbing porous materials when used as layered vibration dampers". PhD thesis. Purdue University, 2019.

[30] A. Hurrell. “Acoustical properties of polymeric fibres and their characterisation”. Mar. 2020.

[31] G. Matheron. *Elements pour une theorie des milieux poreux*. Vol. 166 pages. Masson Paris, 1967.

[32] M. He, C. Perrot, J. Guilleminot, P. Leroy, and G. Jacqus. “Multiscale prediction of acoustic properties for glass wools: Computational study and experimental validation”. In: *The Journal of the Acoustical Society of America* 143.6 (2018), pp. 3283–3299.

[33] J. Vassal, L. Orgéas, and D. Favier. “Modelling microstructure effects on the conduction in fibrous materials with fibre–fibre interface barriers”. In: *Modelling and Simulation in Materials Science and Engineering* 16.3 (2008), p. 035007.

[34] J. Dirrenberger, S. Forest, and D. Jeulin. “Towards gigantic RVE sizes for 3D stochastic fibrous networks”. In: *International Journal of Solids and Structures* 51.2 (2014), pp. 359–376.

[35] H. Altendorf, D. Jeulin, and F. Willot. “Influence of the fiber geometry on the macroscopic elastic and thermal properties”. In: *International Journal of Solids and Structures* 51.23 (2014), pp. 3807–3822.

[36] S. Gazzo, M. Cuomo, C. Boutin, and L. Contrafatto. “Directional properties of fibre network materials evaluated by means of discrete homogenization”. In: *European Journal of Mechanics-A/Solids* 82 (2020), p. 104009.

[37] E. Bosco, R. Peerlings, and M. Geers. “Asymptotic homogenization of hygro-thermo-mechanical properties of fibrous networks”. In: *International Journal of Solids and Structures* 115 (2017), pp. 180–189.

[38] C. Boutin. “Study of permeability by periodic and self-consistent homogenisation”. In: *European Journal of Mechanics-A/Solids* 19.4 (2000), pp. 603–632.

[39] M. Thiery and C. Boutin. “Static and dynamic permeability assessment of granular and fibrous porous media”. In: *Poromechanics II*. CRC Press, 2020, pp. 575–581.

[40] T. Ghafour, C. Balbinot, N. Audry, et al. “Permeability of flax fibre mats: Numerical and theoretical prediction from 3D X-ray microtomography images”. In: *Composites Part A: Applied Science and Manufacturing* 151 (2021), p. 106644.

[41] J.-M. Tucny, L. Spreutels, F. Drolet, S. Leclaire, F. Bertrand, and D. Vidal. “Impact of fiber diameter polydispersity on the permeability of fibrous media”. In: *Chemical Engineering Science* 262 (2022), p. 117984.

[42] H. Altendorf, D. Jeulin, and F. Willot. “Influence of the fiber geometry on the macroscopic elastic and thermal properties”. In: *International Journal of Solids and Structures* 51.23-24 (2014), pp. 3807–3822.

[43] E. Bosco, R. Peerlings, B. Lomans, C. van der Sman, and M. Geers. “On the role of moisture in triggering out-of-plane displacement in paper: From the network level to the macroscopic scale”. In: *International Journal of Solids and Structures* 154 (2018). Multiscale Modelling of Fibrous and Textile Materials, pp. 66–77.

[44] H. Darcy. *Les fontaines publiques de la ville de Dijon: exposition et application des principes à suivre et des formules à employer dans les questions de distribution d'eau*. Vol. 1. Victor dalmont, 1856.

[45] D. L. Johnson, J. Koplik, and L. M. Schwartz. "New pore-size parameter characterizing transport in porous media". In: *Physical Review Letters* 57.20 (1986), p. 2564.

[46] V. Tarnow. "Airflow resistivity of models of fibrous acoustic materials". In: *The Journal of the Acoustical Society of America* 100.6 (1996), pp. 3706–3713.

[47] V. Tarnow. "Compressibility of air in fibrous materials". In: *The Journal of the Acoustical Society of America* 99.5 (1996), pp. 3010–3017.

[48] V. Tarnow. "Calculation of the dynamic air flow resistivity of fiber materials". In: *The Journal of the Acoustical Society of America* 102.3 (1997), pp. 1680–1688.

[49] O. Umnova, D. Tsiklauri, and R. Venegas. "Effect of boundary slip on the acoustical properties of microfibrous materials". In: *The Journal of the Acoustical Society of America* 126.4 (2009), pp. 1850–1861.

[50] B. Semeniuk and P. Göransson. "Microstructure based estimation of the dynamic drag impedance of lightweight fibrous materials". In: *The Journal of the Acoustical Society of America* 141.3 (2017), pp. 1360–1370.

[51] B. P. Semeniuk, P. Göransson, and O. Dazel. "Dynamic equations of a transversely isotropic, highly porous, fibrous material including oscillatory heat transfer effects". In: *The Journal of the Acoustical Society of America* 146.4 (Oct. 2019), pp. 2540–2551.

[52] A. Koponen, D. Kandhai, E. Hellen, et al. "Permeability of three-dimensional random fiber webs". In: *Physical Review Letters* 80.4 (1998), p. 716.

[53] N. Martys and E. Garboczi. "Length scales relating the fluid permeability and electrical conductivity in random two-dimensional model porous media". In: *Physical Review B* 46.10 (1992), p. 6080.

[54] M. M. Tomadakis and T. J. Robertson. "Pore size distribution, survival probability, and relaxation time in random and ordered arrays of fibers". In: *The Journal of Chemical Physics* 119.3 (2003), pp. 1741–1749.

[55] M. M. Tomadakis and T. J. Robertson. "Survival and relaxation time, pore size distribution moments, and viscous permeability in random unidirectional fiber structures". In: *The Journal of Chemical Physics* 122.9 (2005).

[56] K. Schladitz, S. Peters, D. Reinel-Bitzer, A. Wiegmann, and J. Ohser. "Design of acoustic trim based on geometric modeling and flow simulation for non-woven". In: *Computational Materials Science* 38.1 (2006), pp. 56–66.

[57] H. Altendorf and D. Jeulin. "Random-walk-based stochastic modeling of three-dimensional fiber systems". In: *Physical Review E* 83.4 (2011), p. 041804.

[58] C. Peyrega, D. Jeulin, C. Delisée, and J. Malvestio. "3D morphological characterization of phonic insulation fibrous media". In: *Advanced Engineering Materials* 13.3 (2011), pp. 156–164.

[59] H. T. Luu, C. Perrot, V. Monchiet, and R. Panneton. "Three-dimensional reconstruction of a random fibrous medium: Geometry, transport, and sound absorbing properties". In: *The Journal of the Acoustical Society of America* 141.6 (2017), pp. 4768–4780.

[60] H. T. Luu, C. Perrot, and R. Panneton. "Influence of porosity, fiber radius and fiber orientation on the transport and acoustic properties of random fiber structures". In: *ACTA Acustica united with Acustica* 103.6 (2017), pp. 1050–1063.

[61] P. Soltani, M. S. Johari, and M. Zarrebini. "Effect of 3D fiber orientation on permeability of realistic fibrous porous networks". In: *Powder Technology* 254 (2014), pp. 44–56.

[62] C. Peyrega and D. Jeulin. "Estimation of acoustic properties and of the representative volume element of random fibrous media". In: *Journal of Applied Physics* 113.10 (Mar. 2013), p. 104901.

[63] M. Delany and E. Bazley. "Acoustical properties of fibrous absorbent materials". In: *Applied Acoustics* 3.2 (1970), pp. 105–116.

[64] D. Bies and C. H. Hansen. "Flow resistance information for acoustical design". In: *Applied Acoustics* 13.5 (1980), pp. 357–391.

[65] Y. Miki. "Acoustical properties of porous materials-generalizations of empirical models". In: *Journal of the Acoustical Society of Japan (E)* 11.1 (1990), pp. 25–28.

[66] M. Garai and F. Pompoli. "A simple empirical model of polyester fibre materials for acoustical applications". In: *Applied Acoustics* 66.12 (2005), pp. 1383–1398.

[67] J. Manning and R. Panneton. "Acoustical model for Shoddy-based fiber sound absorbers". In: *Textile Research Journal* 83.13 (2013), pp. 1356–1370.

[68] P. Kerdudou, J.-B. Chéné, G. Jacqus, C. Perrot, S. Berger, and P. Leroy. "A semi-empirical approach to link macroscopic parameters to microstructure of fibrous materials". In: *The 44th International Congress and Exposition on Noise Control Engineering (Inter-Noise2015)*. San Francisco, United States, Aug. 2015, pp. 122–154.

[69] Y. Xue, J. S. Bolton, R. Gerdes, S. Lee, and T. Herdtle. "Prediction of airflow resistivity of fibrous acoustical media having two fiber components and a distribution of fiber radii". In: *Applied Acoustics* 134 (2018), pp. 145–153.

[70] M. T. Pelegrinis, K. V. Horoshenkov, and A. Burnett. "An application of Kozeny–Carman flow resistivity model to predict the acoustical properties of polyester fibre". In: *Applied Acoustics* 101 (2016), pp. 1–4.

[71] M. R. Stinson and G. A. Daigle. "Electronic system for the measurement of flow resistance". In: *The Journal of the Acoustical Society of America* 83.6 (1988), pp. 2422–2428.

[72] P. Leclaire, L. Kelders, W. Lauriks, M. Melon, N. Brown, and B. Castagnede. "Determination of the viscous and thermal characteristic lengths of plastic foams by ultrasonic measurements in helium and air". In: *Journal of Applied Physics* 80.4 (1996), pp. 2009–2012.

[73] C. Ayrault, A. Moussatov, B. Castagnede, and D. Lafarge. “Ultrasonic characterization of plastic foams via measurements with static pressure variations”. In: *Applied Physics Letters* 74.21 (1999), pp. 3224–3226.

[74] J. Lux. “Comportement thermique macroscopique de milieux fibreux réels anisotropes: étude basée sur l’analyse d’images tridimensionnelles.” PhD thesis. Université Sciences et Technologies-Bordeaux I, 2005.

[75] C. Peyrega, D. Jeulin, C. Delisée, and J. Malvestio. “3D morphological modelling of a random fibrous network”. In: *Image Analysis & Stereology* 28.3 (2009), pp. 129–141.

[76] D. Depriester, S. Rolland du Roscoat, L. Orgéas, C. Geindreau, B. Levrard, and F. Brémond. “Individual fibre separation in 3D fibrous materials imaged by X-ray tomography”. In: *Journal of Microscopy* 286.3 (2022), pp. 220–239.

[77] E. Sanchez-Palencia. “Fluid flow in porous media”. In: *Non-Homogeneous Media and Vibration Theory* (1980), pp. 129–157.

[78] A. Bensoussan, J.-L. Lions, and G. Papanicolaou. *Asymptotic Anlysis of Periodic Structures*. Vol. 5. Jan. 1978.

[79] J.-L. Auriault et al. “Etude du comportement macroscopique d’un milieu poreux sature déformable.” In: *Journal de Mécanique* (1977).

[80] G. Bhat and S. Malkan. “4 - Polymer-laid web formation”. In: *Handbook of Nonwovens*. Ed. by S. Russell. Woodhead Publishing Series in Textiles. Woodhead Publishing, 2007, pp. 143–200.

[81] S. Gramsch, A. Klar, G. Leugering, et al. “Aerodynamic web forming: process simulation and material properties”. In: *Journal of Mathematics in Industry* 6.1 (2016), pp. 1–23.

[82] A. Ahmed. “8 - Nonwoven fabric finishing”. In: *Handbook of Nonwovens*. Ed. by S. Russell. Woodhead Publishing Series in Textiles. Woodhead Publishing, 2007, pp. 368–400.

[83] W. Albrecht, H. Fuchs, and W. Kittelmann. *Nonwoven fabrics: raw materials, manufacture, applications, characteristics, testing processes*. John Wiley & Sons, 2006.

[84] Y. Salissou and R. Panneton. “Pressure/mass method to measure open porosity of porous solids”. In: *Journal of Applied Physics* 101.12 (2007), p. 124913.

[85] J. F. Allard, B. Castagnede, M. Henry, and W. Lauriks. “Evaluation of tortuosity in acoustic porous materials saturated by air”. In: *Review of Scientific Instruments* 65.3 (1994), pp. 754–755.

[86] N. Kino. “Ultrasonic measurements of the two characteristic lengths in fibrous materials”. In: *Applied acoustics* 68.11-12 (2007), pp. 1427–1438.

[87] R. Panneton and X. Olny. “Acoustical determination of the parameters governing viscous dissipation in porous media”. In: *The Journal of the Acoustical Society of America* 119.4 (2006), pp. 2027–2040.

[88] X. Olny and R. Panneton. "Acoustical determination of the parameters governing thermal dissipation in porous media". In: *The Journal of the Acoustical Society of America* 123.2 (2008), pp. 814–824.

[89] M. Henry, P. Lemarinier, J. F. Allard, J. L. Bonardet, and A. Gedeon. "Evaluation of the characteristic dimensions for porous sound-absorbing materials". In: *Journal of Applied Physics* 77.1 (Jan. 1995), pp. 17–20.

[90] A. Tamayol and M. Bahrami. "Parallel flow through ordered fibers: an analytical approach". In: *Journal of Fluids Engineering* 132.11 (2010).

[91] F. Pompoli and P. Bonfiglio. "Definition of analytical models of non-acoustical parameters for randomly-assembled symmetric and asymmetric radii distribution in parallel fiber structures". In: *Applied Acoustics* 159 (2020), p. 107091.

[92] L. Lei, N. Dauchez, and J. Chazot. "Prediction of the six parameters of an equivalent fluid model for thermocompressed glass wools and melamine foam". In: *Applied Acoustics* 139 (2018), pp. 44–56.

[93] B. Castagnède, A. Moussatov, and V. Tarnow. "Parametric study of the influence of compression on the acoustical anisotropy of automotive felts". In: *Comptes Rendus de l'Académie des Sciences-Series IIB-Mechanics* 329.4 (2001), pp. 295–301.

[94] D. Stoyan, J. Mecke, and S. Pohlmann. "Formulas for stationary planar fibre processes II-partially oriented-fibre systems". In: *Statistics: A Journal of Theoretical and Applied Statistics* 11.2 (1980), pp. 281–286.

[95] R. J. Brown. "Connection between formation factor for electrical resistivity and fluid-solid coupling factor in Biot's equations for acoustic waves in fluid-filled porous media". In: *Geophysics* 45.8 (1980), pp. 1269–1275.

[96] D. Johnson, J. Koplik, and R. Dashen. "Theory of dynamic permeability and tortuosity in fluid-saturated porous media". In: *Journal of Fluid Mechanics* 176 (1987), pp. 379–402.

[97] M.-Y. Zhou and P. Sheng. "First-principles calculations of dynamic permeability in porous media". In: *Physical Review B* 39.16 (1989), p. 12027.

[98] T. Lévy. "Propagation of waves in a fluid-saturated porous elastic solid". In: *International Journal of Engineering Science* 17.9 (1979), pp. 1005–1014.

[99] A. Bensoussan, J.-L. Lions, and G. Papanicolaou. *Asymptotic analysis for periodic structures*. Vol. 374. American Mathematical Soc., 2011.

[100] E. Sánchez-Palencia. "Non-homogeneous media and vibration theory". In: *Lecture Note in Physics, Springer-Verlag* 320 (1980), pp. 57–65.

[101] D. Lafarge, P. Lemarinier, J.-F. Allard, and V. Tarnow. "Dynamic compressibility of air in porous structures at audible frequencies". In: *The Journal of the Acoustical Society of America* 102.4 (1997), pp. 1995–2006.

[102] L. Chapelle, M. Lévesque, P. Brøndsted, M. Foldschack, and Y. Kusano. "Generation of non-overlapping fiber architecture". In: *20th International Conference on Composite Materials*. ICCM Copenhagen. 2015, pp. 1–12.

[103] G. E. Archie. "The electrical resistivity log as an aid in determining some reservoir characteristics". In: *Transactions of the AIME* 146.01 (1942), pp. 54–62.

[104] M. T. Pelegrinis, K. V. Horoshenkov, and A. Burnett. "An application of Kozeny–Carman flow resistivity model to predict the acoustical properties of polyester fibre". In: *Applied Acoustics* 101 (2016), pp. 1–4.

[105] M. Avellaneda and S. Torquato. "Rigorous link between fluid permeability, electrical conductivity, and relaxation times for transport in porous media". In: *Physics of Fluids A: Fluid Dynamics* 3.11 (1991), pp. 2529–2540.

[106] Y. Champoux and J.-F. Allard. "Dynamic tortuosity and bulk modulus in air-saturated porous media". In: *Journal of Applied Physics* 70.4 (1991), pp. 1975–1979.

[107] X. Tang and X. Yan. "Acoustic energy absorption properties of fibrous materials: A review". In: *Composites Part A: Applied Science and Manufacturing* 101 (2017), pp. 360–380.

[108] J. Ning and Y. Li. "Dynamic flow resistivity and sound absorption of compressed fibrous porous materials: Experimental and theoretical". In: *Physics of Fluids* 32.12 (Dec. 2020), p. 127103.

[109] J. Auriault. "Dynamic behaviour of a porous medium saturated by a Newtonian fluid". In: *International Journal of Engineering Science* 18.6 (1980), pp. 775–785.

[110] R. Burridge and J. B. Keller. "Poroelasticity equations derived from microstructure". In: *The Journal of the Acoustical Society of America* 70.4 (1981), pp. 1140–1146.

[111] O. Umnova, K. Attenborough, and K. M. Li. "Cell model calculations of dynamic drag parameters in packings of spheres". In: *The Journal of the Acoustical Society of America* 107.6 (2000), pp. 3113–3119.

[112] G. Núñez, R. Venegas, T. G. Zieliński, and F.-X. Bécot. "Equivalent fluid approach to modeling the acoustical properties of polydisperse heterogeneous porous composites". In: *Physics of Fluids* 33.6 (June 2021), p. 062008.

[113] V. Langlois. "High-frequency permeability of porous media with thin constrictions. I. Wedge-shaped porous media". In: *Physics of Fluids* 34.7 (July 2022), p. 077119.

[114] V. Langlois, C. T. Nguyen, and C. Perrot. "High-frequency permeability of porous media with thin constrictions. II. Porous media containing thin holed membranes". In: *Physics of Fluids* 34.7 (July 2022), p. 077120.

[115] A. M. Chapman and J. J. L. Higdon. "Oscillatory Stokes flow in periodic porous media". In: *Physics of Fluids A: Fluid Dynamics* 4.10 (Oct. 1992), pp. 2099–2116.

[116] Q. V. Tran, C. Perrot, R. Panneton, et al. "Effect of polydispersity on the transport and sound absorbing properties of three-dimensional random fibrous structures". In: *arXiv preprint arXiv:2309.09388* (2023).

[117] R. Storn and K. Price. "Differential Evolution - A Simple and Efficient Heuristic for Global Optimization over Continuous Spaces". In: *Journal of Global Optimization* 11 (Jan. 1997), pp. 341–359.

[118] K. Price, R. Storn, and J. Lampinen. *Differential Evolution-A Practical Approach to Global Optimization*. Vol. 141. Jan. 2005.

[119] R. Hufenus, Y. Yan, M. Dauner, and T. Kikutani. “Melt-Spun Fibers for Textile Applications”. In: *Materials* 13 (Sept. 2020), p. 4298.

[120] J. Schindelin, I. Arganda-Carreras, E. Frise, et al. “Fiji: an open-source platform for biological-image analysis”. In: *Nature Methods* 9.7 (2012), pp. 676–682.